University of Southern Queensland

School of Engineering

Evaluation of a low-cost machine vision detection method for Varroa Destructor mites on honeybees

A dissertation submitted by

Tristan Dean Lyon

in fulfillment of the requirements of

ENP4111 Professional Engineer Research Project

towards the degree of

Bachelor of Engineering (Honours) (Mechatronics)

Submitted November, 2024

2024

This page intentionally left blank

University of Southern Queensland

School of Engineering

ENP4111 Dissertation Project

(This is a 2-unit research project in Bachelor of Engineering Honours Program)

Limitations of Use

The Council of the University of Southern Queensland, its Academic Affairs, and the staff of the University of Southern Queensland, do not accept any responsibility for the truth, accuracy or completeness of material contained within or associated with this dissertation.

Persons using all or any part of this material do so at their own risk, and not at the risk of the Council of the University of Southern Queensland, its Faculty of Health, Engineering and Science or the staff of the University of Southern Queensland.

This dissertation reports an educational exercise and has no purpose or validity beyond this exercise. The sole purpose of this dissertation project is to contribute to the overall education within the student's chosen degree program. This document, the associated hardware, software, drawings, and other material set out in the associated appendices should not be used for any other purpose: if they are so used, it is entirely at the risk of the user.

1.1 CERTIFICATION

I certify that the ideas, designs and experimental work, results, analyses and conclusions set out in this dissertation are entirely my own effort, except where otherwise indicated and acknowledged.

I further certify that the work is original and has not been previously submitted for assessment in any other course or institution, except where specifically stated.

Student Name **Tristan Dean Lyon**

Student Number: [redacted]

Signature

3 November 2024

Date

1.2 ABSTRACT

Varroa Destructor mites are an incredibly destructive parasitic mite that feeds upon honeybees, and can cause the collapse of beehives in high infestation levels(Plant Health Australia nd.-a). These mites are a relatively new pest to Australia, having only arrived in NSW in 2022 (Plant Health Australia nd.-a) ending the country's status as one of the last countries free from the pest. The introduction of this pest has the potential for enormous economic impacts of up to $70 million per year (Australian Government Department of Agriculture 2024) in addition to environmental impacts from the loss of pollination provided by feral bees.

While there are many studies around the world, including some work in Australia (Wheeler 2021a) for the detection of Varroa mites, most utilise expensive industrial cameras or rely on uploading images for remote processing. These methods present problems for widespread deployment in Australia due to the cost and lack of data reception in remote locations. This research aims to investigate a low-cost, machine vision system for detecting Varroa mites in hives that can work remotely in Australian weather.

For this research a system was built utilising a camera that is sensitive to both visible and infra-red light based on previous research by Bjerge et al. (2019a). The camera was connected to a Raspberry Pi 4 for local image capture and processing, with the system powered by a battery charged by a solar panel for remote operation. This system would capture images of bees entering the hive in an area of NSW with Varroa mites, and these images would be used to develop the machine vision algorithm for detecting the mites.

From the resulting images it was discovered that there were problems with the developed system, including camera focus issues and excessive heat in the processor. The result of this

was that the collected images were not of sufficient quality for an algorithm to be developed for detection of mites during the timeframe of the project. Prior research indicated that good discrimination between bees and mites should be expected with the illumination wavelengths in use, however that was not seen. This is most likely because of the cheaper single sensor camera being used in this research. Changes to the wavelengths of illumination being used may be necessary to achieve the expected discrimination, if it is at all possible with the camera used.

1.3 ACKNOWLEDGEMENTS

Sincere thanks to Ben Brown of Waradaa Honey for his experience in the beekeeping industry and the access to his bees, without which this research would not have been possible.

The inspiration for this research was in part driven by the machine vision courses taught by Tobias Low, the supervisor for this research. Tobias provided guidance and feedback helping improve the standard of the research delivered. Thank you, Tobias.

Many thanks to my family for putting up with my study commitments over the years culminating in my focus on this project. Without their support over so many years I would not have been able to pursue my dream.

Thanks to David, for providing access to a beehive to allow testing of an early prototype design and being ready to provide a hive for a mite-free comparison if it had been required.

University of Southern Queensland, for providing the opportunity to study and conduct this research. Being a professional engineer has been a dream that is finally close to being realised.

Thanks to my work and my colleagues, for allowing me time to dedicate to my studies, and enduring my enthusiastic talks about this research.

1.4 TABLE OF CONTENTS

PAGE

1.5 LIST OF TABLES

1.6 LIST OF FIGURES

1.7 NOMENCLATURE

V_f = Forward voltage drop

V_{OL} = Output voltage drop

1.8 GLOSSARY

ADC = Analog to Digital Converter

AI = Artificial Intelligence

BOM = Bureau of Meteorology

BRIEF = Binary Robust Independent Elementary Features

CNN = Convolutional Neural Network

FAST = Features from Accelerated Segment Test

FCN = Fully Convolutional Network

FPS = Frame/s Per Second

HSV = Hue, Saturation, Value

IO = Input/Output

IR = Infra-Red

ISM = Implicit Shape Model

ISO = International Organization for Standardization

LED = Light Emitting Diode

MFLM = Multi-channel Fourier-Legendre Moments

NoIR = No IR

ORB	=	Oriented Rotated and BRIEF
PWM	=	Pulse Width Modulation
RGB	=	Red, Green, Blue
ROI	=	Region/s Of Interest
RPI	=	Raspberry Pi
RTC	=	Real Time Clock
SSD	=	Single Shot multibox Detector
SIFT	=	Scale-Invariant Feature Transform
SURF	=	Speeded-Up Robust Features
SVDD	=	Support Vector Data Description
SVM	=	Support Vector Machine
YCbCr	=	(Y) Luminance, (Cb) Blue difference chrominance, (Cr) Red difference chrominance
YOLO	=	You Only Look Once

CHAPTER 1 INTRODUCTION

This research project is a machine vision based method for detecting Varroa Destructor mites on honeybees (Apis Mellifera) in Australia. Many solutions have been examined around the world to detect and combat this mite, as it impacts honey production and pollination world-wide. A cheap solution that can be deployed remotely will aid in the monitoring of the mite progression in Australia and allow for faster treatment of affected hives. With appropriate treatment the effects of Varroa mites on honeybee hives can be reduced so that the hives can continue pollinating plants and producing honey.

Varroa Destructor mites have the potential to cause massive damage to the Australian economy, and to commercial and hobby apiarists in the country as the mites can cause the complete failure of infested hives. Now that Varroa have established a foothold in NSW and the efforts to eradicate them have failed, tracking the progress of the mites is more important than ever. Tracking the progress of mites not only informs policies and regulation, but also aids in informing beekeepers where they should be watching for mites so treatments can be applied in a timely manner.

Commercial solutions for tracking of Varroa mites have been researched for several years, with most research focusing on cloud-connected and machine learning processing of images captured by expensive industrial cameras. This research project focuses on expanding on the previous research and targeting lower cost hardware that is more accessible to hobbyist beekeepers. If more available hardware is capable of detecting Varroa mites, there is an opportunity for this system to be deployed by more commercial and hobby apiarists affording a faster and more granular tracking of the spread of Varroa mites.

Under current NSW regulations hives are checked for Varroa mites at intervals not exceeding 16 weeks. This is potentially a long time between infestation and detection of the mites in hive, allowing the number of mites to increase and spread to other hives. Removing barriers to the widespread adoption of methods, and systems for tracking the spread of Varroa mites is the focus for this research.

By investigating the viability of replacing the expensive multispectral industrial cameras infra-red (IR) sensitive sensor with No IR (NoIR) cameras the cost barrier can reduced. Similarly, a Raspberry Pi (RPI) is a widely available and relatively cheap local processing solution. Combined with using machine vision techniques rather than Artificial Intelligence (AI) and machine learning reduces cost and limits the amount of data being transmitted.

Expensive hardware, ongoing costs to access cloud software, and the potential of poor cellular data reception in remote areas of Australia are aspects that are being addressed with this research. If a system can be developed that is cheap to deploy and maintain, while keeping good accuracy detecting Varroa mites there is potential to help control the spread of Varroa mites in Australia. Such a system could be beneficial to beekeepers all around the world by providing monitoring of the mite levels in hives to assist in determining appropriate treatment times.

CHAPTER 2 BACKGROUND AND LITERATURE REVIEW

2.1 BACKGROUND ON VARROA

2.1.1 What is Varroa?

Varroa is the name of a group of species of mites that parasitise honeybees, with one species being Varroa Destructor which has recently arrived in Australia (Australian Government Department of Agriculture 2024). This mite is common to almost all continents of the world, with Australia being one of the only places in the world that was free from the mites until 2022 (Plant Health Australia nd.-a). These mites are small, being around 1mm in diameter and have a distinctive reddish-brown colour so they are visible to the naked eye as shown in Figure 1 - Bee with mite from Australian Government Department of Agriculture Fisheries and Forestry (2024)

Figure 1 - Bee with mite

Female Varroa Destructor mites are the only ones that feed on adult honeybees, with the males remaining in the brood cells once they have hatched. Female mites enter the brood cells with larva and remains inside when the cell is capped by the bees. Inside the capped cell the female mite feeds on the growing bee while laying eggs. The newly hatched mites also feed on the

growing bee, mature and mate within the closed cell. Once the bee emerges from the cell, the female mites emerge with it ready to find new hosts, continue the life cycle and spread amongst the bees (Plant Health Australia nd.-b). This life cycle can be seen in Figure 2 - Varroa Destructor life cycle from Huang (2012).

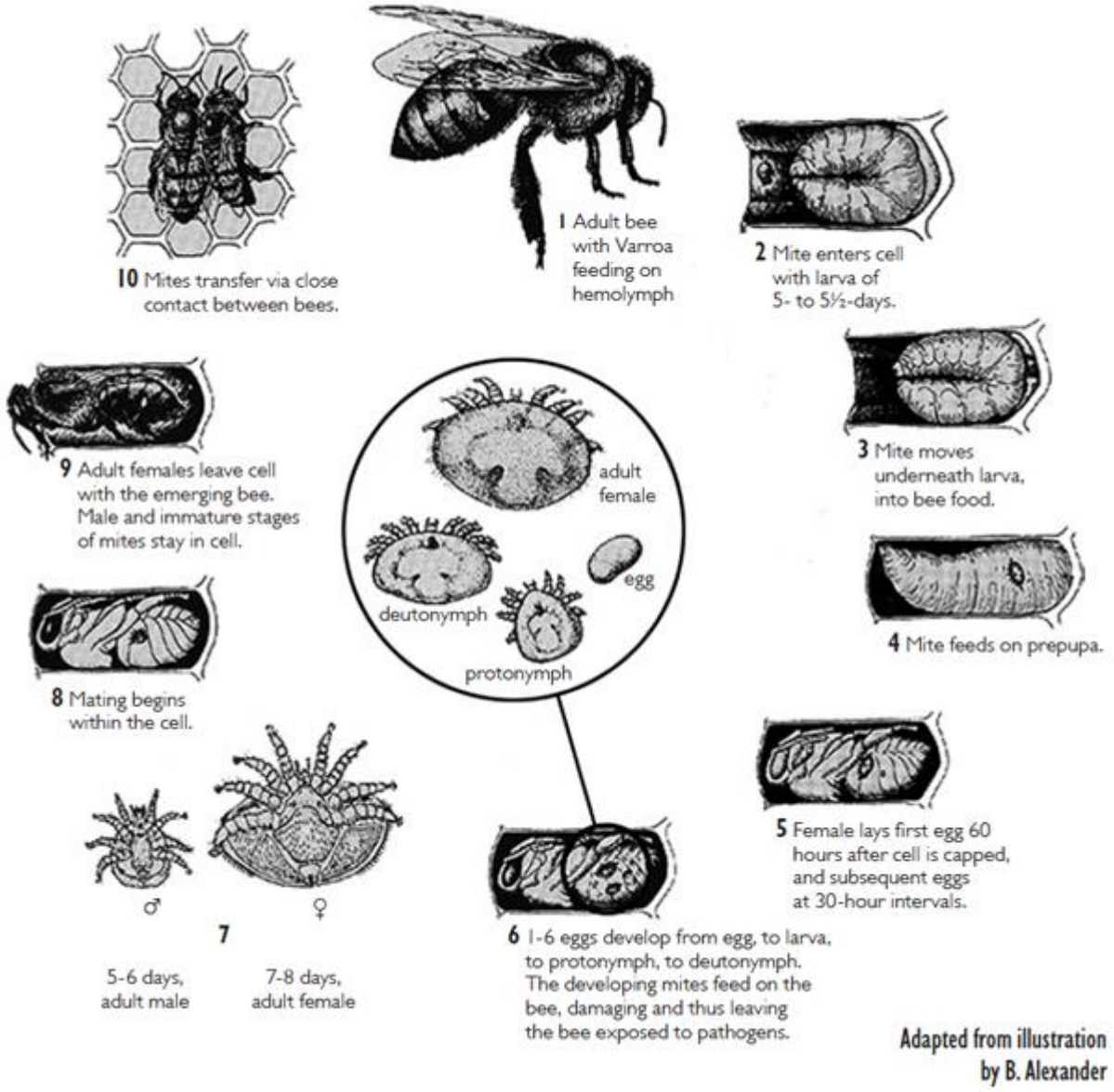

Figure 2 - Varroa Destructor life cycle

2.1.1 What effect does it have on bees/hives?

Varroa destructor feeds on the bees in a hive reducing the strength of the hive and potentially allowing other threats to overwhelm them, in addition to carrying diseases themselves (NSW Department of Primary Industries 2023). An untended (feral) honeybee colony can survive for up to 3-4 years after infestation by the Varroa mites. By feeding on the bees, these mites weaken the bees and allow otherwise harmless viral infections to take over and kill the bees (Plant Health Australia 2014).

The mites feed on the haemolymph (the bees equivalent of blood) of adult bees as well as the brood, weakening future generations before they can even contribute to the hive. By feeding on the bees within the capped brood cells, the mites are protected from being discovered by the bees and other pests. This also means that viruses carried by the mites can be passed to the bees when they are young, weak and still developing (Plant Health Australia nd.-b). Bees that were parasitised while developing can be smaller and weaker when they emerge, and are not likely to live as long as their un-parasitised counterparts. In cases of heavy infestation the bee hives may show symptoms similar to American Foulbrood, European Foulbrood and Sacbrood viruses before progressing into Colony Collapse Disorder (Plant Health Australia nd.-b). The misidentification of the cause of these symptoms can result in a delay in appropriate treatment, increasing the chance of the colony failing.

2.1.2 Impacts on the environment

Australia is fortunate to have native bees that are unaffected by Varroa mites (NSW Department of Primary Industries 2023) which provides some protection from the environmental damage that Varroa can cause. The main cause for environmental damage from Varroa is in the form of a reduction of pollinators available to propagate plants (Plant Health

Australia 2014). Significant pollination in Australia is provided by wild honeybee colonies, and these are the most susceptible to Varroa Destructor. In the Americas and Europe Varroa has destroyed almost all the wild honeybees causing significant impact to pollination (Plant Health Australia 2014).

Varroa infected bee colonies are also shown to have reduced effectiveness pollinating plants. This is due to the combined effects of shorter flower visits and a reduced number of pollen gathering worker bees from the hives (Plant Health Australia 2014). When this effect is considered alongside the reduction in wild honeybees there will be a significant impact to free pollination in Australia. This effect will be tempered by the fact that Australian native bees are unaffected by the Varroa mite, and as such the natural pollinators will continue to be effective.

2.1.3 Impacts to economy

Reduction in pollination provided by both feral and commercialised honeybees due to Varroa infestation in Australia was estimated to cost much as $70 million per year (Australian Government Department of Agriculture 2024). Plant Health Australia (nd.) state that the horticultural sector of the industry will have the largest losses of up to $50 million per year, in addition to the potential for many beekeepers to quit due to the difficulties in managing the pest.

Using New Zealand as a case study for the impacts of Varroa, some idea of what can be expected for Australia can be gathered. Varroa arrived on the North Island in 2000, and almost all feral colonies have disappeared. This has led to an almost 100% increase in pollination costs in just over 10 years (Plant Health Australia 2014). New Zealand uses commercial pollination by honeybees for many crops including kiwifruit (which has more than doubled in pollination costs), avocados, summerfruit and onions (Plant Health Australia 2014).

An additional cost to be borne with Varroa is the treatment cost of the hives, the costs in New Zealand were around $25 per hive in 2012 with costs expected to increase as the mites developed resistance to treatments. A reduction in the number of beekeepers willing to keep up with treatments may also lead to a shortage in bees available for pollination in addition to increased cost of honey as production falls off.

2.1.4 Available treatment

Several treatment methods for Varroa mite infestations are available in Australia in accordance with the Biosecurity (Varroa Mite) Control Order (No. 2) 2024 (Hetherington 2024). These include the products Thymol and Amitraz and miticide strips. Other chemical treatments are not available for use in Australia to combat Varroa under the same order.

Thymol is an organic chemical gel that can only be applied to the hives when the ambient daytime temperatures are between 15°C and 40°C, which makes it applicable for a wide area of Australia, though not in some places at the height of summer or depths of winter. The prescribed treatment time for Thymol is one tray for 2 weeks, and a second tray for 4 weeks. During this time ‘supers’ cannot be on the hive, so no honey can be collected for sale in this time (Australian Honey Bee Industry Council 2024).

Amitraz is a synthetic chemical which is supplied as plastic strips, 2 of which are used for each brood box of a hive. These strips are in place for between 6 and 10 weeks for the treatment to be effective and no supers can be on the hive during this treatment process either. Additionally one type of Amitraz has a period of 2 weeks after the strips are removed before the supers can be put back on the hive (Australian Honey Bee Industry Council 2024).

A standard honeybee hive will have a brood box at the bottom, where the queen lives and lays eggs. Some honey and pollen may be stored in this box if it is not full of brood. A queen

excluder screen keeps the queen from climbing into the super boxes that are placed on top to give more room for the colony to store honey. These supers, in conjunction with the queen excluder allow for easier collection of honey without having bee brood included. Both above methods require the supers to be removed from the hives, so the bees do not have access to most of their honey stores to feed themselves if there are no flowering plants nearby. This also means that no honey can be collected for sale during the treatment time.

In America testing has been conducted on the effectiveness of oxalic acid as a treatment method (Gregorc, Knight & Adamczyk 2017), though this treatment is not approved for use in Australia at this time, though has shown promise achieving 98% cumulative efficacy (Gregorc, Knight & Adamczyk 2017). Oxalic acid is progressing through the permit and application process for use in Australia (Australian Honey Bee Industry Council 2024), and may alleviate some of the issues with other treatment methods pending full registration details.

Drone brood trapping is another approved treatment method and involves encouraging the production of drone (male bees) brood which are a preferred food source of Varroa mites. Once these cells are capped, the comb containing the capped drones are removed and destroyed (Hetherington 2024).

2.2 CURRENT METHODS OF DETECTION

2.2.1 Manual methods

Varroa mites in NSW can be detected on bees by several manual methods that are approved under the Biosecurity (Varroa Mite) Control Order (No. 2) 2024 (Hetherington 2024). Under this order beehives must be examined for Varroa at an interval not exceeding 16 weeks. This

gives an up to 16-week interval for Varroa to grow within a hive between inspections. Additionally if the beekeeper has more than 10 hives at one location, only a subset of the hives need to have a surveillance action carried out at once (Hetherington 2024, p. 6)

Sugar shake test requires the beekeeper to take a sample of at least 300 bees from the hive into a container and gently shake them with fine sugar which can be seen in Figure 3 - Sugar shake process from NSW Department of Primary Industries (2024a, p. 2). This causes the mites to fall off the bees, and the bees can safely be released back to the colony. Other bees from the colony will clean off the sugar leaving the sample bees unharmed. The mites remaining in the sugar container can then be counted to determine the estimated level of infestation (Hetherington 2024, p. 7).

Figure 3 - Sugar shake process

Sugar shaking can be of limited effectiveness when ambient temperature and humidity are high (Gregorc, Knight & Adamczyk 2017, p. 74) affecting the accuracy of these results. Temperatures of 32 degrees Celsius and relative humidity of 76% were shown to reduce the effectiveness of the sugar shake test from 94% down to 66%. The same study identified that a reduction in effectiveness was also evident when using powdered sugar combined with corn starch, commonly known as icing mixture or powder in Australia.

Roasted soybean flour has been examined as an alternative for powdered sugar, which is also harmless to the bees (Ogihara et al. 2020). During testing the powdered sugar started to clump

after 3 days exposed to relative humidity of 75% making it difficult to sift and use for sugar shaking. The roasted soybean flour did not show the same tendency, remaining free even after seven days (Ogihara et al. 2020, p. 430).

Soapy water washing and alcohol washing follow a similar method to the sugar wash, except that the sugar is replaced with either soapy water or an alcohol mix, and the bees are killed as a result of the testing (Hetherington 2024, p. 7).

Sticky miticide strips placed in the hive cause the mites to get stuck as the bees walk over the strips and the number of stuck mites can be counted (Hetherington 2024, p. 7). Detection by of Varroa mites by miticide strips is not deemed as accurate enough to determine the hive infestation rate, requiring follow up testing by one of the other methods with those results reported (Hetherington 2024, p. 9).

These methods require opening of the hive and interacting with the bees to achieve indication of the presence of mites. Two of these methods also kill several hundred bees every time the test is performed. This is not ideal due to the manual effort required, the potentially long time between testing events allow Varroa to build up and the loss of bees from the colony.

2.2.2 Automated detection methods

Research into methods for detecting Varroa mite using cameras and AI has been conducted many times around the world with varying technologies used.

Schurischuster, Zambanini and Kampel (2016) used a Raspberry Pi 3 model B and a V2.1 camera module and explored the different software methods that could be used for automatic detection and classification of mites. The software methods will be examined in a later section.

Two notable limitations of this hardware that was identified is the focal length of the image sensor, and the need to trade-off between image brightness and blur.

In order to test the prototype device a sample of honeybees infested with Varroa were placed inside a testing apparatus so that a large amount of photography could be captured and examined. Schurischuster, Zambanini and Kampel (2016) examined several different camera parameters for their setup to determine the best settings for clear detection of Varroa mites. Since these parameters are specific to the hardware and equipment setup used, they offer a valuable point of reference for configuring other setups but cannot be copied. The difference between effective video and sequential images was also examined by the study. The rate of image capture required is determined by the time taken for a bee to traverse the path in front of the camera.

One of the outcomes from Schurischuster, Zambanini and Kampel (2016, p. 4) is that mite detection becomes more problematic when the mites are occluded by parts of the bee, such as the wing. Otherwise, the colour of the Varroa mite provides a good contrast with the colour of the bee aiding the detection capability. This study also notes that examining the visibility of Varroa under different light wavelengths may aid detection, and this has been examined in other studies.

A Jetson Nano and Raspberry Pi V2.1 camera module were used by Narcia-Macias et al. (2023) for detecting Varroa destructor as well as pollen on the bees. As with many of the other methods, the bees were funnelled into a detection area in front of the hive where the camera could be perfectly positioned for detection. The IntelliBeeHive presented in this study uses cloud connectivity to allow remote monitoring of the hive. Unfortunately Narcia-Macias et al.

(2023) did not have access to a Varroa mite infested hive to train their AI and evaluate the detection capability of the system.

IntelliBeeHive functions as a means of tracking the overall health of a bee colony by being able to track foraging success by pollen load and a temperature sensor for determining the hive temperature (Narcia-Macias et al. 2023). These other features may be useful for remote monitoring of beehives by beekeepers and may be useful addon features to a Varroa detecting system if the industry desires it.

Bjerge et al. (2019a) examined the use of multispectral industrial cameras to further discriminate between Varroa mites and honeybees. They determined that combining near infra-red (NIR) and visible light wavelengths produced a high level of discrimination between honeybees and Varroa mites using their chosen methodology.

In the setup used by Bjerge et al. (2019a) the camera was placed to view the underneath of the bee as it entered the colony as this was determined to be the best location to detect mites (Bjerge et al. 2019a, p. 2) and (Bowen-Walker, Martin & Gunn 1997, p. 153). To achieve this a mirror was placed in front of the camera, allowing a more compact arrangement while maintaining the correct focal length for the camera. Light Emitting Diode (LED) illumination of the underside of the bees was used with narrow spectrum blue, red and infrared light to aid in the discrimination between bees and Varroa (Bjerge et al. 2019a, p. 9). Part of the analysis that was performed to determine the optimal wavelengths of light to use can be seen in Figure 4 below, which was taken from Bjerge et al. (2019b)

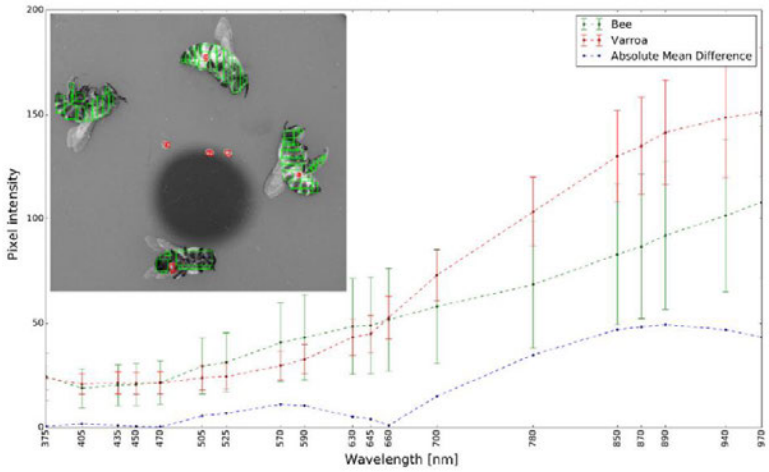

Fig. 3. Mean pixel intensities for pixels in images of bee and varroa mites as a function of wavelength recorded using VideometerLab 4. Bees and mite pixels were manually labeled (see an example of labeling image in upper left corner; actual data used for the plot consist of multiple images) and the μ/σ value pairs for all bee or mite pixels are plotted against wavelength.

Figure 4 - Bee and Varroa mite discrimination by wavelength by Bjerge et al. 2019

Visible light industrial cameras were used by Liu et al. (2023) along with AI methods to design a system that would identify Varroa and honeybees. In this study the images of the bees were captured from above using an industrial camera connected to a laptop for storage. Due to the relatively small number of Varroa mites compared to bees in the images captured the AI training data used was augmented. The team took images of the mites in various lighting conditions and added them to bees in other images to inflate the number of bees with mites for training (Liu et al. 2023, p. 1646). Since this study did not use a custom enclosure to isolate the bees, the AI had to extract the bees from the background imagery in addition to identifying the mites. This exposed limitations where bees where partially visible in the frame, when they were crawling vertically and out of focus due to different flying heights (Liu et al. 2023, p. 1657).

This study also identified a limitation in detecting Varroa mite on flying bees when the hive infection rate is high. With high levels of Varroa infestation bees suffer from wing malformation (Liu et al. 2023, p. 1660) reducing the number of flying bees and potentially hiding the full extent of the infestation. From this it is perhaps best to use this type of Varroa

monitoring for early detection and trend monitoring rather than infestation estimation in established hives.

2.2.3 Technologies in development

Purple Hive Project is a project being run in Townsville with the support of Bega, developing and operating a Varroa mite detection system (Wheeler 2021a). As this is a commercial product there is limited information on the exact processes and technologies inside, though a picture is shown in Figure 5 - The Purple Hive's components from Wheeler (2021b). However, the system uses two cameras plus an AI processing system to detect the bees as they enter through a restrictive slit. Early prototypes of the device produced blurry images as the entrance was too large, allowing the bees to fly through and straight into the hive (Wheeler 2021a). Newer revisions of the system now have a restrictive opening to force the bees to land and slow down as they pass the cameras.

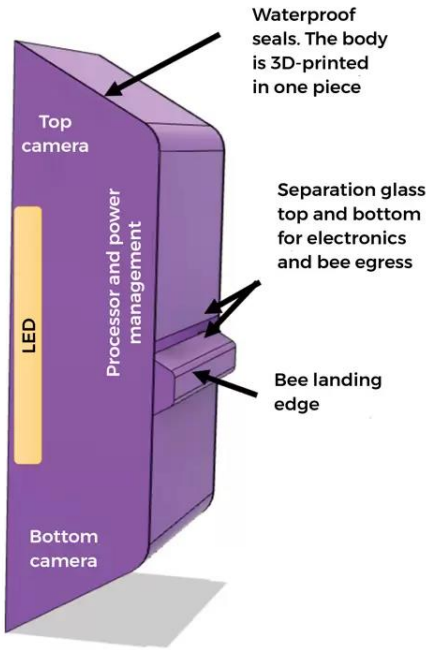

Figure 5 - The Purple Hive's components

The two-camera system employed by the Purple Hive Project allows for full coverage of the bees to be imaged as they enter the hive, getting maximum capture of any mites riding on the bees. This is especially important as these hives are currently located in Townsville and serve an important role in detecting incursions of Varroa jacobsoni and Varroa destructor mites that might arrive at ports there (Wheeler 2021a).

Solar power and a monitoring system that switches the power-hungry processes off when they are not in use is another important part of the Purple Hive Project process. One of the unique aspects of Purple Hive Project is that the cloud processing system is designed to learn and improve over time with all connected hives. This means that the more of these hives are rolled out the more effective the AI algorithm it runs should become, though it does require cloud connection for full functionality (Wheeler 2021a).

Another method that has been examined is using vibrational measurement to detect the movement of Varroa mites within the brood comb (Hall, Bencsik & Newton 2023). The study was focused on detecting and determining the difference in vibrational patterns caused by honeybees and Varroa mites walking. The hardware necessary for implementing such detection within a functional honeybee hive was not presented in the paper, and limitations in the sensitivity of accelerometers may restrict the practical application of this technology now.

Despite these limitations, Hall, Bencsik and Newton (2023) present that other methods of detecting Varroa have limitations that warrant thinking outside the box for new solutions. Visual methods contend with a large amount of collected data for detecting mites, difficulty discriminating between bees and mites (which can be in different positions on the bee) and the hive entrance being the only place to effectively capture images. Another method that is being

studied is using gas sensors to sample the chemical composition of air in the hive, and those need to contend with the nature of bees to seal up gaps such as those used to sample the air.

To measure the vibration and walking gait of the Varroa mite, accelerometers were placed in petri dishes along with mites and in some cases comb to measure the effect of different substrates on the measured vibrations (Hall, Bencsik & Newton 2023). How this would be applied in a hive was not discussed in the paper, though potentially embedded in the comb substrate material creating a ‘smart comb’ would be possible.

2.3 MACHINE VISION AND AI

2.3.1 Machine Vision

Bjerge et al. (2019a) used a sequential multistage approach for image processing making the process not real-time. First the captured image streams needed to be matched in time, as a visible light in Red Green Blue (RGB) and NIR are captured separately. This can then be combined into the R – NIR – B image that is used for further processing. Background segmentation was applied to the image stream by subtracting an image of the background, then applying thresholding to extract the bees. Scale-Invariant Feature Transform (SIFT) was used to identify the bees as they may have been close together.

The main bee detection used was a trained Implicit Shape Model (ISM), utilising features found using SIFT, Speeded-up Robust Features (SURF) and Oriented Rotated Fast and BRIEF (ORB) to form a codebook of features describing a bee. Various machine vision and machine learning processes were examined by Bjerge et al. (2019a) for identifying the Varroa mites, with pixel classifying methods yielding low accuracy.

Mites were detected on the bees by colour masking the bee objects and applying a Hough transformation to detect circular objects with a bound of pixel areas of 10-90 pixels (Voudiotis, Moraiti & Kontogiannis 2022, p. 514). Each positive detection was then annotated onto the colour Convolutional Neural Network (CNN) image along with contours was then stored.

Background subtraction and thresholding was demonstrated by Manoukis and Collier (2019) for isolating the insects caught on a trap. No further classification or counting was shown to expand on this, and this background subtraction and thresholding is a common theme in the studies that were examined.

2.3.2 You Only Look Once (YOLO)

In (Bilik et al. 2021) three different machine learning processes were evaluated and compared for detecting bees and Varroa mites, YOLOv5, Single Shot multibox Detector (SSD) and Deep Support Vector Data Description (Deep SVDD). This paper did not deploy this model on edge hardware but focused on training and evaluating the models with a goal of deploying it on an Nvidia Jetson Nano.

YOLOv5 is identified as an object detector algorithm that is an open-source implementation of YOLO. This method detects features in the image, creating feature maps at several different resolutions, then comparing them at different scales (Mrozek et al. 2021b).

The results from the testing identified that the YOLOv5 algorithm would run at around 1 Frame Per Second (FPS) on an Nvidia Jetson Nano, which was the fastest inference time (Mrozek et al. 2021b, p. 13)

Mite detection by Liu et al. (2023) was performed by YOLOX, a baseline of the YOLO process that was used by several other papers. This was chosen as it is an object detection process that

is capable of real-time processing and performs well (Liu et al. 2023, p. 1649). The YOLOX algorithm was customised and called F-YOLOX-b then compared against other object detection algorithms Faster R-CNN, YOLOv4 and the baseline YOLOX. The results showed that R-CNN was the worst performing of those tested, and F-YOLOX-b was the most accurate for detecting bees and Varroa.

The algorithms used by Liu et al. (2023) were trained and tested on desktop computer hardware and may not be suitable for lower power, field deployable hardware.

To make use of the YOLOv7 object detection algorithm, Narcia-Macias et al. (2023) used a YOLOv7-Tiny model trained in one class annotate “honey bee” to reduce the computational load and allow it to run faster on the Nvidia Jetson Nano. They found that passing a video stream of 1280 x 720 at 10 frames per second through the YOLOv7-Tiny model took 57ms per frame. To improve the speed of processing the model was converted to Open Neural Network Exchange (ONNX) format to make use of the Tensor RT cores provided by the Nvidia Jetson Nano. This improved the processing time to 27ms per frame of video (Narcia-Macias et al. 2023, p. 5).

Pollen and mite tracking was performed using a second YOLOv7-Tiny model that had two classes. The pollen class was trained using manually extracted images of bees that were carrying pollen from the sample videos. Since mite availability was limited, this class was trained using opaque red beads glued to dead bees (Narcia-Macias et al. 2023, p. 6).

Once the bees were identified and boxed, additional data could be extracted including the direction of travel, and the size of the bee could be used to identify between a worker and drone bee (Narcia-Macias et al. 2023, p. 7). The number of drone bees entering and leaving a hive could be useful information for beekeepers and is worth examining.

Zhong et al. (2018) proposed a system for identifying flying insects around crops using a YOLO object detection method followed by a classification and counting method based on Support Vector Machines (SVM). The YOLO model in this case is trained to detect only one class since the fine detection will be handled later. The authors chose to use a pre-trained YOLO model and add a new convolution layer to convert it from a classification model into a detection model (Zhong et al. 2018, p. 7). The YOLO model required the images to be scaled and cropped quite small (448 x 448 pixels) to run through, which reduces the detail, but this does not pose a problem in this case as the model is only detecting insects not classifying them.

A different approach is presented by Noriega-Escamilla et al. (2023) comparing DeepLabV3 and YOLOv5 models which excel in semantic segmentation and object detection, with Multi-channel Fourier-Legendre Moments (MFLM). Additionally, for the MFLM model different colour spaces were examined, RGB, Hue Saturation Value (HSV) and Luminance Chrominance (YCbCr). MFLM are presented as the successor to Quaternion processing of RGB images (Noriega-Escamilla et al. 2023, p. 6). Fourier-Legendre moments are scale invariant, but only when the image being analysed only contains the image of the object, so accurate cropping of the source image is essential to this process.

When the models were trained using a publicly available Varroa dataset captured in laboratory conditions and evaluated the MFLM model was the top performer, with the YCbCr colour space providing the most accurate results (Noriega-Escamilla et al. 2023, p. 12). The results of this study show that examining the performance of object detection can be influenced by the colour space that is utilised and various combinations should be examined to maximise discrimination.

2.3.3 Convolution Neural Network (CNN)

Many processes used for identifying insects rely on machine learning and AI processes that are most efficiently run in dedicated computers. This poses a problem for applying this technology to identifying Varroa mites on bees where there may be limited ability to upload images for cloud processing (Mrozek et al. 2021b, p. 2). One way to get around this problem is to include a device such as a Google Coral accelerator to allow more powerful local processing like was proposed by Mrozek et al. (2021b). The system utilised by Mrozek et al. (2021a, p. 5) is shown in Figure 6 - IoT detection system from Mrozek et al. (2021a, p. 5).

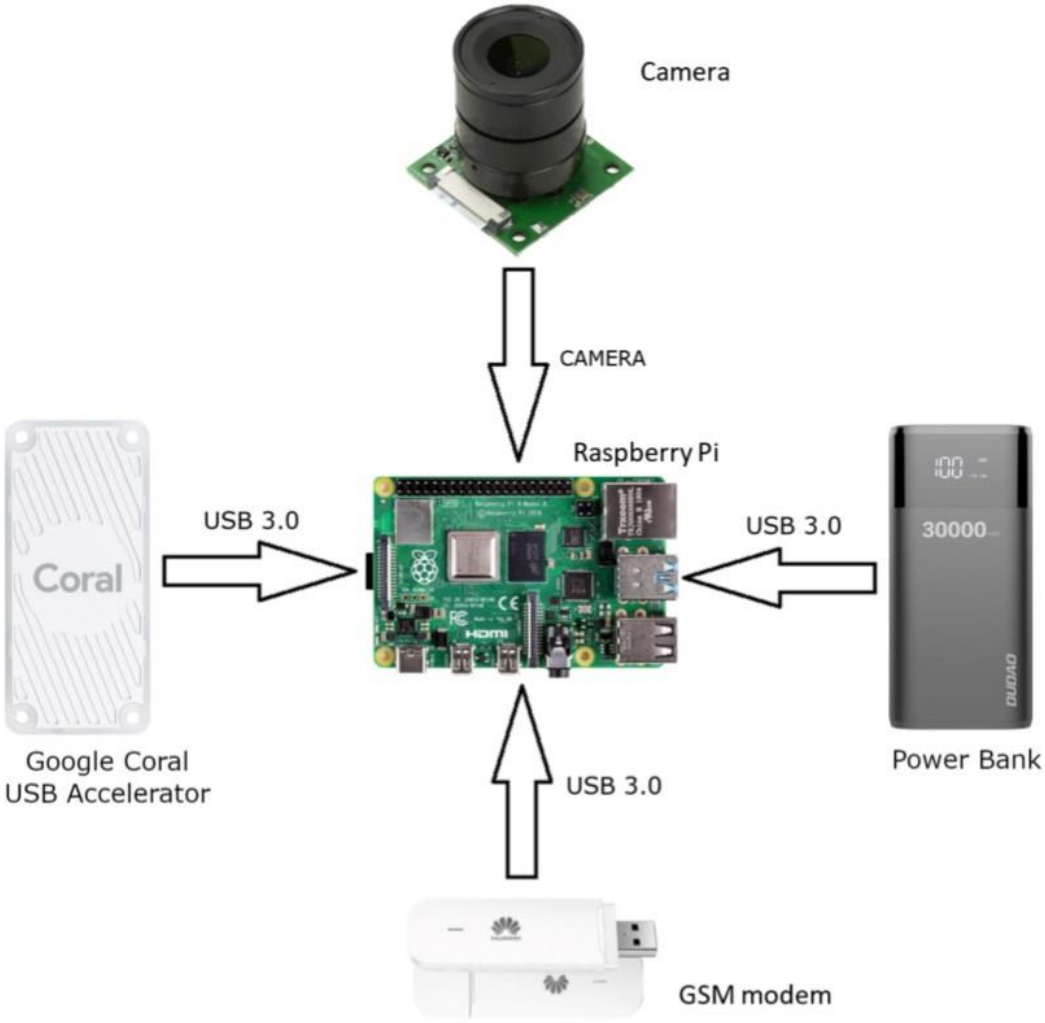

Figure 6 - IoT detection system from Mrozek et al. (2021a, p. 5)

A study of methods used in other paper was carried out by Mrozek et al. (2021b, p. 3), and they produced a CNN model for identifying bees and Varroa destructor. Using the Google Coral, frames from the video feed are extracted and bees are identified as Regions of Interest (ROI). These regions are then assessed by the model to determine if the bee is infected, with any resulting infection results uploaded to the cloud for model improvement (Mrozek et al. 2021b, p. 6). The general CNN process for image processing used by Mrozek et al. (2021a, p. 8) can be seen in Figure 7 - General CNN process.

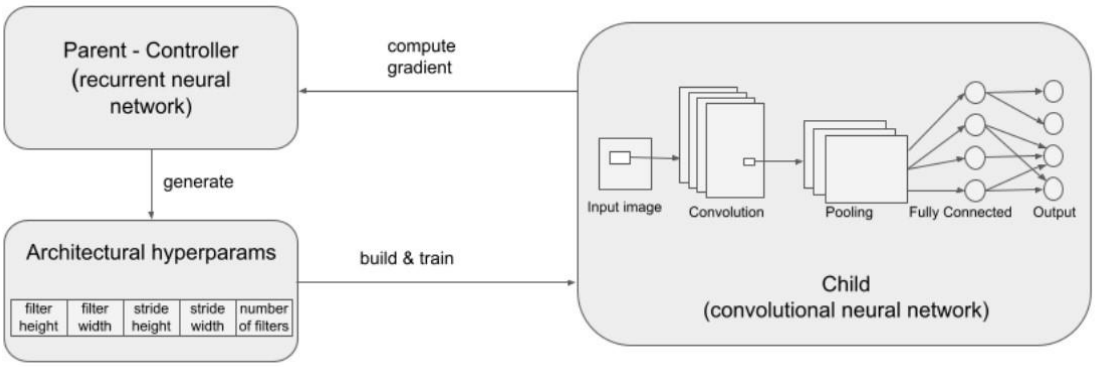

Figure 7 - General CNN process

Similarly the SSD algorithm is an object detection algorithm that uses feature maps, convoluted through several layers of increasing features for fast object detection (Mrozek et al. 2021b). This algorithm had the issue of being unable to identify small features, and therefore may miss Varroa mites on the bees if not enough pixels are visible.

Deep SVDD is a CNN algorithm that is designed for identifying anomalous samples. For this reason, this algorithm can identify bees that do not conform to the class of a normal bee. This means that deformations of the bee, such as wing deformation which can be caused by Varroa, are identified even if the mite cannot be seen (Mrozek et al. 2021b, p. 8).

Bjerge et al. (2019a) selected a CNN process for classifying the mites, as it had higher accuracy than other methods that were tested. It was noted however that a CNN method used to classify the mites could misidentify the tongue of the bee as a mite, necessitating masking this region. This masking is not mentioned in the other studies examined that used CNN methods.

(Liu et al. 2023) demonstrated a two-stage process for the detection of Varroa. The first stage used a Fully Convolutional Network (FCN) to separate the bees from the background. The FCN model uses VGG16 feature extraction with a fine feature map fused in as the backbone and with the fully connected layer replaced by 3 convolution layers. Since the output feature map was a low-resolution image, this was upscaled to match input image as a segmented image.

In contrast to the findings from Liu et al. (2023), Faster R-CNN and SSD were the chosen algorithms for Voudiotis, Moraiti and Kontogiannis (2022). They used pre-trained models of these two algorithms as they are well known and have a balanced performance. Additionally, the authors compared a heavier CNN with more trainable parameters. These models would perform the first of two steps and detect the bees within the images (Voudiotis, Moraiti & Kontogiannis 2022, p. 512). Identification of the Varroa mites would then be carried out using colour masking and Hough transformation.

The CNN model training and detection was broken up into several steps described in the paper, starting with initial data collection and cleansing, data labelling and smoothing, training the CNN, contouring, finally ROI masking and mite detection. Initial data collection and cleansing involved getting the data from the camera at the appropriate resolution. Data labelling was carried out manually, and the images were filtered, smoothed and scaled prior to using for training the model. Three models were trained by Voudiotis, Moraiti and Kontogiannis (2022, p. 513) using the training image set captured. The output of each trained model was then filtered

for the confidence of bee objects and the resulting high confidence objects were then cubic interpolation Gaussian filtering was applied. This helped extract the contours of the bees.

A comparison between the three CNN models with mite detection, and other studies including Bilik et al. (2021) was performed, with the authors system taking the longest time by far in offline mode. When using cloud computing, each image took 470ms on average for detection (Voudiotis, Moraiti & Kontogiannis 2022, p. 519) where the method used by Bilik et al. (2021) took only 0.05ms. It should be noted though, that the hardware used by each author is not equivalent, and adjusting for operation on an Nvidia Jetson Nano makes the time for Bilik et al. (2021, p. 14) 1.5ms. This adjustment still makes this method much faster, while also being the most accurate analysed by Voudiotis, Moraiti and Kontogiannis (2022).

2.3.4 Other methods

Fine classification and counting were performed using the SVM model that was trained in six classes, and utilised three types of global feature extraction and one local feature. The global features were shape, texture, colour with the local feature being HOG which is related to the gradient within cells in the image. Results from the testing of the system showed a processing time of around 50ms (Zhong et al. 2018, p. 12) with an accuracy of the YOLO/SVM model around 90% (Zhong et al. 2018, p. 17).

One of the downsides of this model and method is that images were captured of static insects on a sticky surface, so the accuracy on moving insects is not known. Also testing on the target Raspberry Pi hardware had a count and classifying time of 5 minutes per cycle. This would be too slow for counting Varroa entering a hive but might be enough to give trend indication if enough bees are in each frame.

Manoukis and Collier (2019) utilised an open-source piece of software called ctrax to perform tracking of the insects in their study. The methods that ctrax uses to perform tracking are not discussed. Additionally, ctrax analysis was performed on lab computers after the video files were gathered. Processing times for the captured data was not discussed and may not be suitable for deployment in an edge processing situation.

2.4 HARDWARE

2.4.1 Cameras

Cameras come in many different types and capabilities, with varying benefits and drawbacks depending on their planned use. One feature that needs to be considered is if the camera has a global shutter or a rolling shutter. Global shutter cameras capture the entire image at a single moment in time, minimising blurring, and other distortions on fast moving objects. Rolling shutter cameras are cheaper and more widely available, however they capture the image sequentially from rows or columns of the sensor elements. This can lead to distortion known as rolling shutter effect on fast moving images. So, the trade-off is cheap and widely available, or more expensive and specialised cameras.

Most cameras used by the public will capture visible light images, as close as possible to what the human eye perceives. To aid in this, digital camera sensors are often fitted with infra-red (IR) filters to cut out the IR light entering the sensor. Multispectral cameras on the other hand can detect a wider range of light wavelengths and can be used for specialised applications. Some multispectral cameras may utilise multiple image sensors along the same light path to capture the wider range of wavelengths such as the AD-130GE (JAI 2024a) used by Bjerge et al. (2019a). Of course, a specialised camera is more difficult to get and more expensive. An

alternative is to use cameras that have had the IR filter removed, like the NoIR series of camera for Raspberry Pi. These are often used as night vision cameras (Klemens, Tripepi & McFoy 2021) for projects due to their cheap price point.

The Raspberry Pi cameras come in a wide variety of types and different sensors that can be used such as the PiNoir Camera Board v2 used by Klemens, Tripepi and McFoy (2021) which uses an 8MP IMX-219 sensor by Sony. This camera functioned well as a night vision camera when using external IR illumination. Zhong et al. (2018) used the same sensor, however this one was not IR sensitive as the IR filter was installed in it.

More recently a more powerful camera has been released for the Raspberry Pi that is designed to accept standard C and CS mount lenses, this is the Raspberry Pi HQ camera using the IMX-477 sensor by Sony (Arducam 2023a). This sensor is only available in rolling shutter, has 12.3MP and can capture video at up to 240FPS to reduce blurring caused by movement and the rolling shutter. Importantly there is a version of the camera that can be purchased with a mechanically switchable IR filter (the B0270 model shown in Figure 8 from Arducam (2023c)) allowing IR light to be captured by the RGB sensor.

Figure 8 - Raspberry Pi with Arducam B0270 camera

Another important factor in selecting the camera is the software required to drive it. The Raspberry Pi community is large and documentation on how to drive the cameras compatible with it is widely available.

2.4.2 Image processing

Once images have been captured by the sensor, they need to be processed and have the detection algorithms run on them. This can be done close to the image capture source, at the edge, or remotely on a dedicated server or in the cloud. Remote processing can take advantage of higher power equipment such as dedicated AI and graphics processing capabilities. The disadvantage of this method is the requirement to transmit the images for remote processing. This will add time, and assumes that there is a connection to the remote processing system, which may not always be achievable if the sensor is in a remote location (Voudiotis, Moraiti & Kontogiannis 2022, p. 511). A hybrid system that makes use of remote processing when it is available, and local processing when that is not possible presents a compromise that is worth investigating. Another factor to be considered with remote processing is the potential for recurring costs such as subscription services and mobile data plans that may be required for the service to be used.

Edge processing of the images raises the power requirements and equipment costs at the sensor site, while offering drastically slower processing times (Voudiotis, Moraiti & Kontogiannis 2022, p. 519). The trade-off is that the system is less reliant on external systems to perform its job and can potentially be purchased once and used indefinitely. There are many processing platforms that can be utilised for edge applications, even including devices that improve edge processing such as the Google Coral used by Mrozek et al. (2021b).

Among the hardware that can be used for edge processing, a laptop such as used by Bjerge et al. (2019a) with internal graphics card is powerful option. Since the specifications and power requirements of laptops vary greatly, a good deal of time would need to be invested to identify a suitable power to processing speed trade-off for this option. Another common option is the various models of Raspberry Pi. These are widely available with a good supporting community and are well suited to edge processing of images with attached cameras demonstrated by Mrozek et al. (2021b), Schurischuster, Zambanini and Kampel (2016) and Zhong et al. (2018). Raspberry Pi computers were also used for capturing images by Klemens, Tripepi and McFoy (2021) and van der Voort et al. (2022) though no image processing was performed in these cases.

The Nvidia Jetson Nano is similar in form factor to the Raspberry Pi, though it is designed with AI and image processing in mind. Because of this, and the compatibility with cameras that can also be used with the Raspberry Pi it is another strong option. One benefit of the Nvidia Jetson Nano, and the reason for its stronger AI processing performance is the inclusion of 128 CUDA cores, a feature which the Raspberry Pi lacks (Bilik et al. 2021). Narcia-Macias et al. (2023) also used the Nvidia Jetson Nano as the edge processor of choice in their paper, making use of it for AI processing.

From the available information the Nvidia Jetson Nano is a strong option where edge processing of AI tasks is required due to being designed for this task. The Raspberry Pi is still a viable option where only machine vision or limited AI task loads are required and has been used for this purpose in several other studies.

2.4.3 Batteries

Any system operating in remote locations will need to have some form of power available to sustain the device between inspections cycles. From Hetherington (2024) the maximum time between manual inspections of apiaries in Varroa areas of NSW is 16 weeks. Supplying a battery system capable of running devices for this length of time without recharging would require a large battery system. The Raspberry Pi 4 model B has a recommended power supply of 5V at 3A (Raspberry Pi Ltd nd.) requiring 15W per hour of operation. Given that bees do not fly at night (Narcia-Macias et al. 2023, p. 15), and assuming 12 hours of daylight operation the full 16 weeks of operation would require 20kWh of power storage. This number does not account for inefficiencies in power conversion and storage systems. Likewise, a Raspberry Pi is unlikely to require 3A continuously as Mrozek et al. (2021b, p. 15) demonstrated a system that would last for over 10 hours on a 30,000mAh (150Wh) power bank.

Even with a solar power system capable of running the processing device continuously during all weather conditions, some amount of battery storage is useful to smooth out power delivery and ensure safe power up and down events for the system. There are three main battery technologies in use these days, traditional lead acid, lithium-ion (Li-ion) and lithium polymer (Li-po). Li-ion and Li-po are very similar in properties both being lithium based and will be considered together.

Lead acid batteries are still quite common, powering cars, motorbikes and many other applications. Solar power setups for vehicles and camping often include deep cycle lead acid batteries. Deep cycle batteries are designed for long, slow power draw applications (Battery World Australia Pty Ltd 2024). Lead acid batteries pose a lower risk of thermal runaway events, and are more tolerant of over and under charging, making them less delicate (Un & Aydın

2021), though they are much heavier and larger for the same power capacity as lithium based batteries.

Lithium batteries such as those used in power banks and many portable rechargeable devices these days are very energy dense (Murashko 2016). The downside is that they are susceptible to thermal runaway events. Exposing these batteries to the harsh Australian summer without adequate monitoring, as is likely the case for a remote site, poses a significant risk of thermal runaway and starting bushfires (Un & Aydın 2021).

A new technology on the market is Sodium-ion batteries, which hold the potential for safer operation than lithium-based batteries though more research and time is needed to prove this satisfactorily. Sodium batteries show lower stored power, and steeper charge/discharge curves (Abraham 2020) than lithium batteries. In addition, different cell voltages means different battery protection circuits are required for safe operation. This is a battery technology that may be viable in the future for remote installations, for now more study is required.

Due to the need for long duration, unsupervised operation in remote locations year-round, the risk of thermal runaway induced fire makes lithium-based batteries an unattractive option. Lead acid batteries would be larger and heavier, however a safer option for such a system. The total storage capacity would be determined once the other components of the system are selected.

2.4.4 Solar Power

Battery power alone is not a practical solution for long term operation of a remote system as presented above, so a system utilising solar power during the day and battery storage to smooth out the supply is considered. A solar powered solution consists of three main parts, the solar panel/s, battery charger/energy converter and the power storage. Power storage has been examined in an earlier section and will not be covered again.

Solar panels are available in three types: monocrystalline, polycrystalline and amorphous. Monocrystalline solar panels have each cell made from a single piece of silicon crystal and typically boast higher energy output per area than other types of panel (Lyons 2022). This output does drop in low temperature conditions to the point where it may be less efficient than other types of panel (Yandi, Puriza & Jumaida 2021). Additionally the monocrystalline panels are more expensive than other types of panel and are susceptible to the cleanliness of the panel (Lyons 2022).

Polycrystalline panels have cells made from many pieces of silicon melted together, and thus suffer from lower efficiency compared to monocrystalline panels. This means that a larger surface area of panel is required to achieve the same output power (Lyons 2022). One of the benefits of polycrystalline panels is that they are cheaper than monocrystalline, potentially offsetting the lower efficiency provided by each panel at the expense of space (Lyons 2022). Depending on the temperature environment at the installation location there may be efficiency gains when using polycrystalline panels (Yandi, Puriza & Jumaida 2021).

Amorphous panels are the cheapest option of the three types and have disadvantages to match. These panels have the lowest efficiency out of all three types, however they are less sensitive to temperatures. Amorphous panels are also more susceptible to damage (Lyons 2022) which would make them less suitable for long term remote operation.

The polycrystalline panels are a good compromise in all areas and would be the most practical for this system. Final selection of the solar panel type will be dependent on availability and cost of the desired rating.

Solar panels do not output stable voltages, they vary with the amount of sun received, among other factors. For that reason, voltage converters are used with them, and since sunlight is rarely

available for the entire operational duration of a system, batteries are used to store excess power. Batteries require a charging system so that the maximum solar panel power stays within safe charging range (Kava et al. 2023). Battery charging and voltage conversion for output are often handled by a single device called a charge controller. This charge controller needs to be selected to match the battery chemistry, expected load and solar panel arrangement required.

Since many charge controllers are designed to output 12V for use with car and camping equipment, further conversion down to 5V or another voltage may be necessary depending on the requirements of the load system.

2.4.5 Environmental conditions

Australia is a large continent and the conditions across it vary quite drastically. This makes designing any system for deployment around the country challenging though not impossible. Several environmental factors should be considered for a device exposed to the elements including water and dust resistance, temperature tolerance and susceptibility to UV radiation.

Water and dust resistance can be accommodated by ensuring the equipment used is inside an appropriately rated enclosure following a standard such as AS65029 (Australian Standards 2018). This standard details the commonly used Ingress Protection (IP) rating system which details how dust and water resistant something is along with the testing methodology. According to this system, a device rated at IP65 would be (6) dust tight and (5) protected against water jets. This would be sufficient for exposure to dust and rain, and even hosing the unit down.

Temperatures across Australia vary considerably, maximum temperatures can reach the mid 40’s Celsius and minimum temperatures as low as -6 Celsius according to the climate maps

from Australian Bureau of Meteorology (2024b). Outliers beyond these temperatures can be expected to occur so some operational tolerance should be maintained outside these values.

Maps provided by Australian Bureau of Meteorology (2024b) also show the average daily solar exposure and average sunshine hours across the country. These maps and the values they contain can be used to help determine an appropriately sized solar system for long term operation around Australia. The actual solar generating capability of a location will be very dependent on shade created by trees and structures. In winter, some areas of Tasmania get as low as 3 hours of daily sunlight on average, so solar operation in these areas may be tricky.

UV exposure causes degradation in exposed plastics and should be considered in systems exposed to the elements. Australia has an almost uniform extreme UV index in the summer months as seen on Australian Bureau of Meteorology (2024b) so equipment needs to be appropriately selected or protected from UV exposure for maximum life. Australia is a harsh and challenging environment for electronics, so careful consideration needs to be given to ensure the longevity of a system that is expected to operate around the country.

2.5 RESEARCH AND TECHNOLOGY GAP

Existing research for detecting Varroa has mainly focused on using RGB or visible light spectrum cameras with multispectral cameras being an exception only found in Bjerge et al. (2019a). In this case the camera used was an industrial camera, which are not as readily available and often come with increased cost. Since it has been proven that combining NIR and visible light produces better discrimination between honeybees and Varroa (Bjerge et al. 2019a), examining the effectiveness of more readily available NoIR cameras for this purpose has merit. If the NoIR cameras have a benefit in detecting Varroa mites on honeybees, the price

point for detection systems could be reduced allowing for greater adoption and better tracking of mite invasion in Australia.

Most studies that have been examined present methods and models that have been trained in the detection of Varroa, though few have been tested on proposed target hardware, and fewer still in the field. Integrating hardware together into a system that is targeted to operate in the harsh Australian environment has been carried out by the Purple Hive Project (Wheeler 2021a). This system however operates with cloud processing and interconnection as its intended purpose. Such connection may not be possible everywhere in Australia, and certainly some users may be reticent to utilise yet another IoT device. Systems that can be operated standalone and without relying on services that may require subscription or become unavailable in the future still find favour in today's world.

The systems that have been examined in this study primarily utilise machine learning methods for the detection of Varroa. Some of the methods have incorporated machine vision techniques for processing images before (Bjerge et al. 2019a) or after (Voudiotis, Moraiti & Kontogiannis 2022) the machine learning process. An area that would be worth further examination is a purely machine vision method process utilising edge computing. This method would have the potential for low-power and cheap computing to be utilised in the detection of Varroa mites.

Combining the three points above into a system that is low-cost, made of readily available technologies and does not rely on subscription services for processing will increase the uptake of such a system. With Varroa now in NSW, monitoring the spread of the pest becomes a vital task for the beekeeping industry (NSW Department of Primary Industries 2024b) and any method of increasing monitoring or reducing the burden of monitoring would be of great benefit.

CHAPTER 3 METHODOLOGY

Driving this research are several questions to be answered, and a set of goals to be achieved which inform and are limited by the scope of the research. To carry out these goals and answer the questions a methodology is presented which will govern the process of the remainder of the research. This methodology covers the system testing, from initial prototype through to the field testing of the system, as well as the plan for data collection and analysis of the collected data. The planned methodology is covered here, with collected results and analysis in later chapters.

Risk assessment for this research was carried out and logged as ref: 4514, see APPENDIX D.

3.1 RESEARCH GOALS

3.1.1 Questions to be answered

This research aims to answer the following questions to improve understanding of the options available in efforts of Varroa mite control:

1. Are NoIR cameras an effective low-cost sensor for detecting Varroa mites?
2. How does the system detection rate compare with other systems in development or use?
3. What is this systems rate of false positive detection of Varroa mites?
4. Are mite detection systems able to play a role in mite treatment and can they be useful in areas that are already mite infested, or only on the borders to track progress of mites?

3.1.2 Goals for this research

The following goals have been set for this research to determine the suitability of the solution for deployment or further development:

1. Examine the effectiveness of NoIR cameras for Varroa mite detection
2. Develop a machine vision process for detection of Varroa Mites capable of running on a Raspberry Pi
3. Develop a low-cost machine vision detection method for Varroa Destructor mites on honeybees in Australia
4. Positively identifies Varroa in hives with known cases
5. Does not detect Varroa in hives confirmed to have no cases of Varroa
6. Solution can operate outside in the Australian weather (exposure to sun and rain)
7. Target system run time without intervention 1 week or longer

3.1.3 Scope of research

Due to time and budget constraints this research will be limited in scope. The research will focus on; the building of the detection system including electronics and enclosure, and the development of the algorithm for detecting mites from the output of the detection system. The method of communicating the resulting mite count from the system to the desired destination is considered trivial and out of scope due to the constraints.

3.2 TIMELINE

See APPENDIX A.

3.3 BUILD TESTING

The electronics for the system will be tested on a breadboard to ensure that there are no major flaws in the design before proceeding to permanent mounting of the components on prototyping board. Testing of the breadboard circuit is carried out in two stages, unpowered tests to verify no short circuits exist in the main power rails followed by powered testing of functionality. These tests steps are shown in *Table 6*, *Table 7* & *Table 8* in APPENDIX B.

After the breadboard testing has confirmed the designed circuit is operating as expected, the circuit is committed to a prototyping board and all components soldered in place. The same suite of tests are repeated to ensure no mistakes have occurred during the manufacturing process.

Software on the RPI will be tested prior to integrating the RPI into the electronics enclosure. Testing of the RPI will be carried out with a monitor, keyboard and mouse to monitor the functions. As soon as boot up of the RPI is completed, images will start being captured at regular intervals in RAW format to retain colour information for later processing. GPIO pins 0, 13, 17, 18 and 26 will be logic high at this time and can be tested with a multimeter to confirm. Connecting GPIO 17 to the RPI ground will initiate shutdown of the RPI. Using a multimeter the state of GPIO 0 will be examined to ensure it gets set to logic low only after shutdown has completed. This will ensure that power is maintained to the RPI until it has safely shutdown in the complete system.

At this stage the electronics can be safely incorporated into the electronics enclosure for system integration testing. This testing incorporates the steps in *Table 8* as well as calibration and configuration steps described later.

End the image capturing process using the kill command and open a live camera preview. Using the live preview the camera focus will be adjusted to ensure the bee tunnel is in clear focus. Place the lid on the system box and use terminal commands to take a photo using the same settings as the automatic process except as a JPEG output. Examine the image looking for an over or underexposed image and adjust the shutter speed to compensate. Repeat this process until the image appears well exposed and apply these setting changes to the automatic process.

Using the power measured from the bench power supply, the voltage and current delivered to/from the battery (using a multimeter for voltage and current monitoring sensor) the approximate load power of the system can be calculated. Losses in solar converter would be treated as load power in this case. This is used to calculate the expected system run time on battery only power as well as the power required from a solar panel to maintain continuous operation.

3.4 DATA GATHERING

Initial image capture will be carried out for 1 day to gather the data that will be used for developing and tuning the mite detection process. The built system will be deployed into the field with a beehive on top for this test. Due to the short run time required for this test, solar power will not be required, however the solar charge controller mode would need to be changed to ‘always on’ in this case.

Captured images are segmented and cropped into 9 sub-images from the mirror array. This will produce images that contain either a bee from the underside with both lateral views, or no bee at all. Mixing of the red, green and blue channels produced by the camera in varying amounts is examined to determine the best ratio for discrimination between bee and mite, this will require iteration and manual examination. Subtracting a previously captured image of the background and applying thresholding allows for the detection of images that contain no bee. If no bee is detected, the image is deleted and no further processing carried out.

Hough transformation is carried out on the image to identify circular objects in the image to isolate mites. The number of circles detected in the image is recorded in a text file as mites detected. Considerable amounts of iteration and tuning of this process are expected, comparing the processed images to the originals for manual comparison of detected mites.

Measuring the time taken for the RPI to carry out the process from image capture to completion of the mite detection process will be logged and averaged. This measurement will determine the maximum rate of image capture that can be carried out by this system and will inform the rate of image capture that is used during field testing. The time for each image capture along with the size of the image will inform the capacity of micro-SD card required for the field test to achieve 1 week of operable use.

The current sensor log will be used to log the power used by the system over the duration of the test. If a solar panel, is used for this test the results will indicate if the solar panel produces sufficient power on this day. If no solar panel is used, the test results will provide confirmation of the power used by the system in operation.

Temperature logs from the DHT11 sensor combined with temperature measurements captured from the local Bureau of Meteorology (BOM) weather station will provide indication of the

suitable operable temperature range of the system. Comparing the temperature recorded in the logs with the local BOM temperatures will give a delta reading, how much above or below BOM temperature the inside of the electronics box is. This delta value should be relatively stable regardless of outside temperature and can be used to determine at what external temperate the inside of the electronics enclosure can be expected to hit 55 degrees Celsius. This is the maximum operable temperature of the solar charge controller and will govern the maximum operating temperature of this system.

The humidity measured by the DHT11 sensor should vary with temperature, however as the electronics enclosure is sealed, an increase in the humidity may be a sign of moisture ingress. At the completion of the data gathering test, the inside of the electronics enclosure can be examined for physical signs of moisture ingress, along with the humidity log to verify that the system prevents moisture ingress. Small amounts of moisture may condensate inside the enclosure, depending on environmental conditions when the box was closed, and may necessitate the addition of silica beads or similar to maintain a dry environment.

3.5 FIELD TESTING

After the mite detection process has been developed and tuned to achieve the best possible result then the system will be returned to the field. This field test will be carried out over 1 week with logging of the temperature, humidity, battery current and number of mite detections (matched to the image ID). The images from this test run will also be kept for manual analysis at the end of the test to verify the performance of the mite detection process. Verification includes both measuring the rate of mite detection, as well as the rate of false detections.

Modifications can be carried out to the system at this time if it is necessary to optimise the system performance, and the system subsequently returned to the field for a longer duration test. The duration of this testing may be limited by the capacity of the battery and solar solution or the space available on the internal SD card for image storage. These images will not need to be kept in the final system, they are retained in these tests for the purpose of manual analysis of the system effectiveness.

Non-infected hive testing will be carried out over a short duration (1-2 days) using identical electronics and imaging systems. A different system box and tunnel will be used to comply with state laws about transport of hives from Varroa infected areas and to adapt the tunnel to a different hive design if necessary.

3.6 DATA ANALYSIS

Data gathered from field testing of the system will be analysed and Varroa mite detections compared to manual analysis of the images to get true positive (TP), false positive (FP), true negative (TN) and false negative (FN) results of mite detections. These results along with the processing time will be used to compare the designed system with results from other literature such as Bjerge et al. (2019a), Mrozek et al. (2021b) and Noriega-Escamilla et al. (2023).

Noriega-Escamilla et al. (2023, p. 10) details how to convert TP, FP, TN, and FN results into the F1 score and accuracy values that are used to describe the results of machine learning systems. Since more literature is available that gives results in F1 score and accuracy, this will be the baseline method of comparison between systems. *Table 1 - Comparison of F1 Scores* shows the comparison of metrics from various studies, with Noriega-Escamilla et al. (2023)

given details in true positive rate (TPR), false positive rate (FPR), true negative rate (TNR) and false negative rate (FNR).

Table 1 - Comparison of F1 Scores

Study	**TP**	**FP**	**TN**	**FN**	**F1**	**Processing Time**
Bjerge et al. (2019a)	103	12	Not given	Not given	0.91	Not given
Mrozek et al. (2021)	Not given	Not given	Not given	Not given	0.8	182.15 ms
Noriega-Escamilla et al. (2023)	TPR 91.7	FPR 8.0	TNR 92.0	FNR 8.3	0.92	Not given
This Research						

This analysis will cover the achievement of objectives 1, 2, 4 and 5. Objective 3 is somewhat subjective, and the results will be an analysis of areas where the cost could be reduced with further effort and industry feedback on the prototype costs. Determining if the system can operate in the Australian environment as required by objective 6 will be an analysis of the temperature, humidity data gathered and design criteria of components selected. The maximum operating temperature calculations discussed in the DATA GATHERING chapter can be compared to maximum and average temperatures around Australia to determine the success of this objective. Moisture ingress to the system will count against meeting this objective.

Objective 7 success will be determined by analysis of the current sensor log, which can show current direction as well as value. Plotting a graph of the log values over time and calculating the area under the graph will determine if the current into the battery is net positive, zero or negative. A net negative result can be used with battery capacity information to determine the maximum run time. Net positive or zero indicate that the system will operate indefinitely with the sunlight available at the time of testing. Further analysis using data from Australian Bureau of Meteorology (2024b) will be used to determine how representative the testing conditions are to average Australian conditions and if the solar panel is under or oversized for the system.

CHAPTER 4 DESIGN AND BUILD

4.1 DESIGN

To capture images of the bees a multi-part system will be used, consisting of an enclosure for the system, a guide tunnel for the bees to follow, charging and power control and the optical system. All the electronics are contained within an IP65 enclosure inside the main box to provide protection from water and dust ingress. The enclosure for the system is shown in Figure 9 and makes use of a standard bee box, with a ventilated baseboard (called the equipment box hereafter). A modified baseboard will be placed on top as a lid, also functioning as the baseboard of the hive brood box.

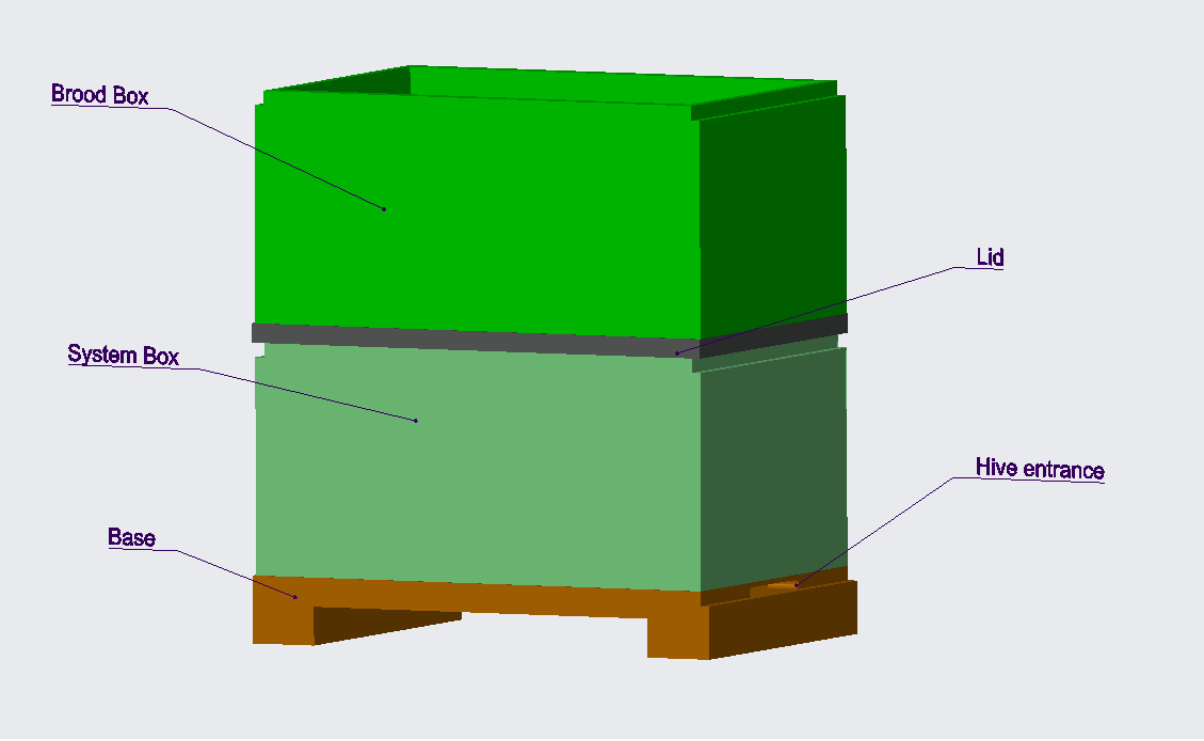

Figure 9 - System with brood box on top (solar panel not shown)

Selecting a processor to use for the system was based on familiarity and availably. The author has prior experience working with Raspberry Pi single board computers and had an RPI 4 8gb model on hand with a metal heatsink case. This board is widely supported by the community

and there are libraries available for many sensors which makes integration and code development easier. Additionally, there are cameras that are manufactured by the Raspberry Pi Foundation (Raspberry Pi Foundation 2024), and other third party companies that are well supported for this board.

A camera for the system has a better chance of successfully detecting mites by combining visible light and NIR based on the results of Bjerge et al. (2019a). To achieve this while keeping costs down a variety of cameras with the IR filter removed were examined, these are sometimes referred to as NoIR cameras. A high resolution camera was identified as the most likely to produce more accurate results by Mrozek et al. (2021b), so a priority was put on selecting a high resolution camera with no IR filter. One of the highest resolution cameras available for the Raspberry Pi is the High Quality (HQ) camera which is also made by other manufacturers such as Arducam. Arducam make several variants of camera that use the same sensor as the HQ camera, including one that has a selectable IR filter and can accept CS-Mount lenses (Arducam 2023b). The ability to switch the filter, and use different lenses offers greater flexibility in the camera if the provided lens proves to be unsuitable for this use.

Using a solar charge controller with a load output enables the system to run from sun-up to sun-down easily. The battery provides additional power when the solar panel is unable to fully supply the system, and a short duration of power at sun-down to allow proper shutdown without data corruption. The charge controller monitors the amount of power it is receiving from the solar panel and uses that to determine sun-up and sun-down conditions for switching the load output on and off. The solar controller was chosen as the cheapest one available that met the requirements of; being IP65 or better, matching the solar panel output voltage and current, compatible with the battery chemistry and having a controllable load output. This last

requirement was later found to be a mistake, as the load output only switches on at night when this design does not need it.

To provide the power switchover at sun-down, a relay is used with diodes to OR the battery power with load output. The relay is held on during the day by an output from the raspberry pi, which will fall low when the RPI has shutdown allowing the relay to relax and cut power. The relay needs to operate on 12V from the battery and be able to handle the full expected current of the system, the solar controller can output up to 10 amps. A relay matching these requirements was available to hand, so that was used. The RPI knows when to shut down by monitoring the voltage on the load output of the charge controller. When this voltage falls to zero, the RPI will begin shutdown. This was later reversed to shut down when load turns on as the load output can only be switched on at night.

Since the power supply from the battery and load output are nominal 12V, a DC-to-DC step down converter is used to provide the RPI with a 5V supply. For ease of integration, a step-down converter designed for use in cars with USB outputs was selected. This could handle the charge voltage of the battery as well as temperatures expected in a car, and the USB A output allows for a USB A to USB C cable to power the RPI.

Darlington pair optocouplers are used to isolate the RPI inputs from the 12V supply and provide the necessary drive to operate the relay. Additional optocouplers are used to allow the RPI to control the LED lights used for illuminating the bees. Darlington pair optocouplers were chosen for the current handling requirements and ease of driving them from 3.3V of the RPI. MOSFETs would have been a better choice, however none could be found with a suitably low gate threshold voltage. The added complexity of designing a method of driving a higher gate

voltage MOSFET was deemed to be unnecessary complications and take up additional space for this system.

The LEDs provide illumination centred at 470nm, 630nm and 850nm for blue, red and NIR respectively. This aligns with Bjerge et al. (2019a) for the blue and red, using 850mn rather than 780nm NIR due to availability still providing good discrimination as seen in Figure 4 from Bjerge et al. (2019b). The LEDs selected are all 5mm diameter for consistent mounting with preference given to wider illumination angles for more consistent light rather than spots. The NIR LED was the most difficult to find as many found were either narrow beam or designed only for pulsed operation rather than continuous illumination. The LEDs are powered from the load output before it is OR'd with the battery, as the LEDs do not need to remain on during the shutdown process. See Figure 10 for a system block diagram, or APPENDIX C for a schematic.

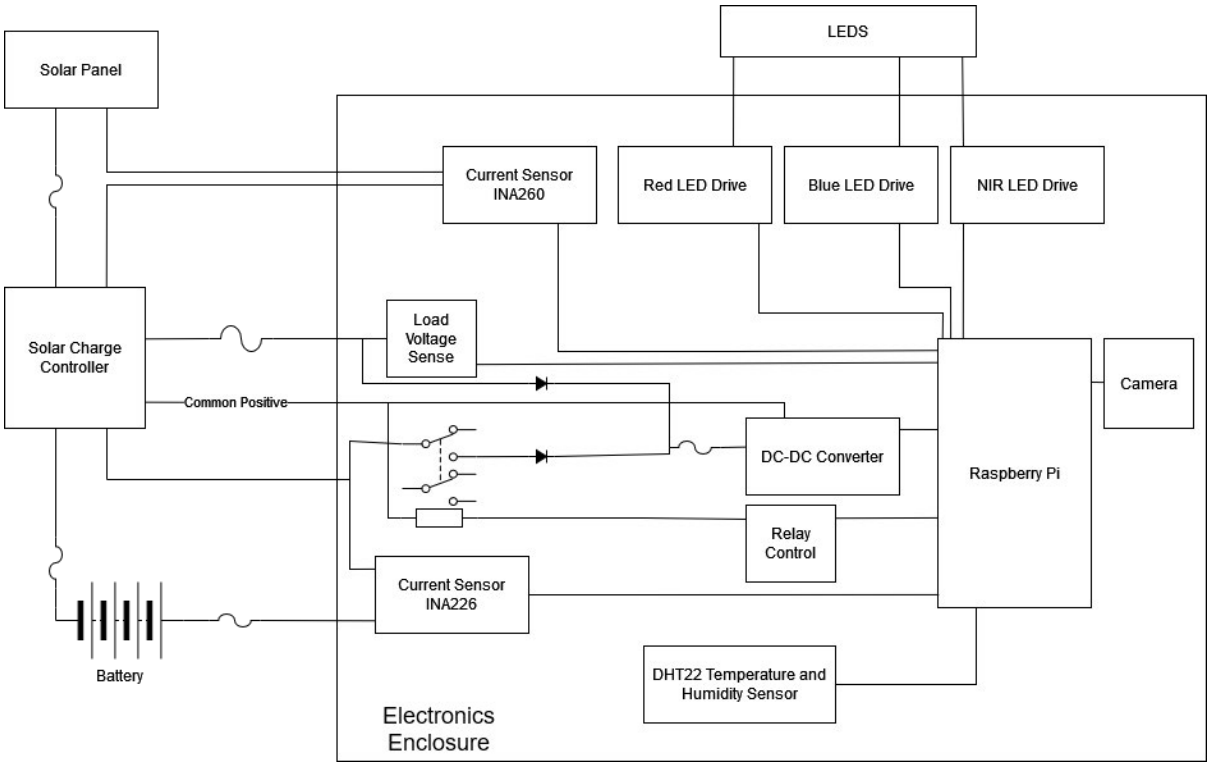

Figure 10 - System diagram

Additional sensors have been added to the system to help quantify the performance and track environmental variables. Two current sensors were added to the system to measure the current going to and from the battery, and the current from the solar panel. The current sensors needed to be able to be mounted on the low (negative) side as the system has common positive from the solar controller. The solar panel and battery do have discrete positive lines that could be used for high side monitoring, to keep the number of wires into the electronics enclosure down these are not fed in. The common positive from the load is the only positive wire that is run into the electronics enclosure. The battery also has the requirement of having to monitor positive and negative currents for charge and discharge. In addition, these sensors must interface to the RPI 3.3V IO, potentially handle 10 amps, and a serial communication method would be preferable to avoid using the slow internal Analog to Digital Converter (ADC) in the RPI. For the solar current sensor, this was found in the INA260 module, and the battery uses a INA226 module.

A Real-Time Clock (RTC) module was fitted to the system to assist with time-stamping the data logs. These timestamps are not required to be particularly accurate as they are only used to aid matching the collected data logs to environmental data collected from the BOM. The clock from the RPI was originally considered for this low accuracy data, however there were concerns that unexpected shutdown if the battery voltage went too low may cause the built-in clock to drift. An external RTC module mitigates these issues due to the battery fitted to the module.

One other sensor was incorporated to monitor the temperature and humidity in the electronics enclosure. This would aid in assessing if the system is resistant to external environmental humidity and tracking how the internal temperature compares to ambient temperature from BOM. Again, this sensor would have to interface with the 3.3V IO of the RPI and it would be

preferable to use serial communication. A common sensor with libraries available for the RPI is the DHT22 combined temperature and humidity sensor. A DHT11 is a slightly cheaper sensor, although with a wider tolerance on temperature and humidity. Given the small price difference, the more accurate sensor DHT22 was selected.

The guide tunnel for the bees is designed to reduce the processing effort required by guiding the bees into an optimal position for imaging. Nine paths will be created from the single hive entrance, with a clear polycarbonate viewing window for illuminating and imaging the bees. Mirrors are placed inside the tunnel at 45-degree angles on each side to facilitate viewing of the bees from both sides as well as underneath as they pass through show to the right of Figure 11. A slot of the same size as the hive entrance is created in the baseboard of the brood box, which forms the lid of the equipment box to allow the bees to enter the brood box from the tunnel. The baseboard is also modified to have continuous side walls ensuring bees enter through the tunnel and providing space for the bees under the brood comb.

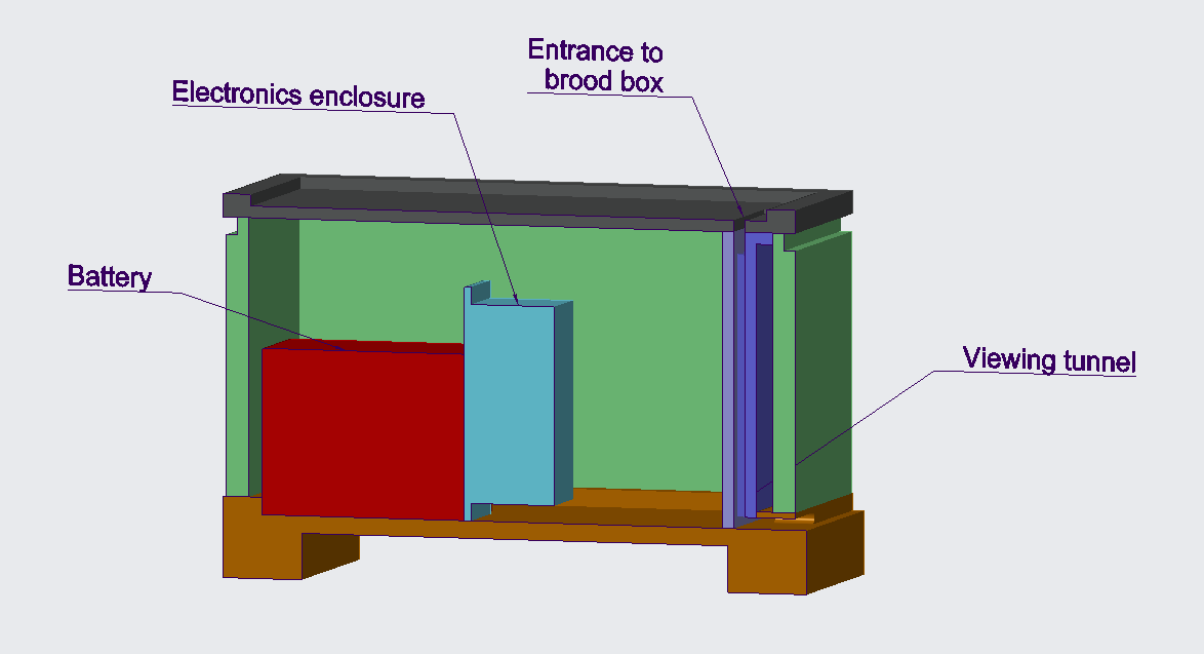

Figure 11 - Sectional internal view of the system box

4.2 EXPERIMENTAL BUILD

Before assembling the system, the value of the resistors in the system needs to be calculated. Each of the LED strings needs a current limiting resistor so they do not get damaged by the battery voltage. Each of the LED strings were kept as close as practical to 9 LEDs so that there would be one of each colour for each channel in the viewing tunnel. The optocouplers also require resistors for the input diodes to adjust for either battery voltage or RPI IO voltage as required. Using the voltage that the solar charge controller is capable of delivering to the battery of 14.8V (Jaycar 2024) the following equations describe the calculations for the current limiting resistors on the LED strings:

The NIR LED (Vishay Semiconductors 2024) has forward voltage (V_f) of 1.5V, so with 2 strings of 5 LEDs in series gives each series voltage of

$$5 \times 1.5V = 7.5V \quad [4.2.1]$$

While these LEDs can handle 100mA of current, the optocoupler can only output a maximum of 60mA (Vishay Semiconductors 2023) which is split between each of the LED strings. This means the current into each NIR LED string must not exceed 30mA, and to reduce stress on the components and heat dissipated, this was limited to 15mA.

At a battery maximum voltage 14.8V, the optocoupler output voltage drop (V_{OL}) nominal is 0.25V (Vishay Semiconductors 2023) at the expected current. Therefore, the resistor needs to drop:

$$14.8V - 0.25V - 7.5V = 7.05V \quad [4.2.2]$$

Now the resistor value can be found using the current per LED string of 15mA, totalling 30mA:

$$7.05V/0.03A = 235\Omega \quad [4.2.3]$$

Using E24 resistor values the nearest easily available resistor value is 240Ω, which can be used to calculate the actual expected current:

$$7.05V/240\Omega = 29.4mA \quad [4.2.4]$$

The power dissipation in this resistor is then:

$$0.0294A \times 7.05V = 0.21W \quad [4.2.5]$$

So, any resistor above 0.25W capacity would be sufficient, and to limit the stress on the part 0.5W or higher would be preferable.

For the blue LED (Visual Communications Company.nd) has V_f of 3.5V, so with 12V nominal battery voltage the LEDs have to be divided into 3 strings to be below this voltage. 3 strings of 3 LEDs in series gives a series voltage of 10.5V each and the resistor for these LEDs needs to drop:

$$14.8V - 0.25V - 10.5V = 4.05V \quad [4.2.6]$$

This resistor value can be found using 15mA per LED string, totalling 45mA:

$$4.05V/0.045A = 90\Omega \quad [4.2.7]$$

The nearest easily available E24 resistor value is 100Ω:

$$4.05V/100\Omega = 40.5mA \quad [4.2.8]$$

This gives a power dissipation of:

$$0.0405A \times 4.05V = 0.18W \quad [4.2.9]$$

Again, any resistor above 0.25W would be sufficient and above 0.5W would be a better choice for reliability.

The red LED (Cree LED 2024) has V_f of 2.1V, so 2 strings of 5 LEDs in series gives a series voltage of 10.5V each keeping below the nominal battery voltage of 12V. This resistor needs to drop:

$$14.8V - 0.25V - 10.5V = 4.05V \quad [4.2.10]$$

At 15mA per LED string, totalling 30mA the resistor value calculates out to:

$$4.05V/0.03A = 135\Omega \quad [4.2.11]$$

Using E24 resistor values, the nearest easily available value is 130Ω. The current through this resistor will then be:

$$4.05V/130\Omega = 31.2mA \quad [4.2.12]$$

The power dissipation of this resistor will be:

$$0.0312A \times 4.05V = 0.13W \quad [4.2.13]$$

Once again, a 0.25W resistor should be sufficient, and 0.5W is safer.

Each of the optocouplers require a current limiting resistor for the input diode, which needs to be sized for either the battery voltage or the 3.3V IO of the RPI. The optocouplers chosen have a current transfer ratio minimum of 400 (Vishay Semiconductors 2023) so the current input can be 400 times less than required at the output. Since the datasheet characteristics were given with a forward current I_f of 1.6mA, this value was chosen for simplicity. At this current the

voltage drop of the diode is V_f between 1.4V and 1.7V, calculating for the maximum current to be 1.6mA, the RPI IO resistor is:

$$3.3V - (1.4V/0.0016A) = 1188\Omega \quad [4.2.14]$$

Which in nearest E24 values is 1200Ω and the power dissipated will be:

$$(3.3V - 1.4V) \times 0.0016A = 0.003W \quad [4.2.15]$$

For the battery inputs to the optocouplers, the resistors will be:

$$(12V - 1.4V)/0.0016A = 6625\Omega \quad [4.2.16]$$

The E24 value closest to this results in a resistor of 6.8kΩ and the power dissipated is:

$$(12V - 1.4V) \times 0.0016A = 0.017W \quad [4.2.17]$$

Now that all the values have been calculated, the parts were ordered from Mouser, Jaycar and Element 14. Due to the availability of required resistor values, the LED resistors were ordered as 2W resistors, this does make them slightly larger but also means they are not under any thermal stress for this load. When the parts had arrived, the electronics were built up on a breadboard for testing the prototype design shown in Figure 12 - Breadboard prototype. The battery relay and connections to the current sensors are not shown in this photo. The LED strings were not connected at this stage, and all connections were checked with a multimeter for short circuits and misconnected parts.

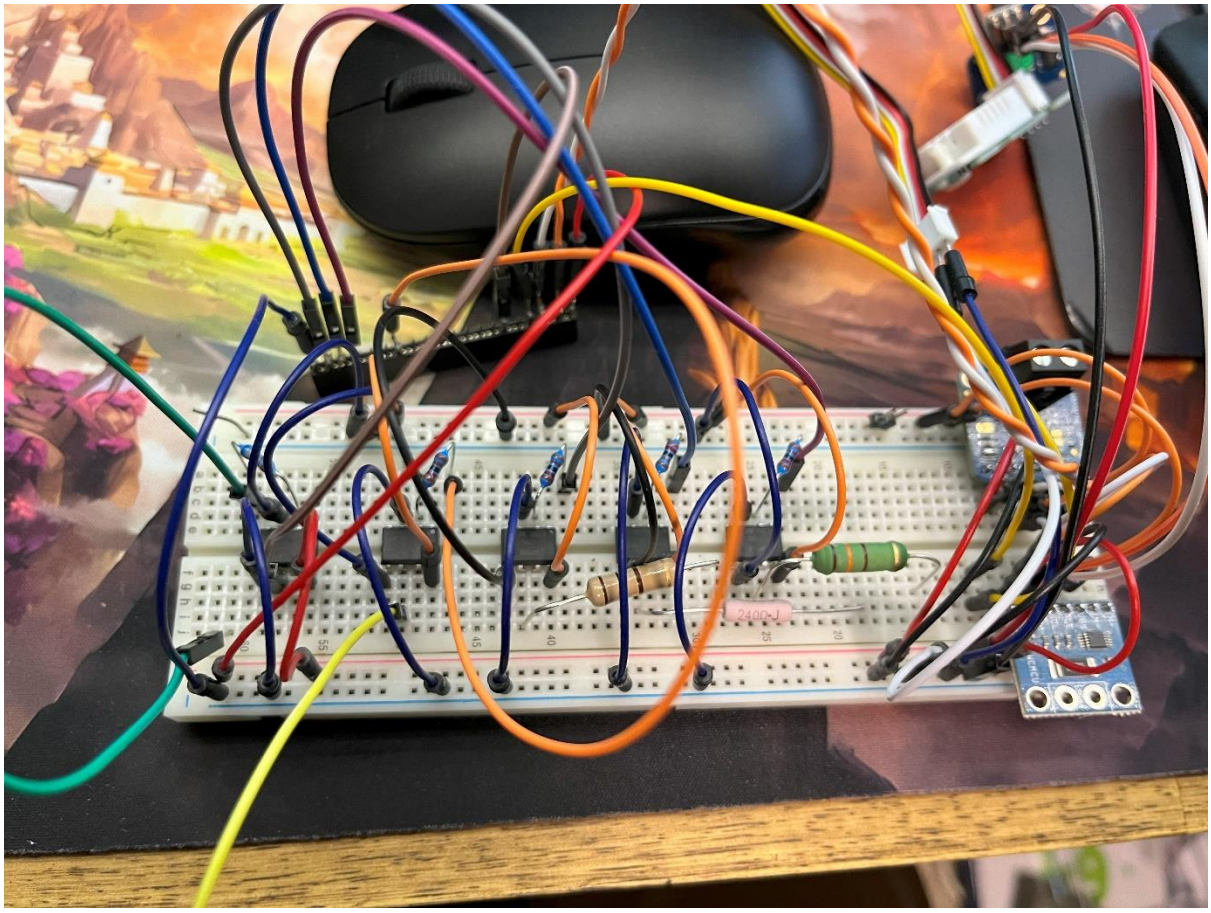

Figure 12 - Breadboard prototype

Once the relay was connected, the breadboard prototype test process was run as detailed above with the results recorded in *Table 2* and *Table 3*.

Table 2 - Unpowered breadboard test results

Breadboard test - unpowered			
Step	**Action**	**Expected Result**	**Actual Result**
1	Using a multimeter, test for resistance between common positive and Solar negative	>10k Ω	>1M Ω

2	Using a multimeter, test for resistance between common positive and Battery negative	>10k Ω	>1M Ω
3	Using a multimeter, test for resistance between common positive and Load negative	>10k Ω	>1M Ω
4	Using a multimeter, test for resistance between common positive and common negative	>10k Ω	>1M Ω
5	Using a multimeter, test for resistance between 3.3V line and RPI negative	>10k Ω	>1M Ω
6	Using a multimeter, test in diode mode with negative probe on load negative and positive probe on the common negative.	<0.7V	0.3V
7	Using a multimeter, test in diode mode with negative probe on load positive and negative probe on the common negative.	.OL	.OL
8	Using a multimeter, test in diode mode with negative probe on relay output and positive probe on the common negative.	<0.7V	0.3V
9	Using a multimeter, test in diode mode with positive probe on relay output and negative probe on the common negative.	.OL	.OL

10	Using a multimeter, test for resistance between Battery negative and relay output.	.OL	.OL

Once the unpowered tests were completed, it was safe to proceed with powered testing of the electronics.

Table 3 - Powered breadboard test results

Breadboard test - powered			
Step	**Action**	**Expected Result**	**Actual Result**
1	Set the bench power supply to 12V, 1A	Setup	
2	Connect the bench power supply to load connection	Setup	
3	Turn on the power supply	Power supply is in constant voltage mode	Confirmed
4	Using a multimeter, probe the 5V converter for voltage	5V is present	5.1V
5	Using a multimeter, probe the relay output for voltage	0V is present	0V

6	Set a second power supply to 12V, 1A	Setup	
7	Turn on the second power supply	Power supply is in constant voltage mode	Confirmed
8	Using a multimeter, probe the relay output for voltage	0V is present	0V
9	Connect U2 (relay control optocoupler) pin 6 to U2 pin 5	Click is heard from the relay	Audible click
10	Using a multimeter, probe the relay output for voltage	12V is present	12V
11	Using a multimeter, test for resistance between U1 (load voltage sense) pin 6 and RPI negative	<1k Ω	56.4Ω
12	Turn off power supply 1	Setup	
13	Using a multimeter, probe the 5V converter for voltage	5V is present	5.1V
14	Using a multimeter, test for resistance between U1 pin 6 and RPI negative	>10k Ω	.OL
15	Using a multimeter, test for voltage on all pins for RPI	0V is present on all	0V

16	Turn off power supply 2	Setup	
17	Remove jumper between U2 pin 5 and pin 6	Setup	
18	Connect RPI to IO connector and power via USB-C power monitor	Setup	
19	Turn on power supply 1, and 2	Setup	
20	Look for power indicator on RPI	Power indicator is on	Power indicator is on
21	Monitor voltage and current on the USB-C power monitor	Record readings	5.08V Peak 730mA
22	Remote connect into the RPI	Setup	
23	Using the terminal, check the state of RPI IO	GPIO 0 is output and high	Confirmed
24	Using a multimeter, probe the relay output for voltage	12V is present	12V
25	Using the terminal, drive RPI GPIO 13 high	Red LEDs turn on	Red LEDs on
26	Using the terminal, drive RPI GPIO 13 low	Red LEDs turn off	Red LEDs off

27	Using the terminal, drive RPI GPIO 19 high	Blue LEDs turn on	Blue LEDs on
28	Using the terminal, drive RPI GPIO 19 low	Blue LEDs turn off	Blue LEDs off
29	Using the terminal, drive RPI GPIO 26 high	NIR LEDs turn on	(Used camera to confirm on)
30	Using the terminal, drive RPI GPIO 26 low	NIR LEDs turn off	(Used camera to confirm off)
31	Load libraries for INA226, INA260 and DHT22 sensors	Setup	
32	Run example code INA226	Expect current and voltage similar to power supply 2	11.6V, 15000mA (10x expected current)
33	Run example code for DHT22	Expect sensible temperature and humidity	18.2°C, 66.8% humidity
34	Using the terminal, drive RPI GPIO 19 high	Blue LEDs turn on	Blue LEDs on

35	Turn off power supply 1	Blue LED's turn off, RPI remains on	Confirmed
36	Shutdown RPI	Remote connection closes, power indicator is off	Confirmed
37	Using a multimeter, probe the 5V converter for voltage	0V is present	0V
38	Connect power supply 1 supply via INA260 to load connection.	Setup	
39	Turn on power supply 1	Power indicator is on	Confirmed
40	Remote connect into the RPI	Setup	
41	Run example code INA260	Expect current and voltage similar to power supply 1	11.5V, 1.25mA (PS2 is supplying load)
42	Turn off power supply 1	Power indicator is on	Confirmed

43	Shutdown RPI	Remote connection closes, power indicator is off	Confirmed
44	Turn off power supply 2	All power is off	Confirmed

These tests have confirmed that the electronics assembly is working properly, except for the INA226 current sensor. With time being short before the system needed to be in Toowoomba, this was noted as being a consistent 10x the expected value and could be manually compensated later.

With testing confirming the circuit is operating, the design was transferred to a solderable prototyping board. Each line was checked against the schematic to ensure it had been soldered correctly, and two wires were found to be in the wrong place. These were fixed and the circuit was ready for integration testing shown in Figure 13 - Testing the built soldered prototype.

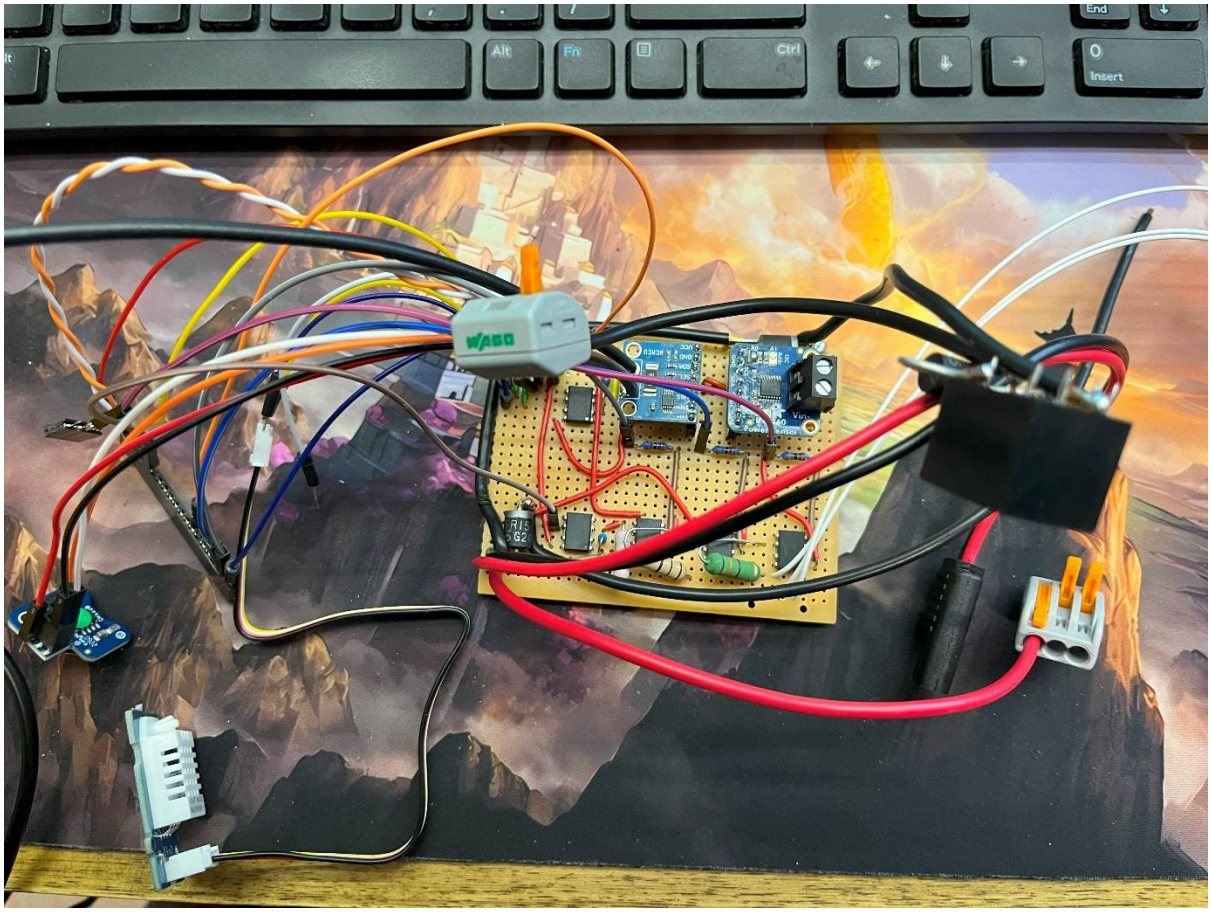

Figure 13 - Testing the built soldered prototype

A quick test program for data capture was written to start when the RPI turns on and continuously loop. It starts a log file for the day and log the temperature, humidity and outputs of the current sensors. The LEDs were programmed to start up with a pulse width modulated (PWM) signal so their intensity could be controlled, then a photo would be taken with the camera, and the LEDs switched off. This reduces the overall power consumption slightly. The filename of this photo is created from the RTC date and time, and this name is also written into the log file. This code incorporates the shutdown when load voltage is lost used in the earlier testing.

All the system components were now connected for integration testing on the bench. The prototype electronics were connected to solar controllers solar, load and battery connections,

and a 12V sealed lead acid battery was connected to the battery terminals. The solar controller was set up in manual mode for ease of operation, and the bench power supply connected to the solar panel inputs. From this point the system integration tests were run with the results recorded in *Table 4*.

Table 4 - System integration test results

Board + solar controller power test			
Step	**Action**	**Expected Result**	**Actual Result**
1	Set the bench power supply to 12V, 1A	Setup	
2	Connect the bench power supply to solar connection	Setup	
3	Connect the battery-to-battery connection	Setup	
4	Turn on the power supply	Power supply is in constant voltage mode	Confirmed
5	Remote connect into the RPI	Setup	
6	Using the terminal, check the state of RPI IO	GPIO 0 is output and high	GPIO 0 is output and high (3.3V)

7	Using the terminal, drive RPI GPIO 13 high	Red LEDs turn on	Red LEDs on
8	Using the terminal, drive RPI GPIO 13 low	Red LEDs turn off	Red LEDs off
9	Using the terminal, drive RPI GPIO 19 high	Blue LEDs turn on	Blue LEDs on
10	Using the terminal, drive RPI GPIO 19 low	Blue LEDs turn off	Blue LEDs off
11	Using the terminal, drive RPI GPIO 26 high	NIR LEDs turn on	(Used camera to confirm on)
12	Using the terminal, drive RPI GPIO 26 low	NIR LEDs turn off	(Used camera to confirm off)
13	Install power test code to RPI	Setup	
14	Run the power test code on RPI	No change observed	INA226 (10x expected current), INA260 matches power supply.

15	Toggle Load power off on solar controller	RPI begins shutdown, terminal closed	Confirmed
16	Using a multimeter, probe the 5V converter for voltage	0V is present (or power indicator light is off)	Power indicator light is off
17	Toggle Load power on, on the solar controller	RPI turns on	RPI is on
18	Remote connect into the RPI	Setup	
19	Install data capture code	Setup	
20	Manually start data capture code	LEDs turn on and off periodically	LEDs turn on and off
21	Examine file structure for a log file and image files	A log file is created, and images are being captured	Log file contains expected values, images are being captured.

An opportunity presented itself at this time to get some control images of bees that were not infected with Varroa due to a trip to Toowoomba, which lies outside the current spread of Varroa in Australia. To avoid any risk of contaminated materials being transported to Queensland, no wood that had been in contact with bees in New South Wales could be used in Queensland. So, an entirely new system box was built out of plywood to match the external dimensions of the target hive, an early Flow Hive.

To protect the electronics, they were fitted into an IP67 enclosure with a sealed connector for the required connections to the rest of the system. The circuit board fits against one side of the enclosure, with the DC-DC converter, connector and camera mounted to the base. Other components including the RPI sit on a mezzanine shelf above these components with cutouts to accommodate the camera lens and wiring as needed. As the solar controller is IP65 and quite bulky it will be mounted outside the electronics enclosure.

The design of this enclosure was almost identical to the design in Figure 11 - Sectional internal view of the system box, with the illumination LEDs taped to a wooden beam between the electronics and bee tunnel. This box was constructed out of 18mm thick plywood that was on hand using a combination of table saw, jigsaw and handsaws as needed, shown in Figure 14. The angled mirrors in the tunnel were achieved with 45-degree wood trimming purchased from a hardware store with adhesive acrylic mirrors on top (Figure 15). The clear polycarbonate viewing window sits in a channel in front of the tunnel allowing for removal for cleaning and replacement.

Figure 14 - Toowoomba system enclosure nearing completion

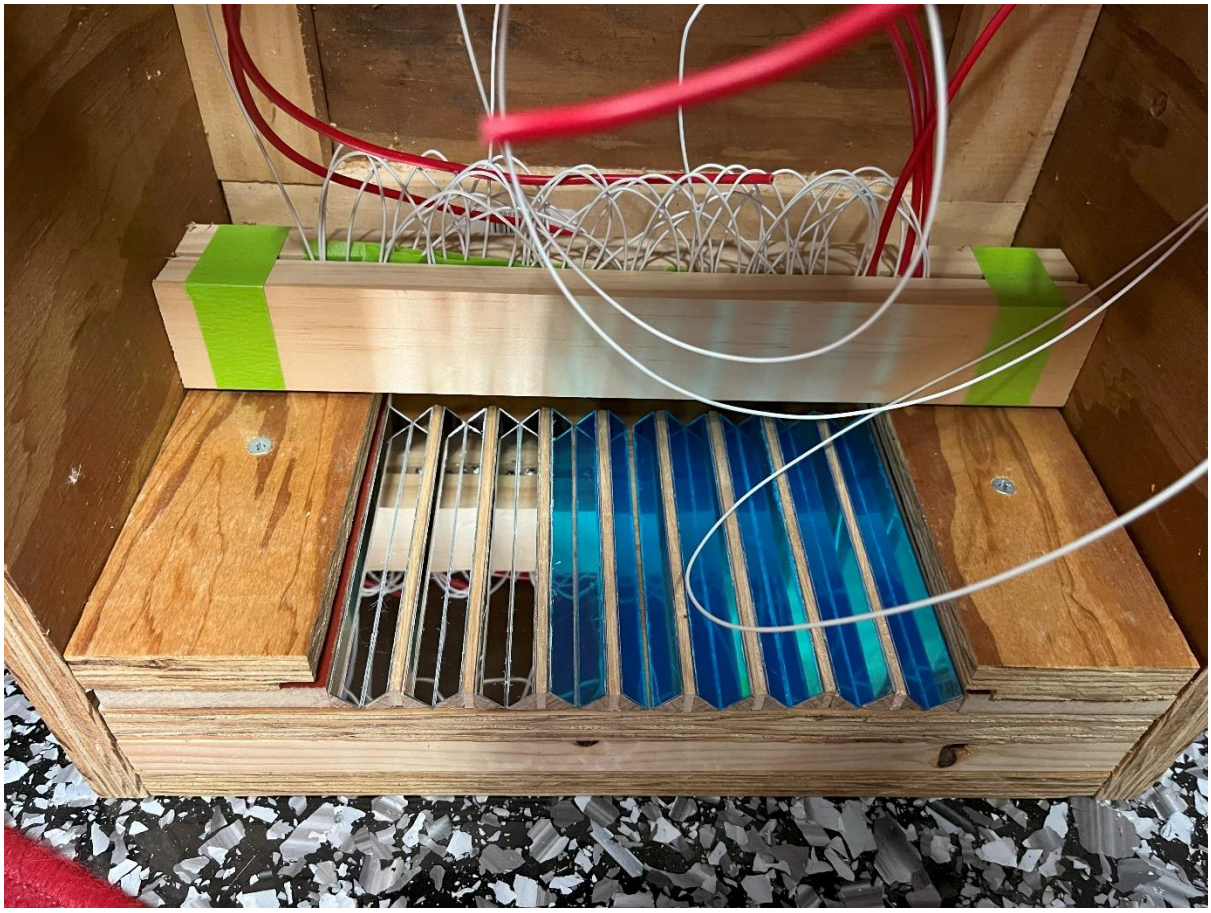

Figure 15 - Angled mirrors fitted to Toowoomba system enclosure

For the illumination LEDs to provide an adjustable light, they were sandwiched between two wooden beams that are screwed to the system box at each end. With only one screw fitted, the angle of the LEDs can be adjusted to give good light with minimal reflections before being secured in place.

The electronics box was affixed to another wooden beam towards the top of the box placed at a distance from the bee tunnel. This distance was determined by monitoring the camera view and finding where the camera had the entire width of the tunnel in frame as the camera has a fixed zoom. The distance ended up at 16cm between the lens and the polycarbonate sheet. As the camera has manual focus, this was adjusted at this time to give the best focus that could be seen in the live camera preview.

For Medowie, the system box was a hive box, lid and base provided by a local beekeeper. Inside this box beams were added to hold the electronics enclosure, the bee tunnel was made from extra lid material also provided by the beekeeper that was cut, glued and screwed in place. Unlike the Toowoomba system, the Medowie system has a removable bee tunnel for easier cleaning, and the polycarbonate panel is held in place with metal bulldog clips seen at the bottom of Figure 16. One other addition to the Medowie system is a dual Anderson plug connector on the side of the system box for connecting a solar panel.

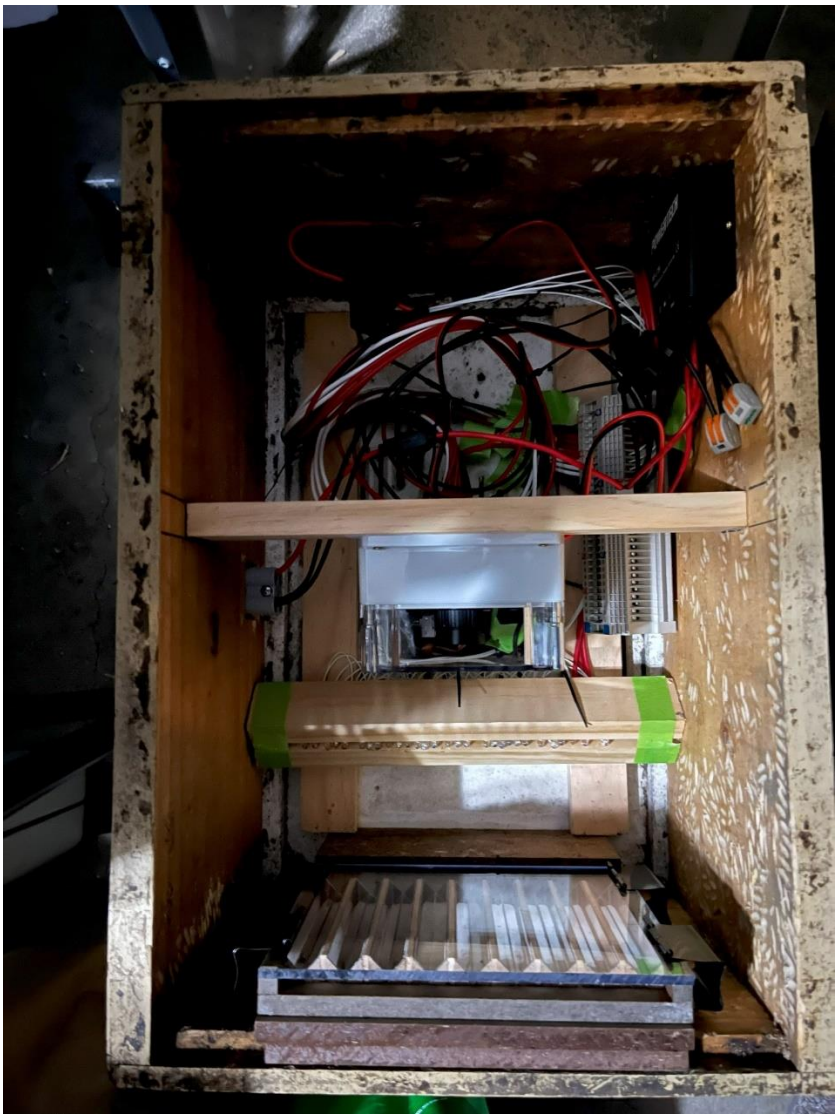

Figure 16 - Medowie system box

CHAPTER 5 FIELD SETUP AND TESTING

Preparation for the field testing of the system included adjusting the PWM values for each of the LED channels to achieve good illumination. Initial adjustments were done by eye with a preference to be slightly brighter in the NIR. This was done because the addition of the NIR wavelengths was previously identified as being effective in differentiating mites from the bees. The images that were captured were using a locked digital gain, and the image metadata was examined to see what ISO (International Organization for Standardization) (a measurement of gain applied to the camera sensor) with lower levels indicating less gain. Higher ISO numbers produce brighter images in low light conditions, but also introduce additional noise. Figure 17 shows images captured during the PWM calibration process for blue, NIR and red LED channels at 15%, 50% and 30% duty cycle respectively. In these images some noise can be seen (exacerbated by the conversion and compression in these pictures) despite showing the lowest ISO an RPI can achieve of 100. This would indicate that the ISO recorded in the metadata is not accurate, and the gain locking is not working.

Figure 17 - LED PWM calibration, Blue 15 - NIR 50 - Red 30

PWM calibration and camera focusing was carried out the night before the system needed to be deployed in the field and the PWM values settled on were blue 15, NIR 30 and red at 20 to reduce the overexposure when all three LED channels were used at the same time. The ISO is still too high in these images, contributing to the overexposure though this was not noticed at the time.

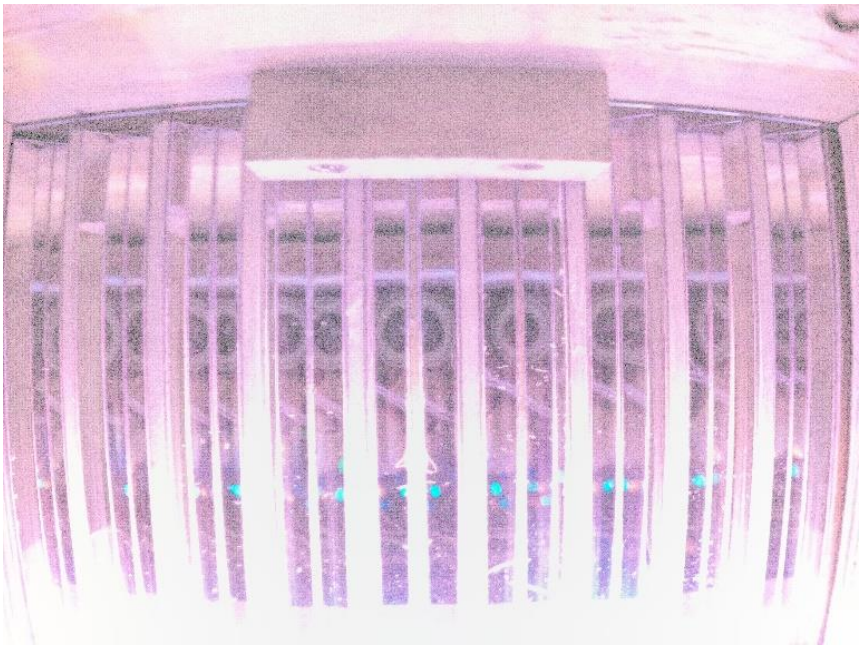

Figure 18 - All LED channels, Blue 15 - NIR 30 - Red 20

In preparation for the first test in Toowoomba, the solar controller was configured to operate in manual mode, intended to have the load output on continuously for the duration of the test. A solar panel was not available in time for this test, and the system could only be deployed for a single day so a sufficiently sized battery would be suitable. A 26Ah battery can power the system at the load current seen during testing (around 360mA) for about 3 days. This would be plenty of capacity for the expected 24 – 36-hour test. The software autostart was adjusted to start the code at 8:30am and shutdown the RPI at 8:30pm, though the storage would be filled up long before this time.

The first field test of the system was carried out in Toowoomba on a Flow Hive late in the evening so the bees would be asleep in the hive. Battery connection was made away from the hive and RPI startup was confirmed prior to moving the system to the hive to minimise the time needed close to the hive. Flow Hives allow for collection of the honey without having to open the hive, and as such is a bit different to standard hives, including a slight tilt to the hive and this one is on a stand. For this reason, the system box was not able to be placed under this

hive, and instead was placed up against the hive entrance, using bricks to achieve the correct height and angle. The top of the system box, that would normally provide the bees access to the hive box instead becomes the hive entrance. The wooden planks on the top of the system box (Figure 19) cover the entrance to provide protection from rain and light straight into the bee tunnel that would have interfered with the camera.

Figure 19 - Testing system deployed in Toowoomba

A picture (Figure 20) received from the beekeeper during the day indicated that the bees were utilising the bee tunnel and system box to access their hive. When the system was retrieved the following evening, the RPI was not shutting down when the load output was manually toggled off. To avoid potential corruption of the storage from a sudden power loss, the system box was brought back inside for diagnosis. Remote access to the RPI confirmed that it was still running, and that the system storage was full after capturing nearly 1400 images over 3 hours. The full

storage capacity had crashed the data capture script. Which is why the load voltage sensing had not worked to turn the RPI off, it is a part of the same code and could not work once the script crashed.

Figure 20 - Toowoomba field test with bees flying

A review of the images collected also identified only one with a confirmed bee, likely due to the 16secs that were elapsing between images. The capture process would have to be sped up to ensure bees could be imaged during their transition through the tunnel. Additionally at this time the poor image quality from excessive noise and out of focus condition of the camera were noticed. These issues would have to be resolved before subsequent deployment of the system back in Medowie.

Changes to the library used to activate the camera, as well as switching to only capturing RAW images rather than RAW and JPEG sped up the capture rate to about one image every 10 seconds. Additional code was added to halt image capture before the storage was full but keep logging data from the sensors. Reducing the time between images should result in less time taken to fill the storage drive to capacity, so the micro-SD card used was upgraded from 32Gb to 512Gb. Rather than use a time-based start to the data capture code, it was set to run as soon as the RPI turned on, though the 8:30pm shutdown was left in case something failed. The change in library used also corrected the gain locking and incorporated a white balance intended for the sensor in the camera used. With those changes made the LEDs and camera shutter speed were adjusted to allow more light into the camera to combat the noise issue.

Reduced shutter speed, increased illumination and locked gain brought the image noise down and yielded a more usable image. To help with the focus issues, the aperture was reduced on the lens requiring an increase in illumination again. A reduction in the aperture produces a greater depth of field meaning the focus did not need to be as precise and the sides of the tunnel should be in good focus despite being further from the centre of the lens.

A review of the log file captured showed a higher current draw than was expected, almost 15A at 12V compared to the maximum of around 1.5A when using the bench power supply reading. Investigation of the 10x current reading revealed that the sensor library was configured for a different range than the sensor that was fitted. Several values were hard coded in the library so as not to be changed despite the setup procedure.

With these changes made, the electronics were transferred to the Medowie system box. Once in place, the camera was carefully focused on the bee tunnel. This focusing was difficult due to a poor remote connection to the RPI only allowing a couple of frames per second of the live

camera preview that was being used to focus. Once a good focus was achieved, a photo was taken and examined at close zoom for focus. When this was determined to be acceptable the focus was locked, and the camera was ready.

A local beekeeper provided the use of one of their hives for testing of the system and handled the installation of the system under guidance. This time the system was installed in the early morning with a 160W solar panel (seen in Figure 21) and smaller internal battery, since the battery should only need to supply the RPI when the solar panel could not produce enough power. A check on the system by remote access the following day was unable to connect, and so was unable to confirm if it was operating at all. The system was removed from the hive and returned for diagnosis.

Figure 21 - Testing system deployed in Medowie

Investigation by connecting the system to a bench power supply resulted in the discovery of a mistake in the system design. The solar controller would only switch on the load when there was no solar power available. This should have resulted in the system switching on at night, though even this did not occur based on the log file, which was not created.

Some changes to the circuit were enacted, allowing the solar panel power to power the system instead of the load power. Load power was still used, but with a code alteration so the RPI would now shutdown if it detected load voltage indicating the solar panel had stopped producing. This setup was tested on the bench power supply, and then in the yard, moving the solar panel into and out of the sun and covering it with blankets. The impromptu testing performed as expected, the system turned on when solar power was available, turned off only when it was totally gone and logged data as expected whenever it was on.

The system was then returned for another day of field testing, which again resulted in failure with no data captured. Extensive testing followed, finally identifying several contributing causes. Each of the current sensors have a diode between the logic ground and the current sense resistor, which would not be a problem if the logic ground is the same or lower voltage than what is on the current sense resistor. However, this is not always the case when the system has a common positive rail and two power sources as this system does. In this case the RPI does not fully power down as the battery voltage can find an alternate path via this diode, bypassing the relay. If the RPI does not have its power fully turned off, it will not shut down and therefore cannot be started back up again.

During this investigation a further issue with the INA226 current sensor was identified. The sensor shipped with the wrong shunt resistor, 0.1Ω which is suitable for 1A rather than the 0.01Ω for 10A range that was ordered. A replacement shunt resistor was ordered and soldered

in place to correct this issue, along with correcting the calibration values in the current sensor library. Once this modification was made, the sensor readings were confirmed to now be logging correctly.

To correct this problem, the ground pins for the current sensors were connected to the spare contact on the relay so they would be disconnected when the relay turns off. This was all tested on a bench power supply with no issues seen. When tested with a solar panel however, the RPI would not switch on properly. The slow build of voltage from the solar panel seemed to cause an issue with the RPI and it refused to boot. A quick build of a voltage level detector (Figure 22) from an LM741 opamp, a spare optocoupler and a BC547 NPN transistor that were on hand successfully detects when the voltage reaches 11.2V. This was connected to the solar panel voltage, and the output used to trigger the relay. All the power for the RPI and associated electronics including LEDs are now supplied from the battery connections, via the relay which can be controlled by the level detector or the RPI itself.

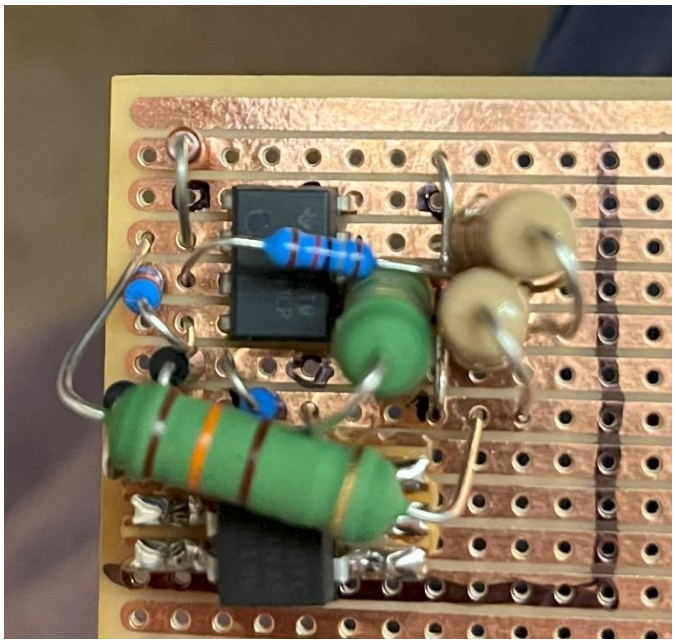

Figure 22 - Voltage level detector

After testing with a solar panel connected, again in a wide variety of lighting conditions to confirm the system turned on and began operating, capturing photos and logging data reliably it was returned to the field. After two days in the field, the system was checked by remote accessing the RPI and found a fault with the system. It was turning on as expected but failing to initiate the data capture code. Manually starting the code revealed that the current sensors were not being detected on the I2C bus, likely due to the change in their ground pin connection even though they functioned correctly in earlier testing. The lines of code using the current sensors were removed, and the code manually started. This time the code began running, a log file was created, and pictures were being captured for data collection.

CHAPTER 6 DATA COLLECTION

Data collection is still in progress at the time of writing, however what has been collected is presented here. While the system was in Toowoomba many photos were collected, though these are mostly unusable for Varroa comparison as the photos are blurry and very noisy as seen in Figure 23. A vast majority of these photos contain no bees that can be seen, likely due to the time interval between images captured as well as the low activity level observed at the hive.

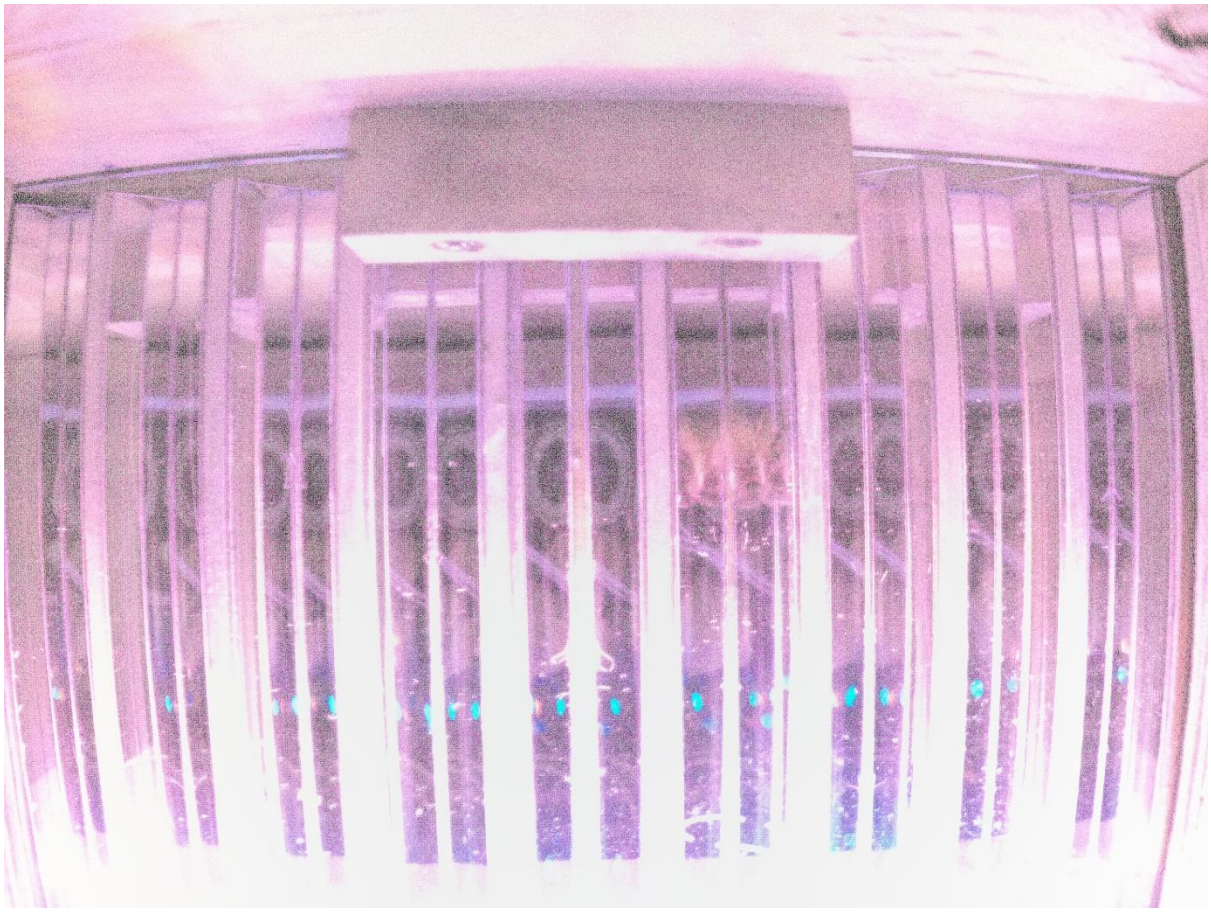

Figure 23 - Image captured from Toowoomba

The log data from Toowoomba in *Table 5* shows the outcome of 3hrs of operation on battery power alone. Unfortunately, this record does not capture the temperature and humidity data for the full day as once the storage was full the application crashed.

Table 5 - Toowoomba log data

Toowoomba		**Min**	**Max**	**Average**
Humidity	%	64.9	79.2	
Temperature	C	15.8	22.8	
Battery Voltage	V	11.905	11.973	
Current	mA	1503.30	1729.28	1568.47

Both the humidity and temperature rose during the operation of the system, while the current remained mostly stable. The battery voltage slowly dropped with time as is expected. More analysis of this data will be covered in a later chapter.

A longer span of data collection was carried out in Medowie, beginning on the 25th of July and ending on the 30th of August, with images captured approximately every 4 seconds for close to 2.5 days. Almost 200 of these images, along with log files were extracted from the system on the 9th of August to start some processing testing and analysis. Due to the large volume of images these have not all been analysed at this time, although a large portion of those appear as though the LEDs are not on (Figure 24) or partially black (Figure 25). It appears that the reduction in time between image collection caused by not logging the current sensors has caused issues with either the camera, or more likely the LEDs not turning on in time for the image capture.

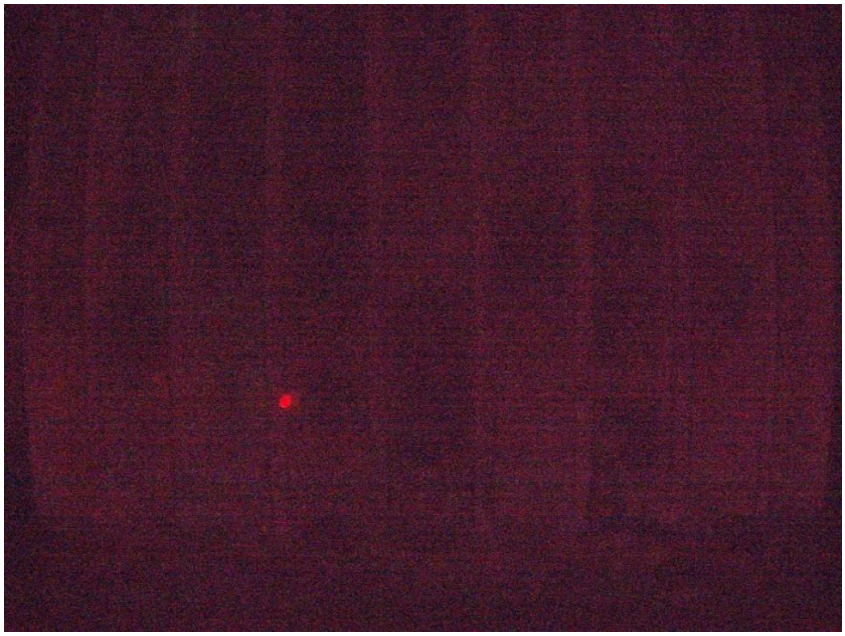

Figure 24 - Medowie image with no illumination

Figure 25 - Medowie image half illuminated

From the images that were successfully captured, images captured early in the day had a lot of condensation evident on the polycarbonate hiding much of tunnel seen in Figure 26 . Additionally, the focus had slipped leading to blurry images making it difficult to see clearly as in Figure 27.

Figure 26 - Medowie image with condensation

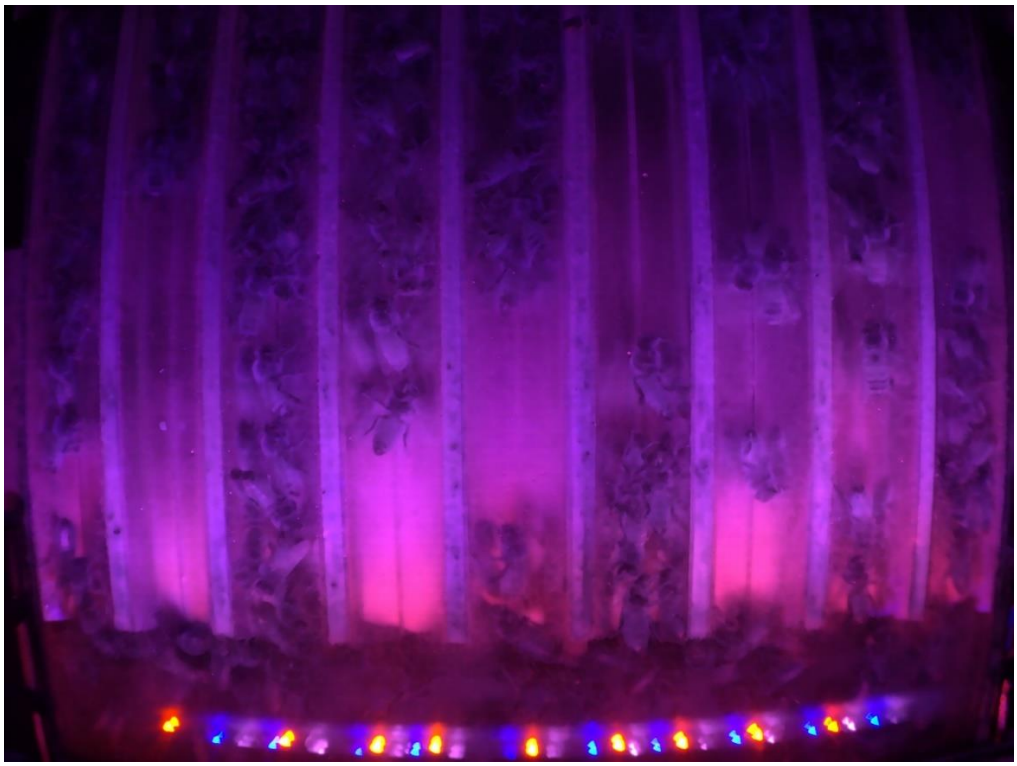

Figure 27 - Image captured from Medowie

Despite the blurry image it is possible to see by eye what are likely Varroa mites clinging to bees as can be seen in Figure 27, with a close-up in Figure 28. The blurry nature of the image makes it more challenging to conclusively identify the mites. Using a static white balance value that does not correct for the illumination wavelengths being used may also contribute to the 'mites' appearing black and difficult to distinguish from the bee. The intent had been to use colour segmentation to help isolate mites from the bees, which is not possible with this image.

Figure 28 - Bee with possible mite

After investigating the system after retrieval, there is significant debris located on both the polycarbonate panel, as well as the angled mirrors used in the bee tunnel (Figure 29). The tracks shown on the polycarbonate in the left image sits between the channels and does not impact the visibility though the panel. With the debris clouding the mirrors after one month, it seems unlikely they would serve their intended purpose for any practical duration without frequent cleaning.

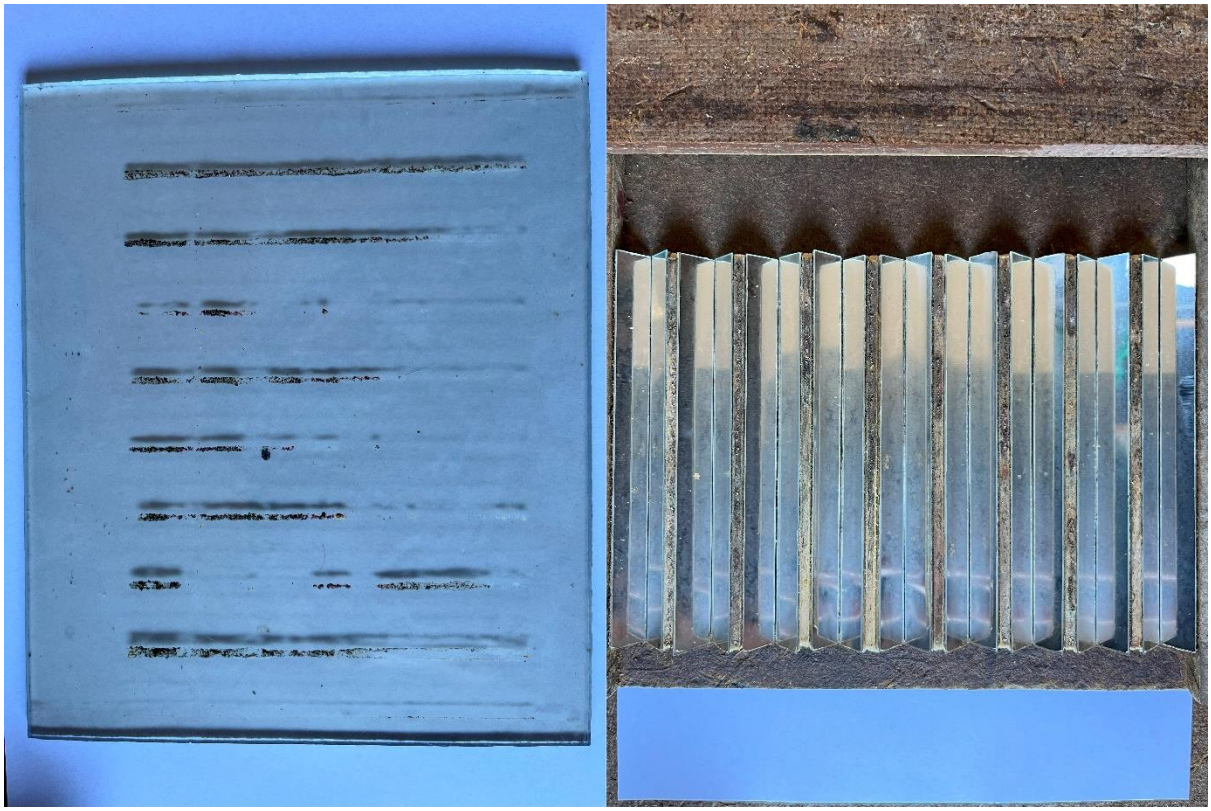

Figure 29 - Debris on bee tunnel after 36 days

The log data gathered from this data collection event contains the start-up and shut-down time of the system, indicating how long effective solar illumination was present in the established location, as well as the internal temperature and humidity data inside the electronics enclosure. An oversight in the logging code when images are not being captured means that each logged line is not tagged with the time. Because of this the time will be estimated based on the start and shutdown times for each day.

Analysis of the gathered log data is ongoing, however currently the humidity in the electronics enclosure appears to be stable throughout the duration of logging indicating no increase in moisture, and the temperature peaks at 38°C, approximately 15°C above the ambient temperature for the day.

Due to the disabling of the current sensors, no measurement was made of the battery charge or discharge rate to evaluate the suitability of the solar system. Looking at the bus voltage measured from the last successful recording of the current sensor (12.264V), the battery voltage is estimated to be around 12.8V as there are diodes and voltage loss through connectors in effect. The voltage of the battery measured after the system was retrieved from the field was 12.85V, so the battery was maintaining charge with the system.

During this data collection event, high winds with gusts up to 70kph were reported by (Australian Bureau of Meteorology 2024a) which resulted in the solar panel being blown over. Fortunately, the beekeeper stood it back up while checking on their hives after this event and no damage was caused to the system. Portable solar panels are needed as the hives get moved periodically by commercial beekeepers, however some means of securing them in place will need to be investigated for future data collection events.

After the data collection even in Medowie, some changes were made to the system to address the issues identified prior to redeploying the system for an additional data gathering event. The changes planned included addressing the blurry images captured, fixing the partially exposed images where the LEDs did not seem to activate, and adding time stamps to the data logging once storage is nearly full. Cleaning of the polycarbonate was also required to remove any debris left behind by earlier testing.

To address the focus issues seen in the images, the camera was carefully focused at the target distance of 165mm. This activity cannot be carried out in-situ due to space constraints in the system, so careful measurements are taken to ensure the camera and target are the appropriate distance apart on the bench. The camera can then be focused with easy access to get the best possible result.

When the code was adjusted to correct the logging function, a delay was added between turning the LEDs on and when the camera captures an image. This was done with the intent of correcting the partially illuminated images. A delay was also added into the code that runs when the storage is near full to slow down the capture of data from the sensors. The delay was added so that data would be captured once every 5 minutes to slow down the filling of the storage. A final addition was made to also capture the CPU temperature in the log so that the system could be examined for performance.

With the polycarbonate cleaned, the system was returned to the field as soon as possible for another round of data collection. This time the system was in the field for only 7 days before it was collected and the data extracted. The changes made to the LED timing was successful at ensuring all images were properly exposed though the focus was no better (Figure 30).

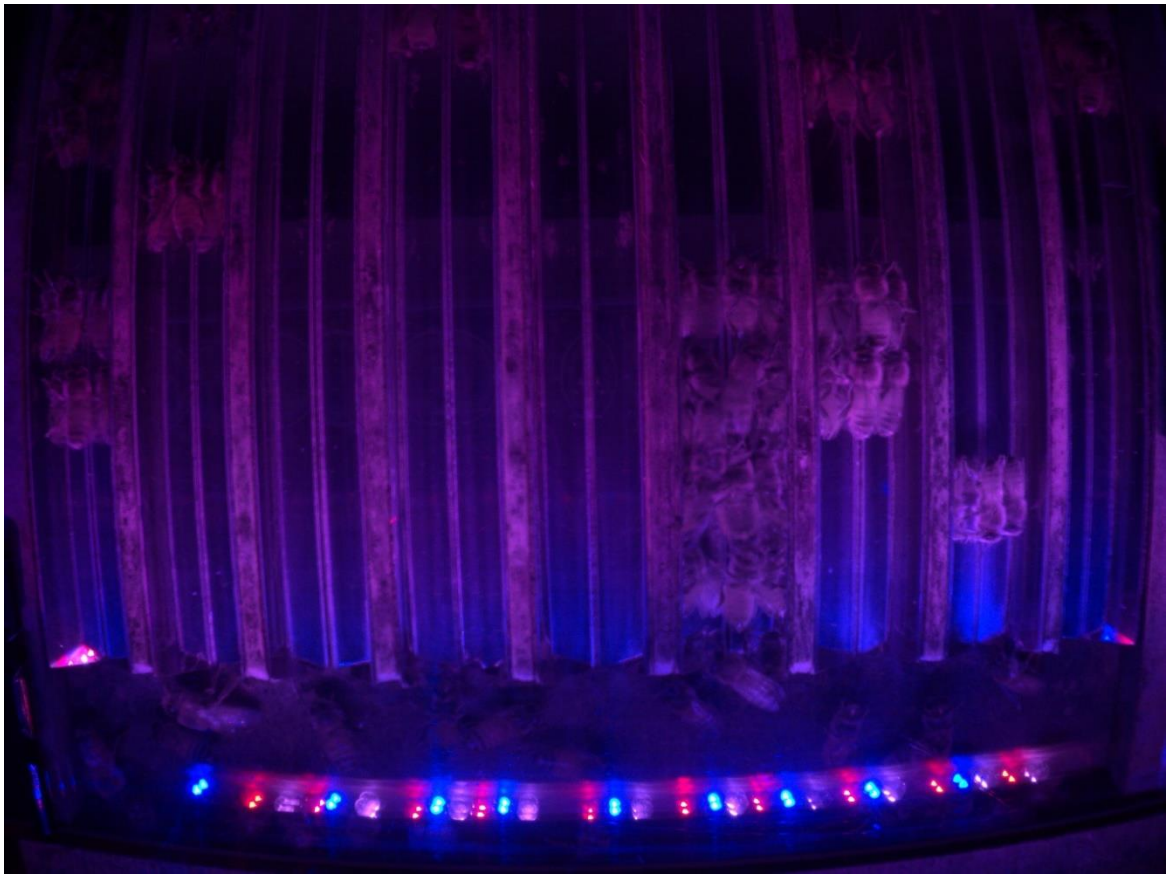

Figure 30 - Image after LED timing and focus adjustment

The logging functions occurred properly until the storage approached full capacity, at which time the time interval between sensor logs extended to 50 minutes due to an extra zero in the delay interval. While this is still sufficient to get an idea of system performance, it is slower than intended.

Due to the focus still being an issue, the possibility of the polycarbonate layers causing reflection or refraction was called into question. A series of images were captured to cover all possible configurations, only the lid fitted, no polycarbonate, only the tunnel panel fitted and with both fitted (Figure 31). A side-by-side comparison of these images shows no discernible difference with all having the same blurriness.

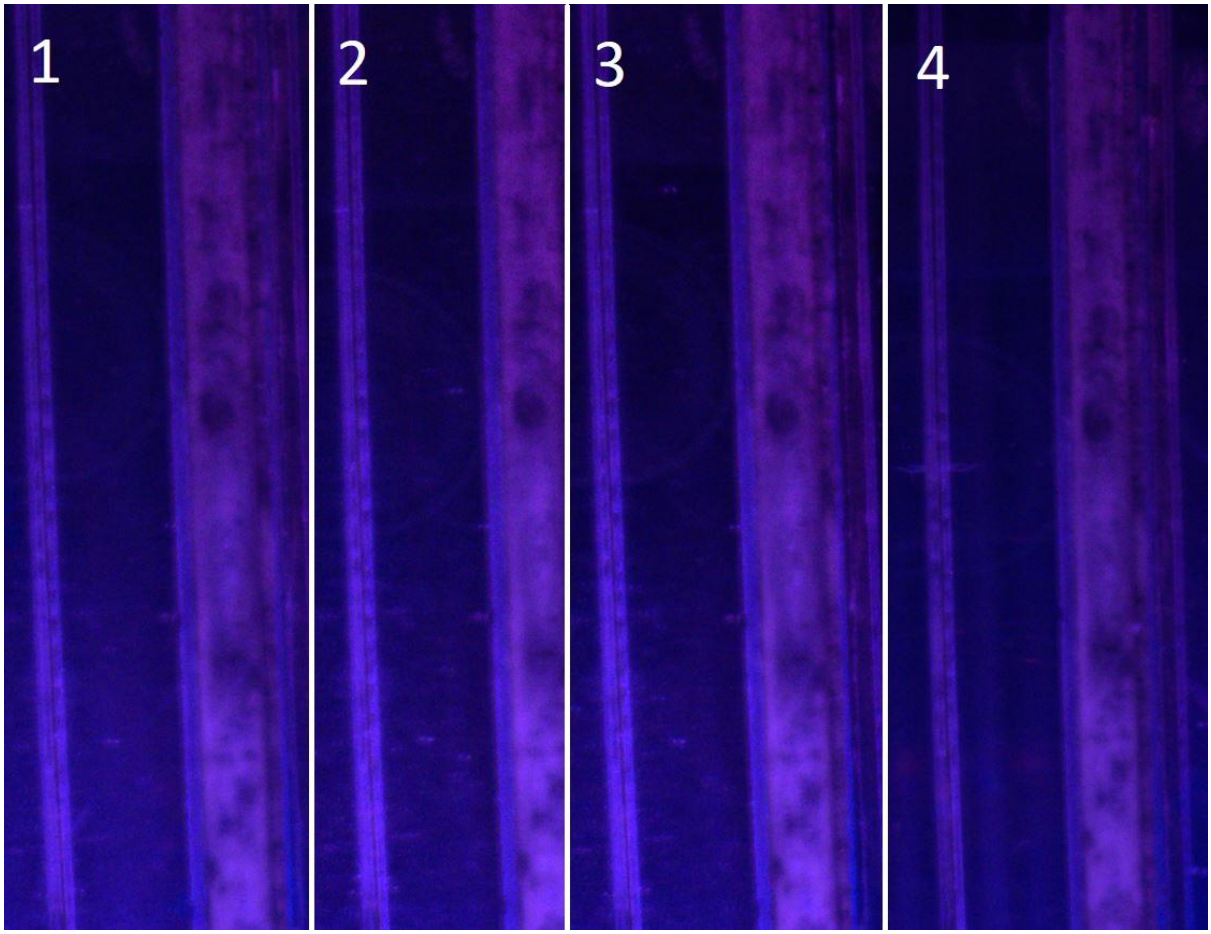

Figure 31 - (1) Lid fitted, (2) No polycarbonate, (3) Tunnel panel fitted, (4) Both fitted

Processing of the log data from both field-testing events identified that the internal system temperature was getting higher than desirable with some peaks above 40°C, shown in Figure 32. The temperature rises rapidly once the system is turned on, and only starts to fall close to when the system turns off in the evening. The humidity data shows that the environmental sealing of the electronics enclosure functioned as expected with the humidity values remaining around the same every day seen in Figure 33.

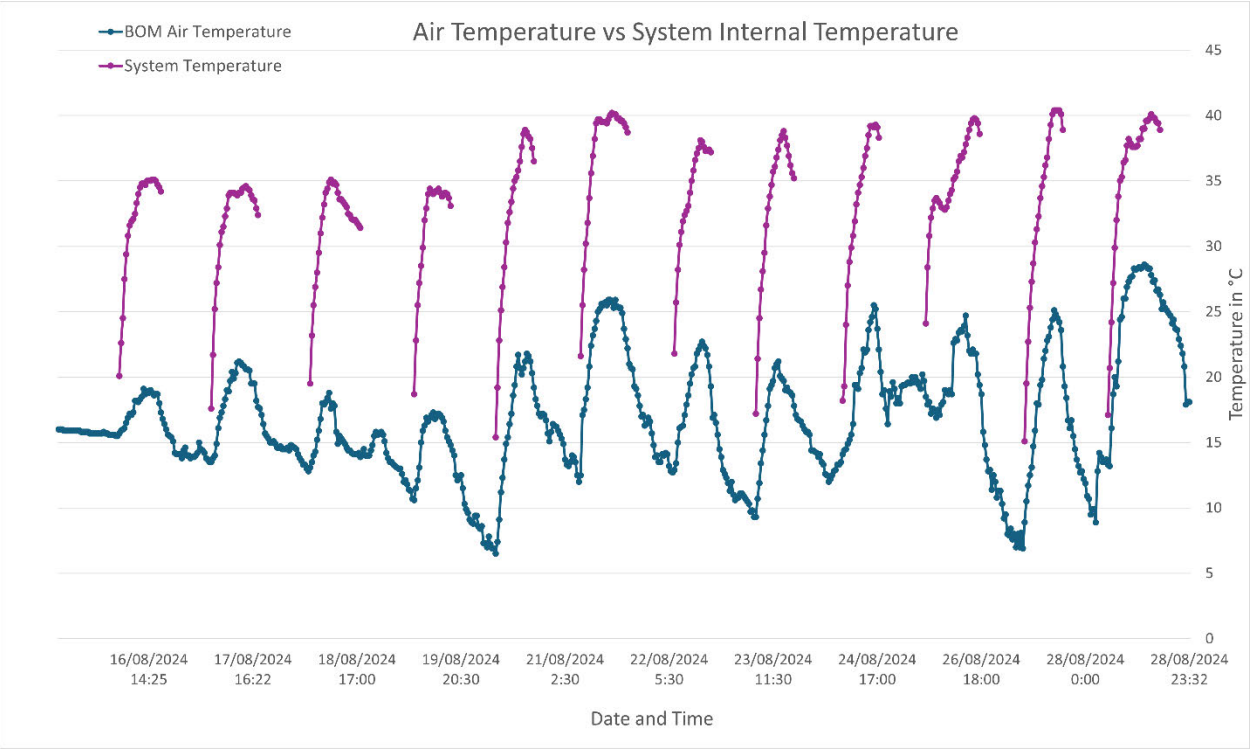

Figure 32 - Ambient air temperature vs system internal temperature

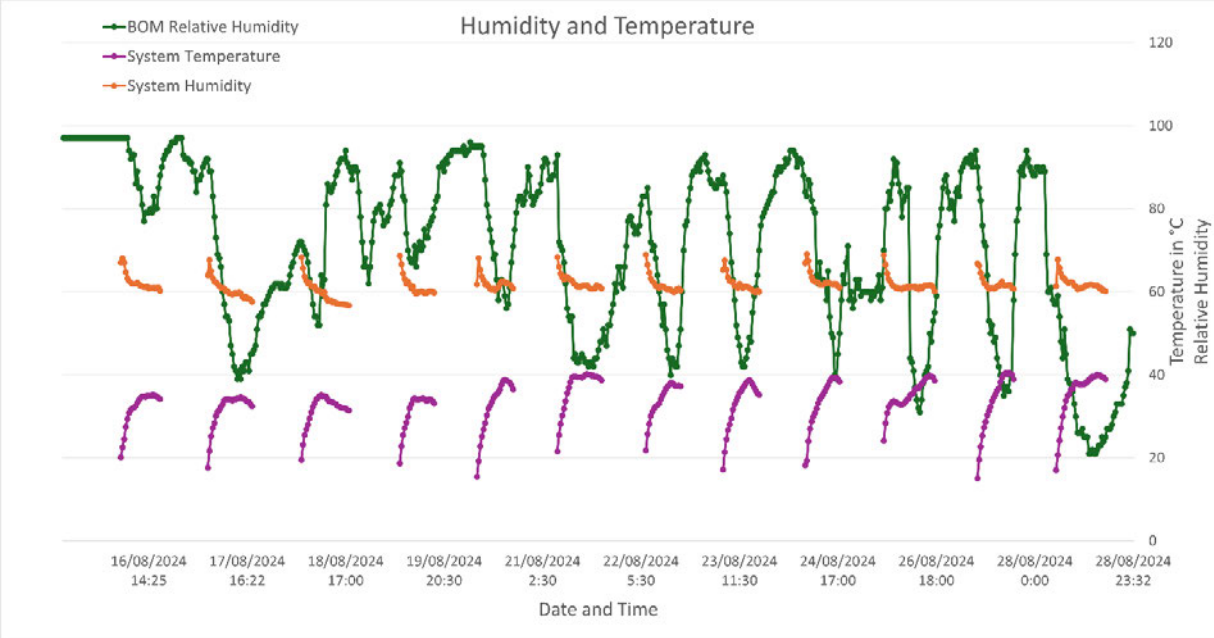

Figure 33 - BOM humidity, system temperature and system humidity measurements

From the second set of data the CPU temperature can be compared to ambient temperature and system internal temperature (Figure 34). The CPU temperature is naturally higher than the system ambient temperature, and approaches 70°C on one day. Further analysis of this data will be covered in a later chapter.

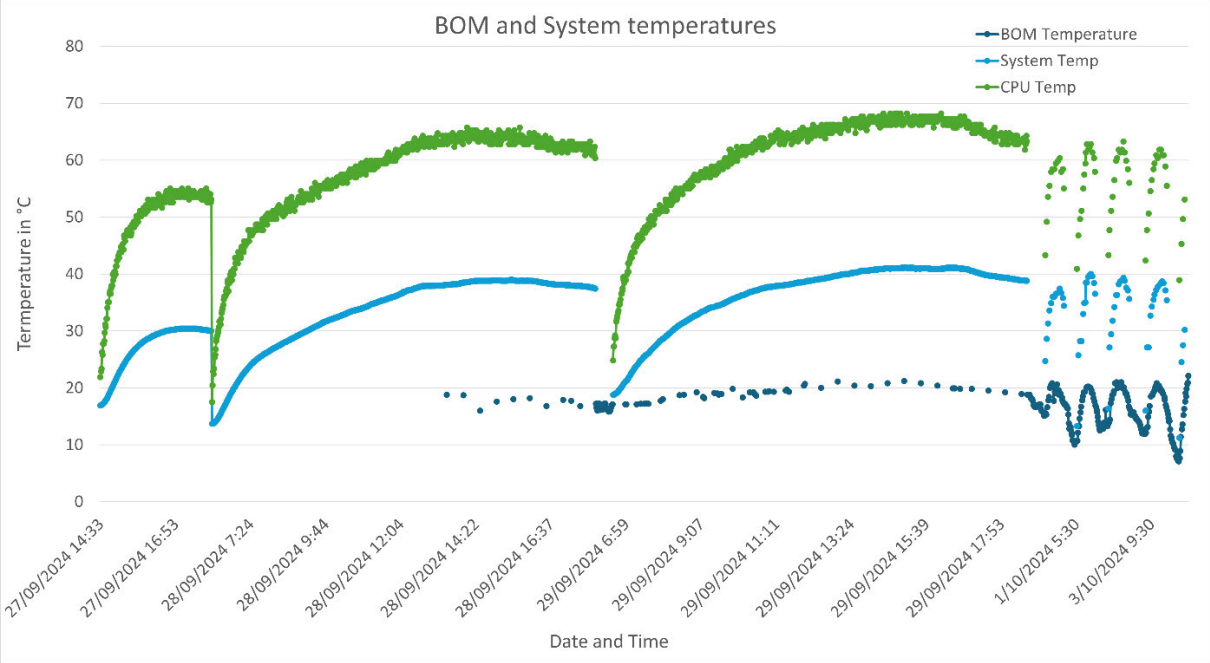

Figure 34 - Ambient, system and CPU temperatures

CHAPTER 7 ALGORITHM

The algorithm for detecting Varroa mites on honeybees is not complete at the time of writing. Much of the initial development and testing of the algorithm processes was carried out using a representative background image with bees from Figure 1 of Mrozek et al. (2021b) scaled and added in. Once the initial images from field testing were captured, testing and development of the algorithm has moved to using these images.

Code for the algorithm uses OpenCV written in Python developed on a Windows desktop before porting to the RPI for deployment. The basic process used for the algorithm is isolating the bees from the background, image cleanup and then mite identification. The image cleanup step involves any steps necessary to help prepare the image of each bee to make mite identification more reliable.

Background subtraction is effected by simply subtracting a captured image (Figure 35 – Top Right) from the background image (Figure 35 – Top Left) (a single 'clean' image of the background containing no bees). Ideally this will leave any pixels of the bees coloured while all others are black. Noise, debris brought into the system, and moisture will also show up in this image (Figure 35 – Bottom Left). The next several steps help combat the unwanted detections at this stage. At this stage the resolution is reduced to improve processing time, while still retaining the original image for later processing. Thresholding only operates on black and white images, so the reduced resolution image is converted to black and white (OpenCV appears to flip the image during this process). Thresholding is then applied to isolate the changed pixels in the image by setting any pixels above the threshold intensity to white, all others as black. Erosion is applied to remove noise, followed by dilation to correct for erosion of desired areas, and make the bee as continuous as possible (Figure 35 – Bottom Right).

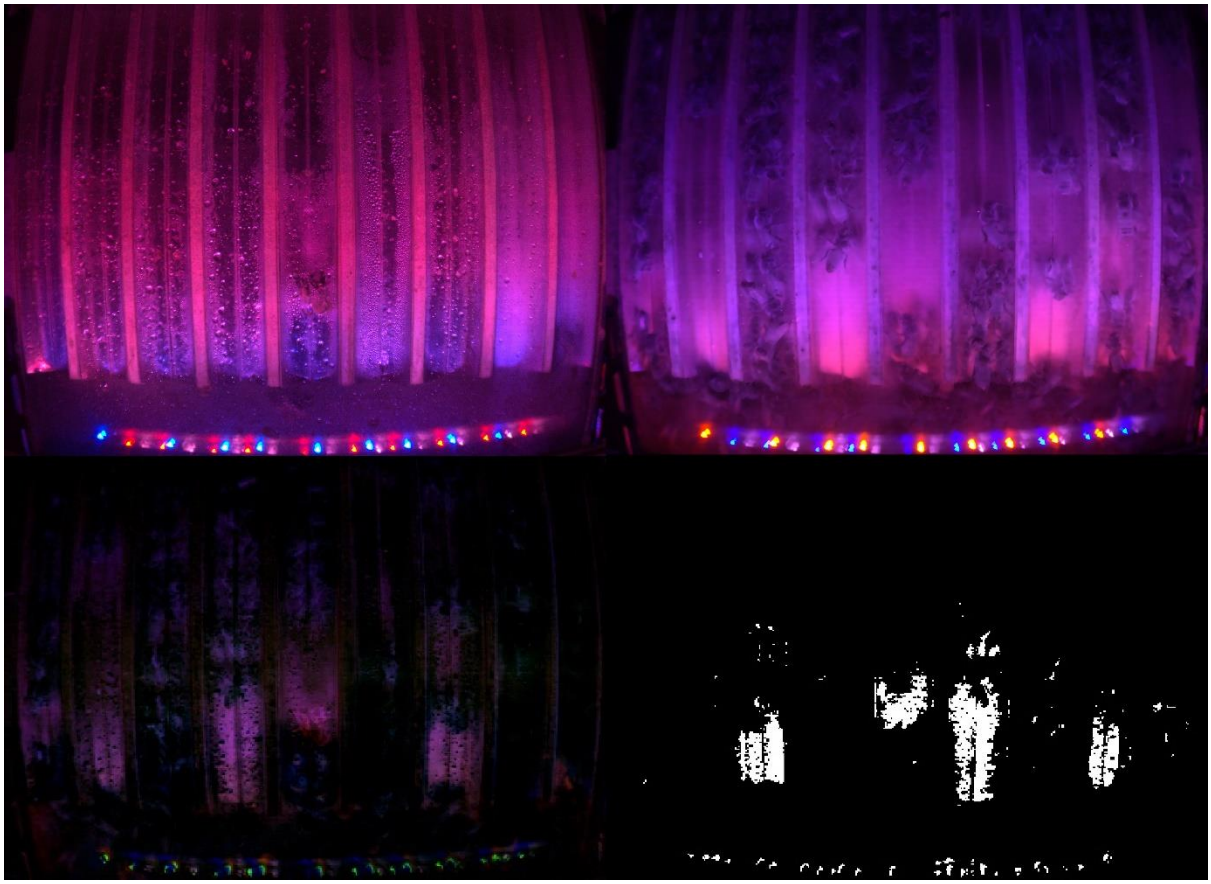

Figure 35 - (Top Left) background, (Top Right) captured image, (Bottom Left) subtracted image, (Bottom Right) thresholded image.

The image is then cropped into each channel of the tunnel and OpenCV findContours applied to identify areas thresholded. The contours are used to apply a bounding rectangle, the dimensions and position of which are applied to the original captured image. This produces cropped images of each location of difference from the background, which should be bees.

From the first field test, the blurry images and moisture on the background image confused this process and yielded inconsistent results. The bees could not be consistently identified from the background in images captured by the system and alternative processes were investigated.

A replacement for the findContours function using SIFT and ORB processes were examined. These processes identify key features of a bee which can be used for object identification in the image. This was hoped to aid in differentiating bees that are grouped close together as seen

in Figure 35 – Top Right. SIFT and ORB were ultimately unsuccessful at identifying the bees in the images. The processes did not seem to be able to identify appropriate key points on any image of a bee cropped out of the entire image, and often struggled to find the same bee in the image.

Hough transform for circles was applied to attempt identification of the mites as was done by Voudiotis, Moraiti and Kontogiannis (2022), on a test image using bee images from Figure 1 of (Mrozek et al. 2021b) which requires further tuning and has not been successful at this time (Figure 36). Some additional pre-processing may be required to help the process isolate the mite such as colour detection.

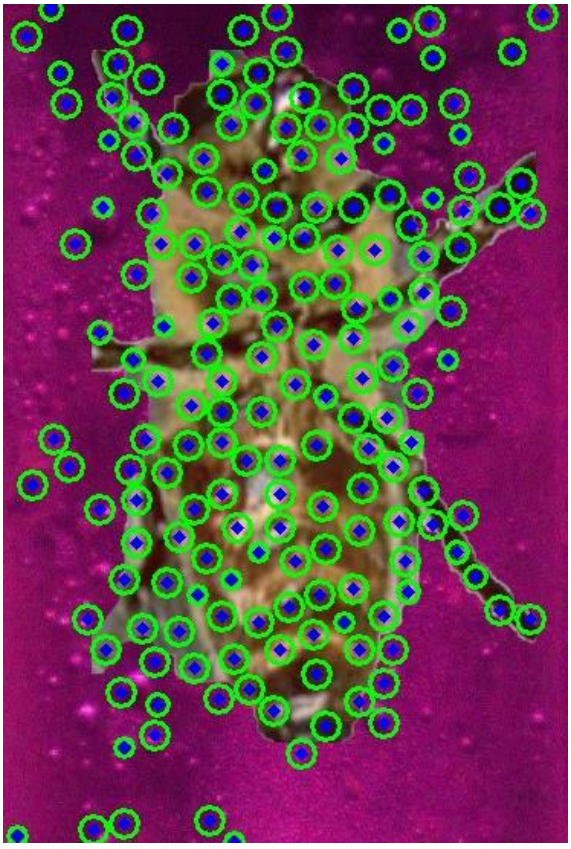

Figure 36 - Early algorithm testing

Based on the images collected by the system, colour detection will be of limited use as the mites and various areas on the bee appear to be the same colour of near black. Other colour

spaces were investigated (HSV and YCbCr) trying to identify a suitable method of extracting the mites from the images. RGB images had the most difference between the mites and bees when viewed by eye, and the mites blended into the black areas of the bees in this colour space.

With a second set of data collected, the image colours and exposure were much more consistent. Additionally, there was no humidity, and a clean background had been collected before deploying the system to the field and with some image brightness and contrast applied individual bees could be extracted. The mite detection process was not working successfully however (Figure 37). A large amount of Gaussian filtering had to be done on the images to reduce the noise present in the images, which when combined with the blurry state of the original images made details difficult to see by eye.

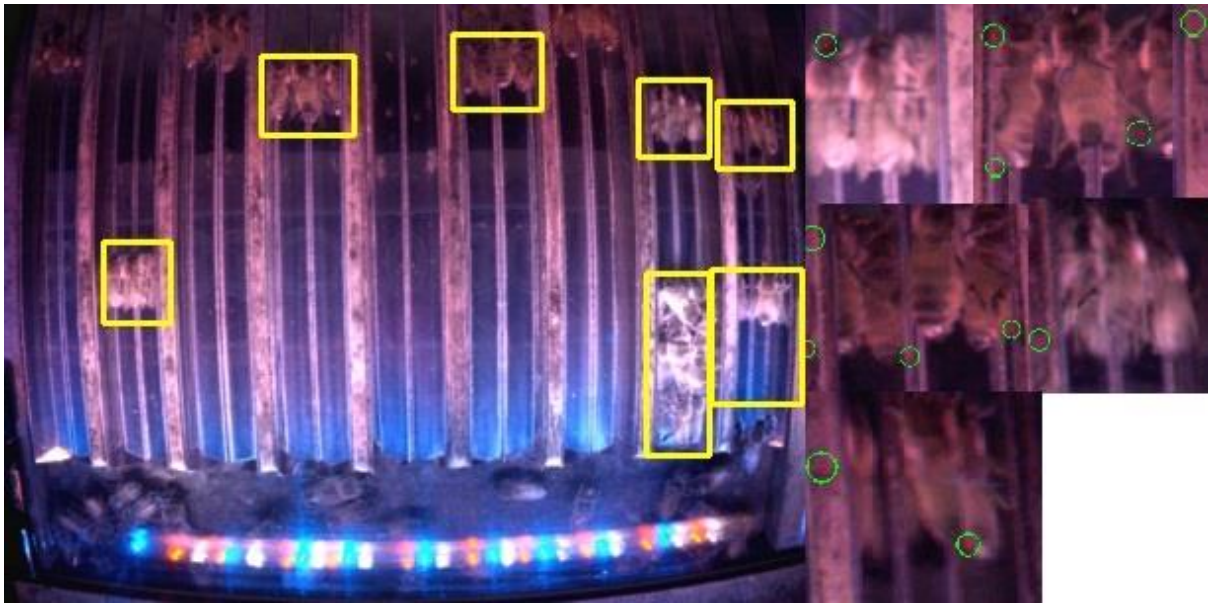

Figure 37 - Bees identified from background image and attempted mite detection

Tuning of the mite detection process was attempted using a single image of a bee with suspected mite cropped from the whole image using varying levels of Gaussian filtering, sharpening, colour segmentation in HSV and YCbCr colour spaces and inverted thresholding. Once a process achieved successful detection of the one mite, it was applied to the dataset to

test. None of the methods examined could avoid numerous false positives such as seen in Figure 37.

The algorithm in use at the end of research timeframe consists of two subprocesses: detecting bees (Figure 38) remains the same process outlined earlier, followed by detecting mites on the bees. Detecting the bees is done by taking an image from the camera, downscaling it and converting it to grayscale and subtracting a grayscale background image. This resulting image has a threshold applied, eroded and dilated to clean up noise. This is then cropped into columns for each of the bee paths (this aids the findContours function to isolate bees from each other). The findContours function is applied to identify areas of difference between the two images which are cropped out of the original image for further processing.

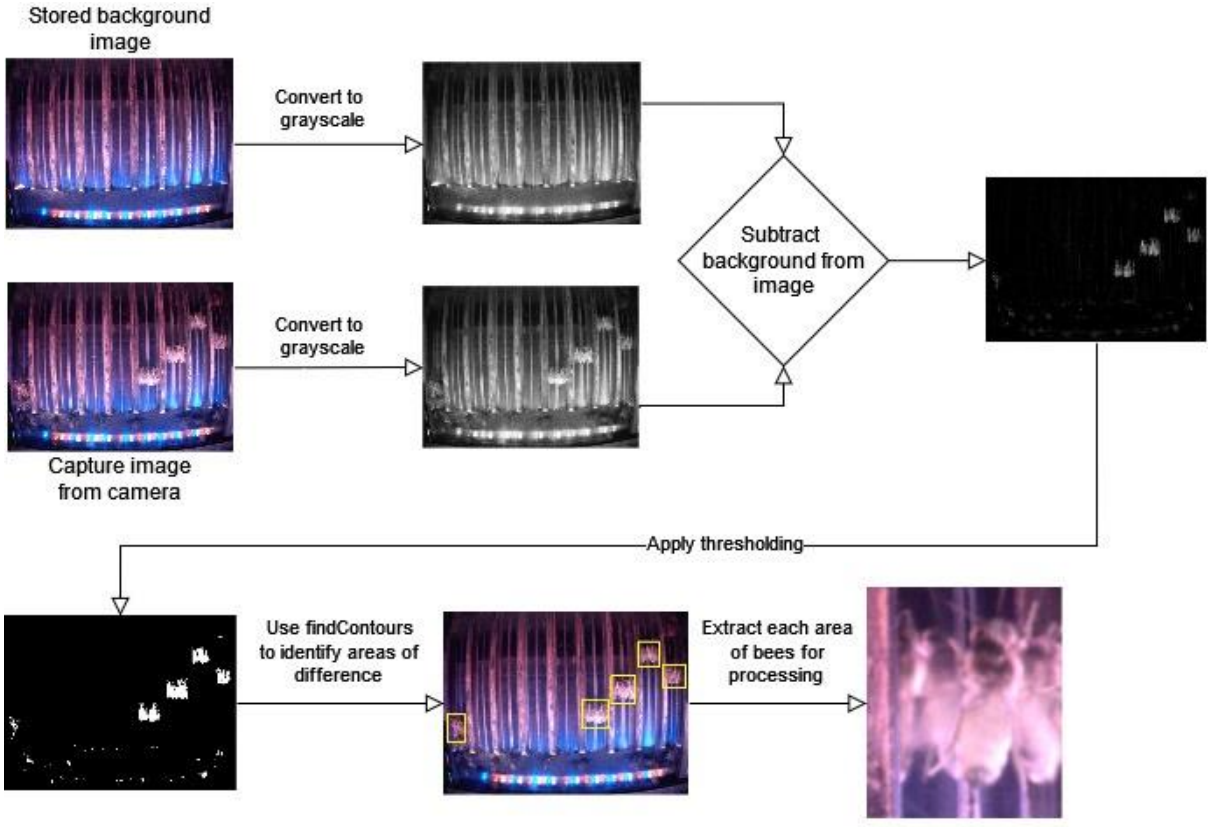

Figure 38 - Bee detection algorithm subprocess

Isolating the mites from bees is a subprocess (Figure 39) run on every region detected by findContours starting with converting the individual bee images to HSV colour space. A mask is generated using upper and lower bounded colour values derived from a manually identified mite image. The mask was applied to the original bee image as a bitwise AND so only the masked pixels were kept. Erosion and dilation were applied after this image was converted to grayscale. Hough circle detection was applied to the resulting image and any detected circles were recorded as mites.

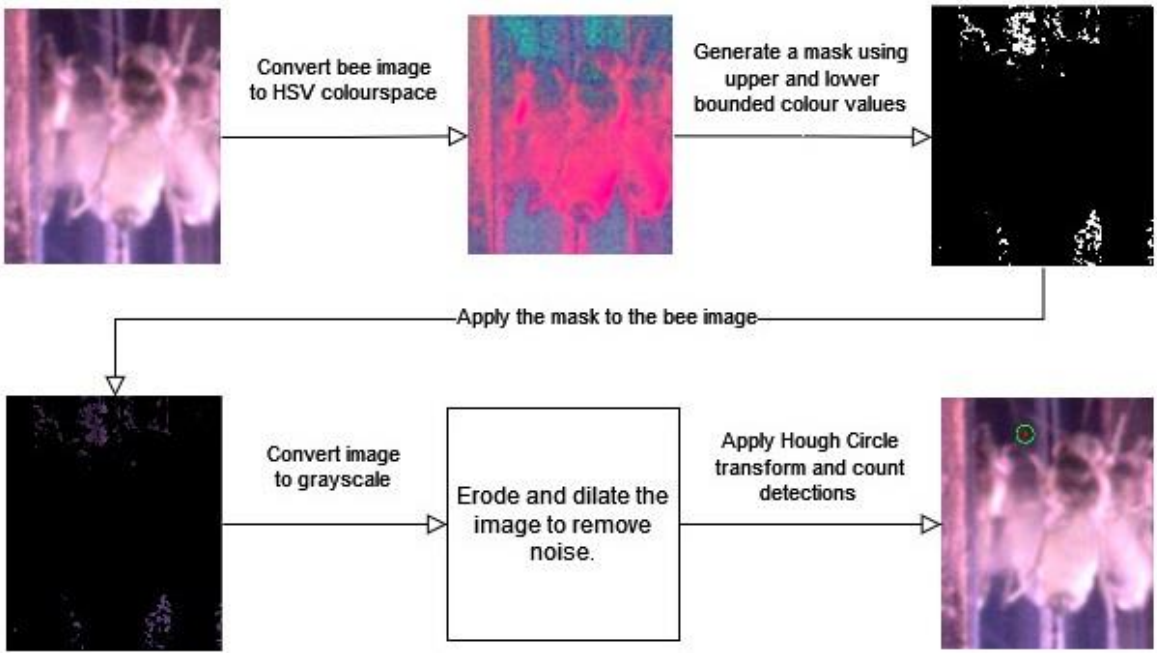

Figure 39 - Mite detection algorithm subprocess

Gradient detection, and second order gradient detection were both attempted using various kernel sizes and values with no success. In most cases these methods made the mites more difficult to see by eye (Figure 40) and circle detection never achieved success in these attempts, though this was not attempted with the newer dataset.

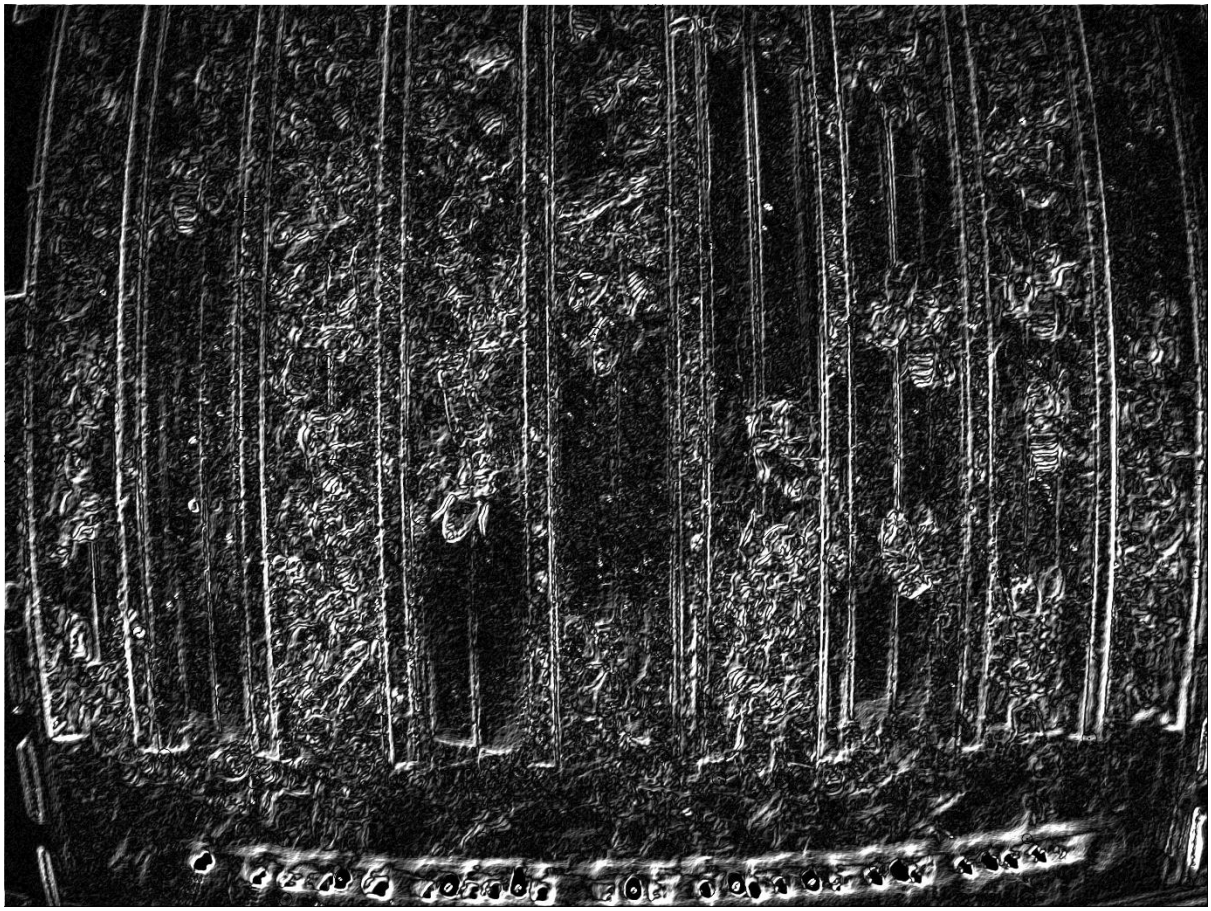

Figure 40 - Edge detection using convolution gradient detection

At this point there was insufficient time to continue attempting to get the image processing to work and this will be left for future research opportunities.

CHAPTER 8 DISCUSSION

Focusing of the camera is a major concern as that affects the ability to accurately detect the mites on the bees. This may be something that can be corrected with another round of careful focusing and ensuring the focus is locked before redeployment. The next field test will occur after focusing, recording and locking the camera so that drift of the focus over time can be examined. If the focus is somehow drifting, perhaps due to environmental factors that would render this camera or lens completely unsuitable for this use. Some additional post processing may be able to help correct this issue as well using image sharpening. Failing this, a different camera module with autofocus capability may be able to avoid the focusing problem, though these have limited lens compatibility.

Following on from research by Bjerge et al. (2019a) the combination of NIR, red and blue illumination was intended to provide good discrimination between mites and bees. This has not been shown with the algorithm and post-processing conducted in this research. The reason for this is not understood at this time and could be related to the cheaper camera used in this research or the data processing methodology used. A slightly different wavelength of NIR illumination was used in this research (850nm versus 780nm used by Bjerge et al. (2019a)) though this wavelength has a higher absolute mean pixel intensity difference from Figure 4.

Comparing the spectral ranges of the AD-130GE camera used by (Bjerge et al. 2019a) and the IMX477 sensor (Arducam 2023a) in the camera used in this project there is a difference. The IMX477 sensor does not show the spectral sensitivity above 700nm (Sony 2018, p. 40) shown in Figure 41, while the AD-130GE has a separate NIR sensor and so shows the spectral sensitivity up to 1000nm, with near 40% sensitivity at 780nm (JAI 2024a) shown in Figure 42 from JAI (2024b, p. 2).

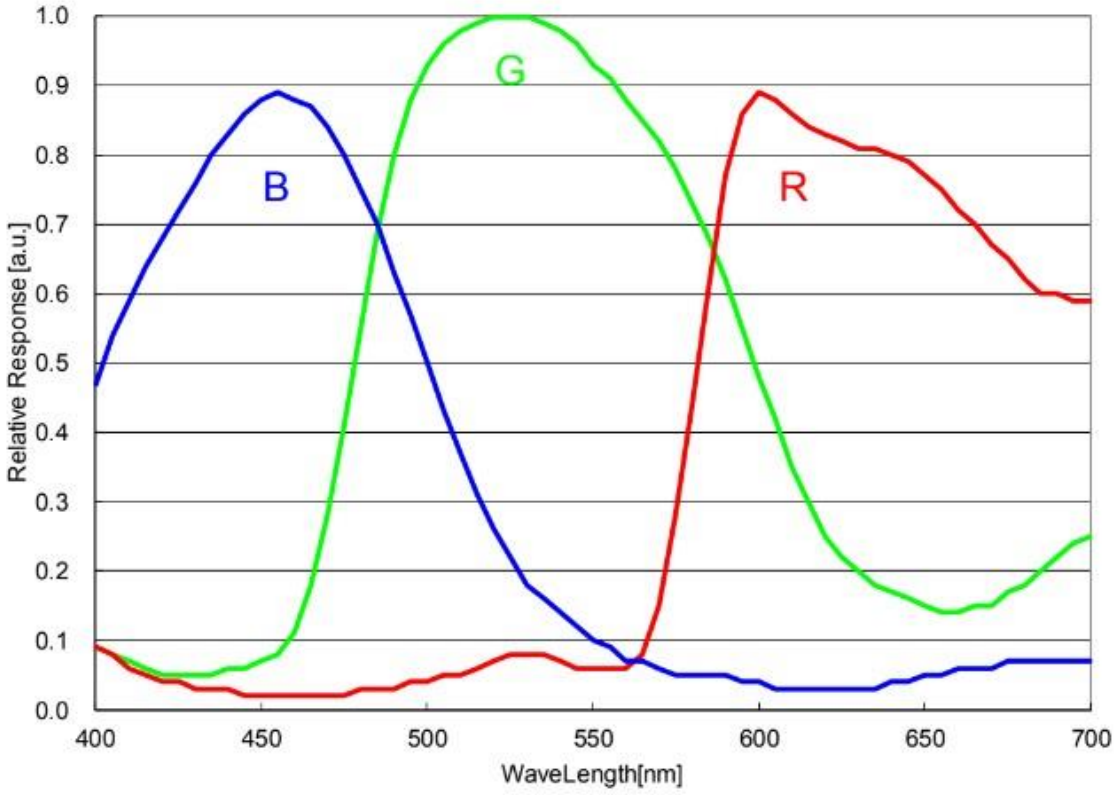

Figure 41 - Sony IMX477 sensor spectral sensitivity

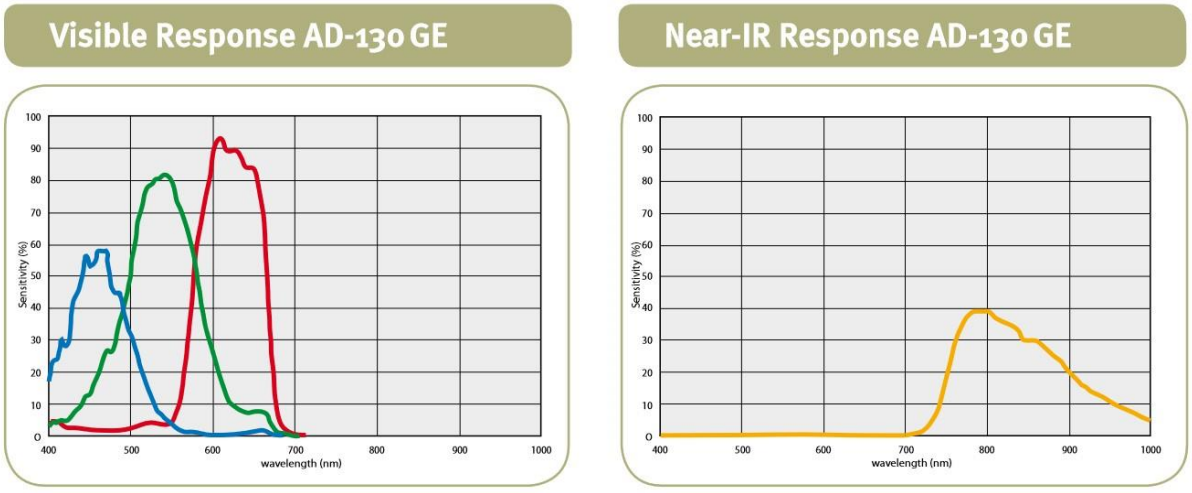

Figure 42 - JAI AD-130GE spectral sensitivity

After some investigation an estimate of the spectral sensitivity of a Sony IMX219 sensor was found (bjswift 2016), though this was from a GitHub page so the accuracy is not known. Figure

43 shows this estimated sensitivity, and from this not only does the NIR sensitivity fall to around 25-30% at 850nm, but the sensor is also equally sensitive on all pixels. Combining these factors together the NoIR sensor does not seem suitable for providing clear discrimination of the NIR wavelength and likely contributes to the failure to easily detect the mites. Since all the pixels are equally sensitive to these wavelengths, the result is everything in the image is brighter. Given that there is no green illumination being used in this system, perhaps the wavelength of blue could be shifted to 430nm, and red to 660nm to minimise the green channel exposure. The green channel could then be used as a proxy for NIR with minimal interference from the other light wavelengths being used. Optimum green channel sensitivity for NIR appears to be at 800nm based on the data presented in Figure 43.

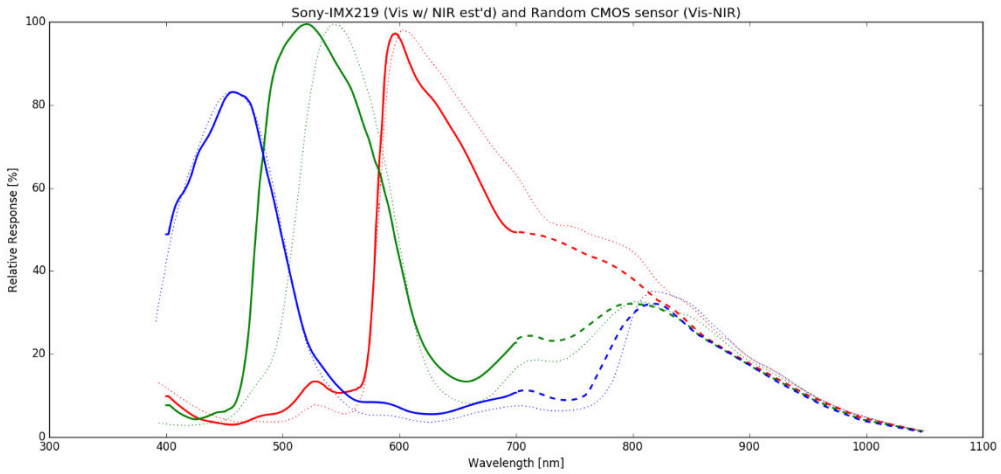

Figure 43 - Estimated spectral sensitivity of the Sony IMX219 sensor

Additional investigation is needed to find alternative methods of processing the images to detect the mites. White balance adjustments were investigated, along with using other colour spaces (RGB, HSV or YCbCr) as used by Noriega-Escamilla et al. (2023). None of these processes were successful in aiding detection of the mites, though white balance and contrast corrections improved detection of the bees.

The angled mirrors in the bee tunnel were intended to provide additional views of the bees for greater coverage and detection. These mirrors gathered enough debris on them in 3 days to only provide a hazy reflection and will not appreciably improve detection of mites due to this. Combined with the fact that this field test was conducted in winter when bees are less active, it is anticipated that the mirrors would require cleaning far more frequently than the benefit they provide. The second set of images collected showed the mirror remaining debris free and functional for the duration of image collection. It is possible that the humidity build-up evident in the first test led to additional debris collecting on the mirrors at a faster rate than can be expected in dryer weather.

Humidity build-up in the bee tunnel impacts the visibility of bees in the morning hours of the testing. Moisture in the tunnel dissipates throughout the day, and additional testing at other times of the year would be needed to determine the full extent of this issue. This is not an issue that has been identified in any other system that was researched in literature. Even when the moisture is not detected as false positives, the time where the tunnel is obscured reduces the effectiveness and efficiency of the system. Redesign of the bee tunnel and electronics system could be used to mitigate the issue by using waste heat of the electronics to keep the bee tunnel above the dew point temperature. This would require careful design to ensure the tunnel does not exceed a temperature that would affect the bees attempting to pass through it. Controlling the temperature of the tunnel would be easier to achieve with a separate heater, though this would cost extra power which is not ideal in a solar powered system.

Having an IP65 electronics enclosure succeeded in protecting the electronics from the external humidity and rain, shown by the measured humidity remaining within the same range for the entire testing duration shown in Figure 33. During this test duration there were some heavy rains and the humidity recorded by BOM and also shown on Figure 33 indicates that the

external humidity reached 100% at one point, and often into the 90% range, well above the 70% maximum of the enclosure.

Temperatures recorded in the electronics enclosure remained within acceptable levels of the equipment contained in there, not getting above 42°C and a delta from ambient air temperature not exceeding 20°C. If this rise does not increase with increasing ambient temperature, then a temperature of 45°C would see the equipment enclosure reach 65°C with the current design. Some care would need to be taken selecting equipment to operate in that temperature, but it is quite achievable.

The RPI CPU temperature is not as safe with a measured peak temperature of 68.17°C without the added load of an image processing algorithm to stress it. This is approaching the throttling temperature of a RPI board of 80°C (Allan 2023), and would not be suitable for operation during summer. For this system to be able to operate in warmer weather a different cooling solution would be needed, such as a metal electronics enclosure that could be used as a heatsink for the processor. It would be ideal if this waste heat could be used to help maintain the bee tunnel above the dewpoint to avoid humidity issues, but the largest amount of heat is generated in the middle of the day and the tunnel needs the heat over night.

Australian winter weather in NSW proved to be no challenge for this system as it exceeded the target of at least 1 week of continuous operation in the field. During the first field test in NSW the system was in the field for over 30 days of continuous operation, being exposed to sun, rain, high winds and storms with no issue beyond the solar panel blowing over. Securing the solar panel to the ground with sandbags or pegs would have aided this and is easy to achieve. As mentioned above, the temperature in summer is likely to have a negative impact on the system performance and additional methods of cooling the system will need to be investigated.

A goal was set for this system to be as cheap as practical to aid a wide rollout of the technology. The total system cost as designed and presented here approaches $900, including the solar panel and battery, but excluding the hive box as it was provided by the beekeeper. Some components could be scaled back in cost, such as the solar panel and battery likely do not need such high capacity. Though the cost saving in this regard is minimal with the main cost being the compute solution, memory and camera accounting for nearly half the system cost. Some cost efficiencies may need to be found, but those are secondary to achieving a functioning system at this time.

With the current design of the system, there are improvements that are needed before it would be useful to beekeepers. One of those is getting a mite detection algorithm functioning, and another aspect is making the cleaning an easier process. From the humidity and fouling seen during the field tests of this system periodic cleaning would be required to maintain optimum system operation. Fouling is likely to be increased during seasons when the bees are bringing in more pollen as the pollen could fall off the bees and accumulate on the polycarbonate window and on the mirrors. It would be ideal to modify the system so that the bee tunnel assembly could be removed without the need to remove the beehive from on top of the system as is currently done. This would improve the maintainability of the system and increase the chances of beekeepers making use of it.

Any additional effort that is required to maintain the system will not only lower the adoption of such a system but will also offset the benefit of not needing to manually count mites. The automated mite counting from such a system would reduce the requirement to interfere with the bees as well as reduce the labour required by the beekeeper. However mandatory mite checks required by the government would still have to be done manually using existing

techniques unless the policy was changed which would necessitate a reliable and accurate counting system.

Some benefit can be gained from faster detection of mite infestation levels to be able to target treatments better. Faster detection is likely the main benefit of this type of system aside from a reduction in manual labour in counting mites as early detection and appropriate treatment of mites means less stress on the bees. It is worth noting that deploying this system onto a hive with high mite infestation would show a lower number of mites than expected based on the research by Liu et al. (2023). Likewise, it would be expected that a hive left untreated for extended time would see the detected mite levels drop as fewer bees are able to leave the hive to fly. The goal of such a detection system would be to enable treatment of the mites before the infestation reaches that level in any case.

To track the progress of mites across NSW, many of these systems would need to be deployed which is only likely to happen if the government provided incentives to beekeepers. The effort required for cleaning of the system periodically and the cost of even this cheap system make it unlikely to be used without such incentives. Some possible options for implementing incentives could be government supplied detection system, or allowing the use of such a system for mandatory Varroa counts could make it worthwhile.

CHAPTER 9 CONCLUSION

In conclusion the Varroa mite detection system presented in this research was unable to meet the goals of distinguishing mites from honeybees. The images captured were of poorer quality than expected, the discrimination between mite and bee that was expected was not evident and the algorithm developed was unable to distinguish the mites.

Investigating the use of NoIR cameras for the detection of mites saw several undesirable effects including blurry images, and the RGB channels of the sensor equally detecting the NIR light. This may be able to be mitigated with changes to the light wavelengths used allowing the unused green channel to function as a proxy for NIR. The red channel is more sensitive to NIR wavelengths, so this does not provide a completely independent NIR channel. Focusing was a major issue with the solution presented and an autofocus camera may have been a better option for this research. Further work is required to identify the cause of the focus issues experienced and decide on a solution.

The detection algorithm used in this research is incomplete at this time, being unable to distinguish mites from other features in the images. Poor image quality and a lack of distinguishing features between the mites and bees presented challenges for the algorithm designed. It is hoped that correcting the image quality and adjusting the light wavelengths will provide better discrimination of the mites and enable the algorithm to be successful in the future with further development.

While the designed system is reasonably low cost coming in at nearly $900 worth of materials this would be a significant investment if it was required on every hive kept by a commercial beekeeper. For this reason, the system more likely to be useful in tracking the progress of mites around NSW by having one such system co-located with each site having hives. Such a

deployment would be reliant on improving the system such that it is able to reliably detect mites and have a sufficiently long maintenance cycle. Currently the cleaning requirements of the bee tunnel are likely to impede the usability of such a system.

Two other problems with the current system design would also prevent its deployment: humidity in the bee viewing tunnel and the processor temperature. These issues are unfortunately present at different times of day and cannot easily be mutually resolved. Humidity in the bee tunnel makes viewing the bees difficult in the early morning when the weather is cold and wet, and the processor approaches its temperature limits during the warmer afternoons. These issues would need to be solved for the system to be reliably usable in the Australian environment.

9.1 FUTURE WORK

Key points for future research are to investigate if using illumination of 430nm, 660nm and 800nm produces better discrimination using a NoIR camera and identify a method for reducing or eliminating the humidity issue in viewing the bees. Any similar system using optical methods to attempt detecting mites on the bees will have to contend with the external air temperature and humidity which contribute to the obscuring of the bees seen in this research.

Issues that need to be corrected for the system presented in this research are appropriate cooling for the processor, identifying a means of reducing the fouling of the bee tunnel or providing an easy means of cleaning, correcting the camera image quality and finalising the mite detection algorithm.

CHAPTER 10 REFERENCES

Abraham, KM 2020, 'How Comparable Are Sodium-Ion Batteries to Lithium-Ion Counterparts?', *ACS Energy Letters*, vol. 5, no. 11, pp. 3544-7.

Allan, A 2023, *Heating and cooling Raspberry Pi 5*, Raspberry Pi Ltd, Cambridge, UK, viewed 21/10/2024, <https://www.raspberrypi.com/news/heating-and-cooling-raspberry-pi-5/>.

Arducam 2023a, *IMX477 Full Report – Datasheet, Specs, Technologies and Camera Modules*, Arducam, Hong Kong, viewed 23/03/2024, <https://www.arducam.com/sony/imx477/>.

Arducam 2023b, *12MP IMX477*, Arducam, Kowloon, Hong Kong, viewed 23/03/2024, <https://docs.arducam.com/Raspberry-Pi-Camera/Native-camera/12MP-IMX477/#ir-cut>.

Arducam 2023c, *12MP IMX477,* Arducam, Kowloon, Hong Kong.

Australian Bureau of Meteorology 2024a, *Latest Weather Observations for Williamtown*, Australian Bureau of Meteorology, Melbourne, Australia, viewed 06/09/2024, <http://www.bom.gov.au/products/IDN60801/IDN60801.94776.shtml>.

Australian Bureau of Meteorology 2024b, *Maps of recent and past conditions*, Australian Bureau of Meteorology, Melbourne, Australia, viewed 27/03/2024, <http://www.bom.gov.au/climate/maps>.

Australian Government Department of Agriculture, FaF 2024, *Varroa mite (Varroa destructor)*, Australian Government Department of Agriculture, Fisheries and Forestry, Canberra, ACT, viewed 24/02/2024, <https://www.outbreak.gov.au/current-outbreaks/varroa-mite#:~:text=This%20mite%20is%20thought%20to,4%20years%20if%20left%20untreated>.

Australian Government Department of Agriculture Fisheries and Forestry 2024, *Varroa mite (Varroa destructor),* bee, Australian Government Department of Agriculture Fisheries and Forestry,, Canberra, ACT.

Australian Honey Bee Industry Council 2024, 'AHBIC Varroa Chemical Treatment Table', no. 09 August 2024, viewed 18/08/2024,<https://honeybee.org.au/ahbic-varroa-treatment-table/>.

Australian Standards 2018, *AS 60529—2004 Degrees of protection provided by*

enclosures (IP Code)

Battery World Australia Pty Ltd 2024, *Why Do I Need A Deep Cycle Battery?*, Battery World Australia Pty Ltd, Goodna, Queensland, viewed 31/03/20224, <https://www.batteryworld.com.au/news/expert-advice/2022/why-do-i-need-a-deep-cycle-battery>.

Bilik, S, Kratochvila, L, Ligocki, A, Bostik, O, Zemcik, T, Hybl, M, Horak, K & Zalud, L 2021, 'Visual Diagnosis of the Varroa Destructor Parasitic Mite in Honeybees Using Object Detector Techniques', *Sensors*, vol. 21, no. 8, p. 2764.

Bjerge, K, Frigaard, CE, Mikkelsen, PH, Nielsen, TH, Misbih, M & Kryger, P 2019a, 'A computer vision system to monitor the infestation level of Varroa destructor in a honeybee colony', *Computers and Electronics in Agriculture*, vol. 164, p. 104898.

Bjerge, K, Frigaard, CE, Mikkelsen, PH, Nielsen, TH, Misbih, M & Kryger, P 2019b, *A computer vision system to monitor the infestation level of Varroa destructor in a honeybee colony,* F 3.

bjswift 2016, *Sony-IMX219 (Vis w/ NIR est'd) and Random CMOS sensor (Vis-NIR),* github, San Francisco, USA.

Bowen-Walker, PL, Martin, SJ & Gunn, A 1997, 'Preferential distribution of the parasitic mite, Varroa jacobsoni Oud. on overwintering honeybee (Apis mellifera L.) workers and changes in the level of parasitism', *Parasitology*, vol. 114, no. 2, pp. 151-7.

Cree LED 2024, *C503B-Rxx/Axx 5-mm Round Red & Amber LEDs Data Sheet*, Cree LED, North Carolina, USA, viewed 01/09/2024, <https://www.cree-led.com/?s=C503>.

Gregorc, A, Knight, PR & Adamczyk, J 2017, 'Powdered sugar shake to monitor and oxalic acid treatments to control varroa mites (Varroa destructor Anderson and Trueman) in honey bee (Apis mellifera) colonies', *Journal of apicultural research*, vol. 56, no. 1, pp. 71-5.

Hall, H, Bencsik, M & Newton, M 2023, 'Automated, non-invasive Varroa mite detection by vibrational measurements of gait combined with machine learning', *Scientific reports*, vol. 13, no. 1, pp. 10202-.

Hetherington, S 2024, *Biosecurity (Varroa Mite) Control Order (No. 2) 2024,* DoPI NSW, Department of Primary Industries NSW, Orange, NSW, viewed 11/02/2024, <https://www.dpi.nsw.gov.au/__data/assets/pdf_file/0004/1529221/Biosecurity-Varroa-Mite-Control-Order-No.-2-2024.pdf>.

Huang, Z 2012, *Varroa Destructor Life Cycle,* Extension Foundation, Missouri, USA.

JAI 2024a, *Discontinued Products*, JAI A/S, Copenhagen, Denmark, viewed 24/03/2024, <https://www.jai.com/uploads/documents/English-Manual-Datasheet/Fusion-Series/Datasheet_AD-130GE.pdf>.

JAI 2024b, *Fusion Series AD-130GE,* JAI, Copenhagen, Denmark.

Jaycar 2024, *10A PWM Solar Charge Controller 12/24V with Timer Function IP67*, Jaycar, Sydney, Australia, viewed 03/08/2024, <https://www.jaycar.com.au/10a-pwm-solar-charge-controller-12-24v-with-timer-function-ip67/p/MP3756>.

Kava, HV, Vala, RG, Makwana, DH, Bhatt, UR, Sojitra, JD, Bhensadadiya, MP, Thoriya, SM, Kariya, SN, Fulbariya, BK, Bhagat Revision, MM, Oza, RD, Keshvani, MJ & Jani, YN 2023, 'Decentralized DC solar power system for remote areas', *Materials today : proceedings*, vol. 73, pp. 590-4.

Klemens, JA, Tripepi, M & McFoy, SA 2021, 'A motion-detection based camera trap for small nocturnal mammals with low latency and high signal-to-noise ratio', *Methods in ecology and evolution*, vol. 12, no. 7, pp. 1323-8.

Liu, M, Cui, M, Xu, B, Liu, Z, Li, Z, Chu, Z, Zhang, X, Liu, G, Xu, X & Yan, Y 2023, 'Detection of Varroa destructor Infestation of Honeybees Based on Segmentation and Object Detection Convolutional Neural Networks', *AgriEngineering*, vol. 5, no. 4, pp. 1644-62.

Lyons, J 2022, *Types of Solar Panels: Polycrystalline vs monocrystalline solar panels*, JFK Electrical, Mandurah, Western Australia, viewed 31/03/2024, <https://jfkelectrical.com.au/polycrystalline-vs-monocrystalline-solar-panels/>.

Manoukis, NC & Collier, TC 2019, 'Computer Vision to Enhance Behavioral Research on Insects', *Annals of the Entomological Society of America*, vol. 112, no. 3, pp. 227-35.

Mrozek, D, Górny, R, Wachowicz, A & Małysiak-Mrozek, B 2021a, *Edge-Based Detection of Varroosis in Beehives with IoT Devices with Embedded and TPU-Accelerated Machine Learning,* Journal of Applied Sciences.

Mrozek, D, Górny, R, Wachowicz, A & Małysiak-Mrozek, B 2021b, 'Edge-Based Detection of Varroosis in Beehives with IoT Devices with Embedded and TPU-Accelerated Machine Learning', *Applied Sciences*, vol. 11, no. 22, p. 11078.

Murashko, K 2016, 'Thermal modelling of commercial lithium-ion batteries', Doctoral thesis, University of Eastern Finland, Finland.

Narcia-Macias, CI, Guardado, J, Rodriguez, J, Rampersad-Ammons, J, Enriquez, E & Kim, D-C 2023, 'IntelliBeeHive: An Automated Honey Bee, Pollen, and Varroa Destructor Monitoring System', p. arXiv:2309.08955, viewed September 01, 2023,<https://ui.adsabs.harvard.edu/abs/2023arXiv230908955N>.

Noriega-Escamilla, A, Camacho-Bello, CJ, Ortega-Mendoza, RM, Arroyo-Núñez, JH & Gutiérrez-Lazcano, L 2023, 'Varroa Destructor Classification Using Legendre-Fourier Moments with Different Color Spaces', *J Imaging*, vol. 9, no. 7.

NSW Department of Primary Industries 2023, *Varroa Mite*, NSW Department of Primary Industries,, Orange, NSW, viewed 11/02/2024, <https://www.dpi.nsw.gov.au/biosecurity/seasonal-pests-and-diseases/spring/varroa-mite>.

NSW Department of Primary Industries 2024a, *Sugar shaking bees to detect external parasites,* F 2, NSW Department of Primary Industries,, Orange, NSW.

NSW Department of Primary Industries 2024b, *Varroa mite emergency response*, NSW Department of Primary Industries,, Orange, NSW, viewed 02/02/2024, <https://www.dpi.nsw.gov.au/emergencies/biosecurity/current-situation/varroa-mite-emergency-response>.

Ogihara, MH, Stoic, M, Morimoto, N, Yoshiyama, M & Kimura, K 2020, 'A convenient method for detection of Varroa destructor (Acari: Varroidae) using roasted soybean flour', *Applied entomology and zoology*, vol. 55, no. 4, pp. 429-33.

Plant Health Australia 2014, *Effect of Varroa on plant industries*, Plant Health Australia, Deakin, Australia, viewed 10/02/2024, <https://beeaware.org.au/pollination/preparing-for-varroa-mite/effect-of-varroa-on-plant-industries/>.

Plant Health Australia nd.-a, *Preparing for Varroa mite*, Plant Health Australia, Deakin, Australia, viewed 12/02/2024, <https://beeaware.org.au/pollination/preparing-for-varroa-mite/>.

Plant Health Australia nd.-b, *Varroa mites*, Plant Health Australia, Deakin, Australia, viewed 12/02/2024, <https://beeaware.org.au/archive-pest/varroa-mites/#ad-image-0>.

Raspberry Pi Foundation 2024, *Raspberry Pi Foundation*, Raspberry Pi Foundation, Cambridge, UK, viewed 31/08/2024, <https://www.raspberrypi.org/>.

Raspberry Pi Ltd nd., *Raspberry Pi 4 Model B specifications – Raspberry Pi*, Raspberry Pi Ltd, Cambridge, UK, viewed 31/03/2024, <https://www.raspberrypi.com/products/raspberry-pi-4-model-b/specifications/>.

Schurischuster, S, Zambanini, S & Kampel, M 2016, 'Sensor Study for Monitoring Varroa Mites on Honey Bees (Apis mellifera)'.

Sony 2018, *IMX477 Spectral Sensitivity Characteristics,* Sony, Kanagawa, Japan.

Un, C & Aydın, K 2021, 'Thermal Runaway and Fire Suppression Applications for Different Types of Lithium Ion Batteries', *Vehicles*, vol. 3, no. 3, pp. 480-97.

van der Voort, GE, Gilmore, SR, Gorrell, JC & Janes, JK 2022, 'Continuous video capture, and pollinia tracking, in Platanthera (Orchidaceae) reveal new insect visitors and potential pollinators', *PeerJ (San Francisco, CA)*, vol. 10, pp. e13191-e.

Vishay Semiconductors 2023, *High Speed Optocoupler, 100 kBd, Low Input Current, Photodiode Darlington Output*, Vishay Semiconductors, Pennsylvania, USA, viewed 04/06/2024, <https://www.vishay.com/docs/83605/6n139.pdf>.

Vishay Semiconductors 2024, *High Speed Infrared Emitting Diode, 830 nm,*

GaAlAs Double Hetero, Vishay Semiconductors, Pennsylvania, USA, viewed 01/09/2024, <https://www.vishay.com/docs/83605/6n139.pdf>.

Visual Communications Company.nd, *LED Through Hole 5mm (T-1 3/4) Blue 470 nm 1500 mcd 3.5V*, Visual Communications Company, California, USA, viewed 01/09/2024, <https://vcclite.com/product/vaol-5lsby4/>.

Voudiotis, G, Moraiti, A & Kontogiannis, S 2022, 'Deep Learning Beehive Monitoring System for Early Detection of the Varroa Mite', *Signals*, vol. 3, pp. 506-23.

Wheeler, M 2021a, *Purple Hive uses artificial intelligence to keep bees parasite-free*, Create Digital, ACT, Australia, viewed 29/03/2024, <https://createdigital.org.au/purple-hive-uses-artificial-intelligence-to-keep-bees-parasite-free/>.

Wheeler, M 2021b, *Purple Hive uses artificial intelligence to keep bees parasite-free,* PH 2, Create Digital, ACT, Australia.

Yandi, W, Puriza, MY & Jumaida, K 2021, 'Comparative study of electrical energy conversion on monocrystalline and polycrystalline solar panel types in fixed position with

various weather conditions in mountain area', *IOP conference series. Earth and environmental science*, vol. 926, no. 1, p. 12053.

Zhong, Y, Gao, J, Lei, Q & Zhou, Y 2018, 'A Vision-Based Counting and Recognition System for Flying Insects in Intelligent Agriculture', *Sensors (Basel, Switzerland)*, vol. 18, no. 5, p. 1489.

CHAPTER 11 APPENDICES

11.1 APPENDIX A

Gannt chart of the planned timeline for the research project

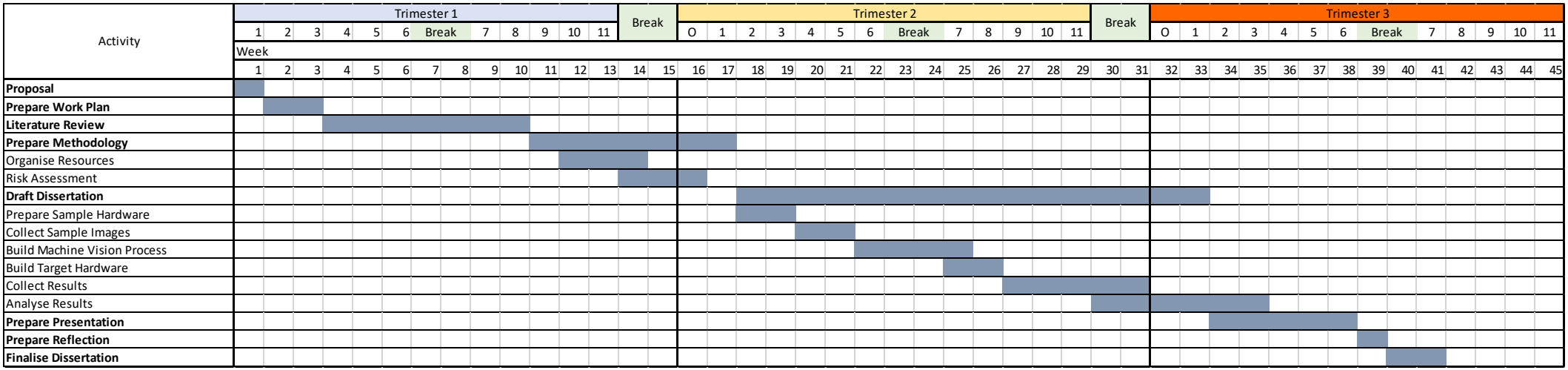

11.2 APPENDIX B

Test procedure tables that will be carried out with actual results filled in during testing.

Table 6 - Unpowered breadboard test procedure

Breadboard test - unpowered			
Step	**Action**	**Expected Result**	**Actual Result**
1	Using a multimeter, test for resistance between common positive and Solar negative	>10k Ω	
2	Using a multimeter, test for resistance between common positive and Battery negative	>10k Ω	
3	Using a multimeter, test for resistance between common positive and Load negative	>10k Ω	
4	Using a multimeter, test for resistance between common positive and common negative	>10k Ω	
5	Using a multimeter, test for resistance between 3.3V line and RPI negative	>10k Ω	
6	Using a multimeter, test in diode with negative probe on load negative and positive probe on the common negative.	<0.7V	

7	Using a multimeter, test in diode with negative probe on load positive and negative probe on the common negative.	.OL	
8	Using a multimeter, test in diode with negative probe on relay output and positive probe on the common negative.	<0.7V	
9	Using a multimeter, test in diode with positive probe on relay output and negative probe on the common negative.	.OL	
10	Using a multimeter, test for resistance between Battery negative and relay output.	.OL	

Table 7 - Powered breadboard test procedure

Breadboard test - powered			
Step	**Action**	**Expected Result**	**Actual Result**
1	Set the bench power supply to 12V, 1A	Setup	
2	Connect the bench power supply to load connection	Setup	
3	Turn on the power supply	Power supply is in constant voltage mode	
4	Using a multimeter, probe the 5V converter for voltage	5V is present	
5	Using a multimeter, probe the relay output for voltage	0V is present	
6	Set a second power supply to 12V, 1A	Setup	
7	Turn on the second power supply	Power supply is in constant voltage mode	
8	Using a multimeter, probe the relay output for voltage	0V is present	

9	Connect U2 pin 6 to U2 pin 5	Click is heard from the relay	
10	Using a multimeter, probe the relay output for voltage	12V is present	
11	Using a multimeter, test for resistance between U1 pin 6 and RPI negative	<1k Ω	
12	Turn off power supply 1	Setup	
13	Using a multimeter, probe the 5V converter for voltage	5V is present	
14	Using a multimeter, test for resistance between U1 pin 6 and RPI negative	>10k Ω	
15	Using a multimeter, test for voltage on all pins for RPI	0V is present on all	
16	Turn off power supply 2	Setup	
17	Remove jumper between U2 pin 5 and pin 6	Setup	
18	Connect RPI to Input/Output (IO) connector and power via USB-C power monitor	Setup	
19	Turn on power supply 1, and 2	Setup	

20	Look for power indicator on RPI	Power indicator is on	
21	Monitor voltage and current on the USB-C power monitor	Record readings	
22	Remote connect into the RPI	Setup	
23	Using the terminal, check the state of RPI IO	GPIO 0 is output and high	
24	Using a multimeter, probe the relay output for voltage	12V is present	
25	Using the terminal, drive RPI GPIO 13 high	Red LEDs turn on	
26	Using the terminal, drive RPI GPIO 13 low	Red LEDs turn off	
27	Using the terminal, drive RPI GPIO 19 high	Blue LEDs turn on	
28	Using the terminal, drive RPI GPIO 19 low	Blue LEDs turn off	
29	Using the terminal, drive RPI GPIO 26 high	NIR LEDs turn on	
30	Using the terminal, drive RPI GPIO 26 low	NIR LEDs turn off	

31	Load libraries for INA226, INA260 and DHT22 sensors	Setup	
32	Run example code INA226	Expect current and voltage similar to power supply 2	
33	Run example code for DHT22	Expect sensible temperature and humidity	
34	Using the terminal, drive RPI GPIO 19 high	Blue LEDs turn on	
35	Turn off power supply 1	Blue LED's turn off, RPI remains on	
36	Shutdown RPI	Remote connection closes, power indicator is off	
37	Using a multimeter, probe the 5V converter for voltage	0V is present	
38	Connect power supply 1 supply via INA260 to load connection.	Setup	

39	Turn on power supply 1	Power indicator is on	
40	Remote connect into the RPI	Setup	
41	Run example code INA260	Expect current and voltage similar to power supply 1	
42	Turn off power supply 1	Power indicator is on	
43	Shutdown RPI	Remote connection closes, power indicator is off	
44	Turn off power supply 2	All power is off	

Table 8 - System integration testing

Board + solar controller power test			
Step	**Action**	**Expected Result**	**Actual Result**
1	Set the bench power supply to 12V, 1A	Setup	
2	Connect the bench power supply to solar connection	Setup	
3	Connect the battery-to-battery connection	Setup	
4	Turn on the power supply	Power supply is in constant voltage mode	
5	Remote connect into the RPI	Setup	
6	Using the terminal, check the state of RPI IO	GPIO 0 is output and high	
7	Using the terminal, drive RPI GPIO 13 high	Red LEDs turn on	
8	Using the terminal, drive RPI GPIO 13 low	Red LEDs turn off	

9	Using the terminal, drive RPI GPIO 19 high	Blue LEDs turn on	
10	Using the terminal, drive RPI GPIO 19 low	Blue LEDs turn off	
11	Using the terminal, drive RPI GPIO 26 high	NIR LEDs turn on	
12	Using the terminal, drive RPI GPIO 26 low	NIR LEDs turn off	
13	Install power test code to RPI	Setup	
14	Run the power test code on RPI	No change observed	
15	Toggle Load power off on solar controller	RPI begins shutdown, terminal closed	
16	Using a multimeter, probe the 5V converter for voltage	0V is present (or power indicator light is off)	
17	Toggle Load power on, on the solar controller	RPI turns on	
18	Remote connect into the RPI	Setup	

19	Install data capture code	Setup	
20	Manually start data capture code	LEDs turn on and off periodically	
21	Examine file structure for a log file and image files	A log file is created, and images are being captured	

11.3 APPENDIX C

System schematic

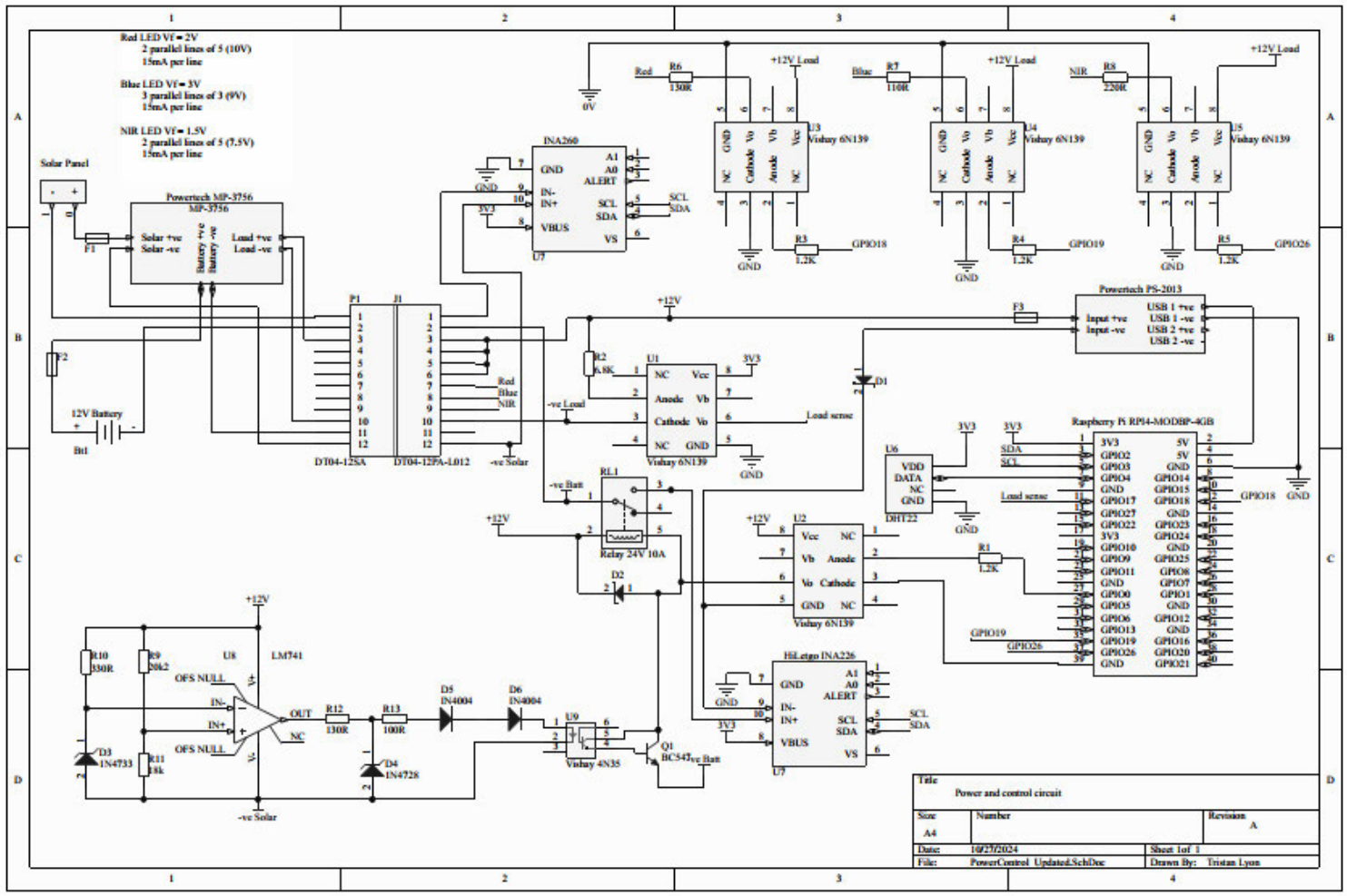

11.4 APPENDIX D

Risk assessment of the practical work to be carried out.

4514	RISK DESCRIPTION	STATUS	TREND	CURRENT	RESIDUAL
	Monitoring varroa infestation in bee hives	Live		Medium	Medium

RISK OWNER	RISK IDENTIFIED ON	LAST REVIEWED ON	NEXT SCHEDULED REVIEW
Tristan Lyon	28/04/2024	28/04/2024	28/10/2024

RISK FACTOR(S)	EXISTING CONTROL(S)	CURRENT	PROPOSED CONTROL(S)	TREATMENT OWNER	DUE DATE	RESIDUAL
Bee hives are located outside. While accessing the hives there is exposure to weather.	Control: Accessing the hives during adverse or inclement weather is not necessary and will be avoided.	Very Low	No Control:			Very Low
1. Working outdoors including exposure to sun.	Control: Work is being conducted in cooler	Low	No Control:			Low

2. Native flora and fauna including bees, spiders and snakes. 3. Manual handling of bee hives and boxes. 4. Bee hives in use are located at a business near place of residence. 5. Driving to hive location (less than 10 minutes).	months with frequent breaks. Short duration is expected. Work will be conducted at times to avoid mid-day temperatures. Handles and surfaces will be checked for spiders before touching. Manual handling techniques will be employed. Local business and family will be notified of personnel location, and time of expected return. _____ Control: Always wearing a wide brim hat (or bee suit). Bee suit will be worn anytime contact with bees is expected. Safety boots and gloves worn at all times on site					
Australia in winter - possibility of snakes/spiders Interacting with honeybees	Control: Handles and surfaces will be checked for spiders before touching. Work is being conducted in cooler months, contact with snakes is unlikely. Care will be taken when walking and touching anything on the ground.	Low	No Control:			Low

	Student is not allergic to bees, but anti-histamines will be kept nearby at all times in case of multiple stings. _____ Control: Bee suit will be worn anytime contact with bees is expected. All other times long sleeves and long pants will be worn. Safety boots and gloves worn at all times on site.					
1. Working outdoors, there is risk of tripping on ground. 2. Moving beehives to install test equipment has a risk of dropping boxes on feet, and pinching fingers.	Control: Introduction to the area with knowledgeable staff and employing manual handling techniques when moving loads. _____ Control: Gloves and safety boots will be work at all times on site.	Medium	No Control:			Medium
The design incorporates a 12V battery and requires assembly, therefore possible contact with low voltage.	Control: Student has training and experience as an avionics technician (Cert IV in Aeroskills Avionics) working with low voltage. _____ Control: When assembly is finished, the device will not have exposed voltage.	Low	No Control:			Low

Soldering - contact with soldering iron. Beekeeping - smoker	Control: Student has training and experience as an avionics technician (Cert IV in Aeroskills Avionics) working with soldering equipment. Control: Gloves will be worn when working with soldering equipment and smoker.	Medium	Student will receive instruction in the use of the smoker from professional beekeepers.		17/05/2024	Low
Leaded solder and flux used during soldering.	Control: Soldering will be conducted in a well-ventilated environment will solder fume extractor.	Low	No Control:			Low

	Control: Gloves will be worn during soldering activities.					
Power tools such as drills and saws may exceed 85dB (exact level is unknown) for short duration.	Control: Earmuffs worn any time power tools are used.	Low	No Control:			Low
Power tools such as drills and saws may cut or sever fingers if used improperly.	Control: Guards provided by tool manufacturers will be checked prior to use for correct fitment and operation. Pusher tools, clamps and such will be used to keep fingers away from saw blades. Loose clothing and hair will be secured, tied back or changed before operating tools. Control: Safety glasses will be used any time power tools are operating.	Medium	No Control:			Medium
May be working alone when attending to the bee hive. Work will be conducted outdoors in daylight hours, so UV exposure is expected.	Control: Family and business will be informed of student location and expected return time before any field activity. Control: Long sleeves, pants and wide brim hat will be worn at all times that a bee suit is not worn. Sunscreen will be applied to any exposed skin.	Very Low	No Control:			Very Low